UTAPRAD

Technical Unit for the development of APplications of RADiations

ACTIVITY REPORT

Year 2010

ENEA – Frascati Research Centre

UTAPRAD

UTAPRAD is the ENEA Technical Unit for the development of APplications of RADiations.

UTAPRAD was started mostly from former Applied Physics Laboratories and a few environmental groups at ENEA Frascati on April 20, 2010, within the process of reorganization of ENEA Agency.

UTAPRAD mission is addressed to research and technological objectives and to qualified technological services in the fields of energy and sustainable development, by means implementation of technologies for the application of ionizing and not-ionizing radiations, the development of particle accelerators, of optoelectronics and photonics.

UTAPRAD is constituted by four major Laboratories aimed at Diagnostics and Metrology (DIM), Mathematical Modelling (MAT), Photonics Micro- and Nano-structures (MNF) and Radiation Sources (SOR), each one including different groups with specific expertise.

UTAPRAD senior direction members have a coordination role of different scientific and management aspects of specific activities aimed at: medical application of particles accelerators, technology transfer to SME, nanotechnology, relations to Italian Ministries.

UTAPRAD has a special care for dissemination aspects, as a part of results of research projects (organization of conferences and workshop, dedicated websites, etc) and for formation activities (teaching at university, PhD and master courses, student tutoring, etc).

Since Nov. 2010 UTAPRAD has its own administration and management service, while before it was relying on the Frascati Centre facilities.

Major scientific results achieved in 2010 are summarized in the following, the list of the involved personnel is given at the end of the report, followed by the relevant research products.

1. Diagnostic and Metrology Laboratory

1.1 Mission and infrastructures

The Diagnostic and Metrology Laboratory (UTAPRAD-DIM), included in the ENEA Frascati Research Centre, is mainly focused in the development of laser sensors for environmental monitoring applications in devoted outdoor campaigns. The implemented laser technologies are dedicated to find the state of the art in the electro-optical spectroscopic tools that are better tailored in terms of discrimination and sensitivity in diagnostic and metrology field of applications. More in details the allocated roles to the Laboratory are:

- development of spectroscopic and optic systems for in-situ or remote (lidar systems) in sensing and metrological applications (the Environment, Cultural Heritage, Security and Health);
- development of compact and miniaturized sensors to be operated in hostile environments and space explorations;
- development of imaging sensors for in-situ applications in different fields of interest supporting also data analysis and images release;
- data merging from different active and passive optical sensors.

Competences available in the Laboratory are originated from expertise in different scientific disciplines as laser spectroscopy, optics, active and passive sensors, terrestrial and marine biology, analytical chemistry and data analysis. This know-how is fruitfully devoted to the development of sensors for scientific and industrial applications. More in details, tasks and roles assigned involve:

- the design, implementation and tests of compact optical systems for environmental active and passive remote sensing including harsh environments (polar and interplanetary explorations), Cultural Heritage and Security.
- the execution of monitoring campaigns with own instruments installed in dedicated payloads to be connected with terrestrial and/or marine autonomous robots or rovers, merging data from other sensors;
- the design, implementation and tests compact and/or imaging spectroscopic sensors for real time analysis of hazardous materials scattered in different matrices, for health applications and for goods characterization;
- the development of optical tools for in-situ and remote sensing on demand of other UTs;
- the hardware upgrading of own mobile laboratories for environmental monitoring (atmosphere, sea and terrestrial campaigns);
- the partnership in research activities within national and international joint ventures.

Facilities and sensors formerly developed by UTAPRAD-DIM and utilized for current activities include:

- Satellite oceanographic data analysis and merging laboratory
- Plant biology laboratory
- Environmental analytic laboratory
- Laser scanning flow cytometry laboratory
- LIBS + XRF laboratory
- Bio-electro-magnetism laboratory

- Atmospheric mobile lidar laboratory
- Molecular spectroscopy laboratory
- Non linear spectroscopy laboratory
- Laser scanning 3D tri-chromatic sensor and artificial vision laboratory
- Laser scanning 3D underwater sensor
- Lidar fluorosensor
- LIF Scanning sensor

1.1.1 Funding and projects

The research activities of the UTAPRAD-DIM Laboratory are mainly funded in the frame of National research programs (MIUR, Industria 2015) either as partner or joining consortia (CETMA and TRAIN), with a strong presence in the EC Framework Programme FP7 (CUSTOM - Drugs And Precursors Sensing By Complementing Low Cost Multiple Techniques), networks of excellence (NDE – Network Detection of Explosive).

The UTAPRAD-DIM Laboratory boasts the collaboration with national and European Small and Medium Enterprises (SMEs) as well as Large Industries, in supporting the development of laser based equipment to be successively delivered on the market. To this respect, it is worthwhile to stress the collaboration with a network of Scotland SMEs and Large Industries, operating in the sector of offshore Oil and Gas industry. In particular, the subsea 3D laser scanner is the subject of ongoing discussions to ascertain the possibility of a technological transfer aimed at its further development into a device qualified to operate under the harsh environmental conditions (high depth) of offshore oil fields.

1.2 Environmental diagnostic related to climate changes

1.2.1 Atmospheric monitoring of volcanic sites

The atmospheric lidar ATLAS (Agile Tuner Lidar for Atmospheric Sensing), mounted on the mobile laboratory ENVILAB (ENVIronmental LABoratory) hosted in a small truck, underwent some major improvements: the laser high voltage circuit was upgraded; the transmitter optics was repolished; the telescope was recoated; a two mirror system, similar to a coelostat, was implemented, in order to scan the whole hemisphere above the horizon. A gain of a factor 3 – 4 in term of signal-to-noise ratio can be estimated as a result of these improvements.

After its deployment in polluted zones and in the Etna areas, recently ATLAS measured the Stromboli volcanic plume (Figure 1). At Etna, the extinction coefficient inside the volcanic plume was retrieved, while at Stromboli also water vapor concentration in cross sections of the plume and wind speed at the crater were measured. Water vapor concentration and wind speed were retrieved by differential absorption lidar and correlation technique, respectively. Lidar returns were obtained up to a range of 3 km. The spatial resolution was 15 m and the temporal resolution was 20 s. By combining these measurements, the water vapor flux in the Stromboli volcano plume was found. To our knowledge, it is the first time that a CO_2 laser-based lidar is used to profile a volcanic plume and a lidar retrieves water vapor concentrations in a volcanic plume.

Figure 1 - The mobile lidar ATLAS at Stromboli, Italy. The laser has been aimed to analyze the volcanic plume.

The prevailing wind during the Stromboli campaign blew the plume south of ATLAS. Pointing the lidar south west with a fixed azimuth angle while varying the elevation angle, cross sections of water vapor concentration in the plume were obtained: an example is given in Figure 2. Once detected the plume center (maximum of water vapor concentration) with two scans, it was possible to determine the wind direction as the unit vector linking the two centers.

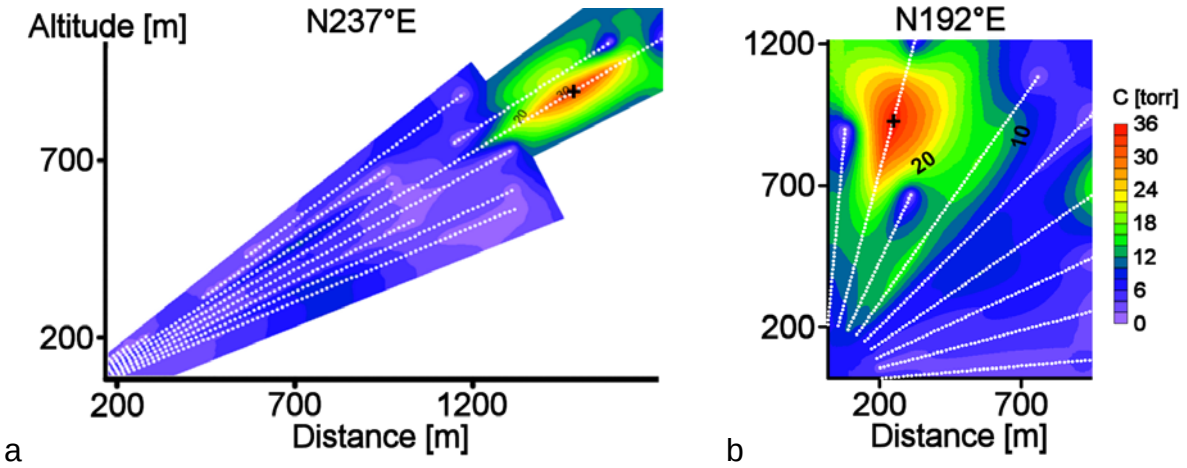

Figure 2 - Water vapor concentration retrieved by ATLAS during two scans at 237° (a) and 192° (b) azimuth angles. The white points are the lidar measurements. The black crosses are the points where the water vapor concentration maxima of the two scans occurred.

The plume was located at the range of 2100 – 2700 m from ATLAS, as it can be inferred by the extinction coefficient profile (Figure 3a). The extinction coefficient was retrieved from the lidar signal with an inversion method derived from the algorithms published by Klett and Fernald. Consequently, the wind speed was obtained from the correlation function was calculated in the range interval 2100 – 2700 m for ten successive lidar profiles (one each 10 s), thus observing the displacement of aerosol inhomogeneities for 100 s. An example of correlation function is given in Figure 3b. Although the correlation technique is not very precise, it allows one to gain information on the wind field from lidar returns exactly in the same space zone and time interval where the water vapor concentration is measured. Moreover, it does not require the deployment of any other instrument. Eventually, combining the measurements of average concentrations and wind speed, the water vapor flux was calculated.

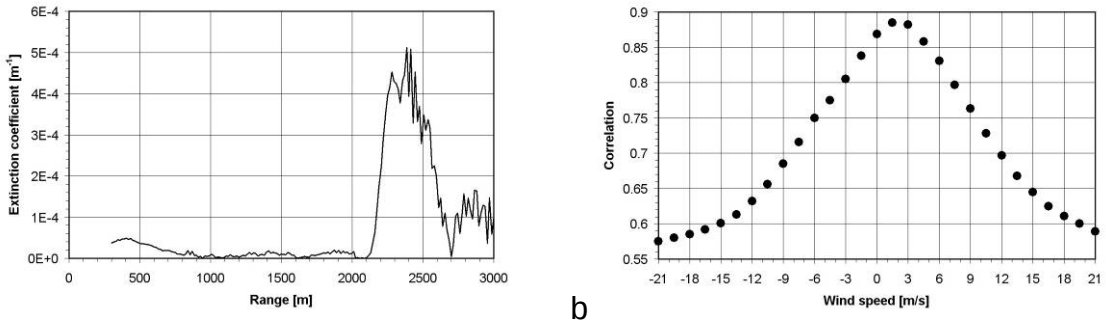

a b

Figure 3 - Extinction coefficient (a) and correlation versus wind speed (b) retrieved at 13:57 pm by ATLAS.

1.2.2 Environmental Analytical Chemistry lab (LCA)

Within the LCA lab research activities related to the environment characterization and protection, a specific attention has been dedicated in the last years to the PAH (polyciclic aromatic hydrocarbons) characterization in atmosphere. PAHs are mutagenic and carcinogenic organic pollutants emitted by incomplete combustion processes. The main sources of these pollutants in the atmosphere are vehicular traffic, industrial activities and waste incineration processes. Within this research topic the LCA lab participates to the MUSS (Mobilità Urbana Sostenibile e Sicura) Project-Industria 2015, coordinated by Piaggio Company and financed by MiSE (Italian Ministry of Economic Development). The project, started in April 2010, lasts 3 years and. The LCA lab objective is to characterize PAHs emitted by vehicular engines feed by biofuels, in particular bioethanol. During the first year of the project a report on the state-of-art of biofuel emissions has been produced. Determination of PAHs will be carried out during the third year of activities. The method that will be used for PAH analysis will be based on EPA TO 13A (USEPA 1999) method, adequately modified and developed in our lab. The 16 PAHs considered with high priority by the US Environmental Protection Agency (EPA) will be determined in our lab by gas chromatography coupled with mass spectrometry (GC-MS) (Figure 4)

Figure 4 - GC-MS systems sited in the LCA lab in Frascati.

1.2.3 Laser scanning flow cytometer CLASS

The experimental apparatus for the laser scanning flow cytometry (CLASS), extension of the more classical flow cytometers, has gone one step further from both the points of view of the instrumental apparatus and of the data analysis. The process intended to transform the CLASS, system able to acquire simultaneously 5 different signals and to provide information on size, refractive index, shape and fluorescence of single particles, in a miniaturized instrument has been carried on. To obtain a further reduction of the apparatus size, the whole optical and hydrodynamic subsystems have been replanned and modified (

Figure 5). Moreover the use of new micro pumps makes now the system independent from the laboratory utilities. This change represents an important step forward the possibility to employ, in the future, the CLASS for in situ measurements. More in general the whole system has been redesigned with the goal to have a transportable apparatus, i.e. small, light and less fragile than the laboratory prototype.

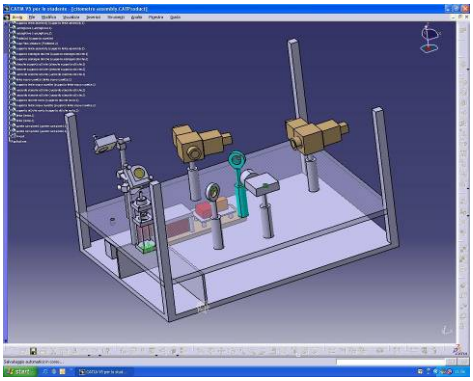

Figure 5 – Design of the new transportable CLASS apparatus.

As far as the data analysis is concerned the work has followed two different directions. So far for the data analysis a software based on a parametric resolution of the Inverse Light Scattering Problem (ILSP) was used. This is an evolution of the Flying Light Scattering Indicatrix method (FLSI), which in turn is based on the spectral decomposition of scattered light pattern detected.

Data sets on algae communities have been re-analyzed with such approach in using a new algorithm that better describes the scattering pattern behaviour for real particles. In this way size, fluorescence and refractive index values have been retrieved and the combination of such different parameters allowed us to distinguish cells with very small differences in both morphological characters and optical properties. In particular was possible to evaluate physiological conditions of different population algae grown in vitro.

However, some limitations connected to the data analysis software are still present when working with data from real particles that strongly deviate from ideality. Moreover, the very large amount of information collected during a LSFC experiment requires techniques of data mining to extract information and allow particle recognition. In this frame a series of tests have been performed using multivariate analysis and a Radial Basis Function Neural Network on purpose developed. In the first step, only patterns of forward light scattering between 6° and 80° have been considered. The analysis has been conducted both with measured data (Figure 6) and with data simulated from Mie scattering algorithm (Figure 7).

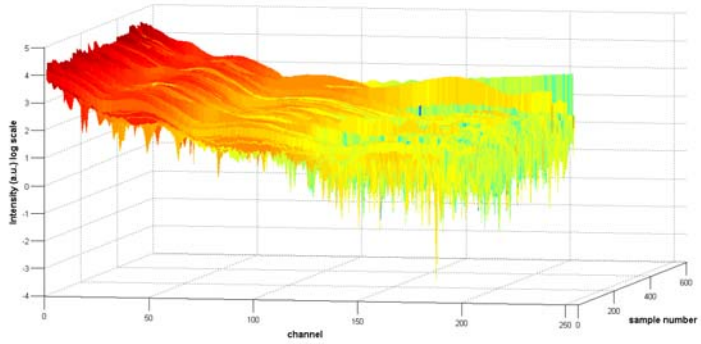

Figure 6 - Forward scattering pattern in the range 6°-80° of calibrated microspheres 2 micron sized.

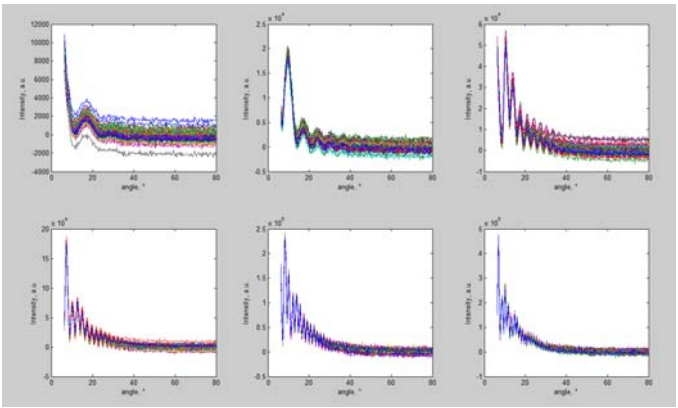

Figure 7 - Forward scattering pattern in the range 6°-80° simulated by the Mie theory for polystyrene microspheres with radius of 1, 2, 4, 6, 8, 10 micron (from the top left clockwise).

1.2.4 *Development of mathematical methods for artificial intelligence applied to diagnostics*

Neural network algorithms are powerful tools to solve complex mathematical tasks in low time frame as the on-line analysis of convoluted and/or multiple information. Work is in progress to implement techniques of Machine Learning able to classify different biological particles arising from the laser scanning cytometer data. The final goal is to upgrade the software in a real time analysis.

The present neural network expertize will be also employed in the frame of the TRAMP (Sistema Integrato di Gestione e Controllo per il TRAsporto in Sicurezza di Merci Pericolose) a MIUR PON project approved which is currently in the final stage of funding.

1.2.5 *Satellite oceanographic data analysis and merging laboratory*

The SST multi-decadal variability in the Atlantic-Mediterranean region and its relation to Atlantic Multidecadal Oscillation (AMO)

Climatic variability can be investigated using univariate or multivatiate time series analysis to describe, understand and eventually predict its variability. Our goal was to identify multidecadal oscillations in the global sea surface temperature (SST) time series focusing, in particular, on the North Atlantic and Mediterranean regions during the last two centuries. Input data are obtained from the ICOADS 2.5 dataset, ERSST.v3 and HadISST that cover the period from 1850 to today. Low frequency oscillations were identified using Singular Spectral Analysis (SSA), an useful technical tools to extract information from short and noisy time series providing some insight into the unknown dynamical system that generated the series. The first two eigenvalues form a pair which contribute about 40% of the total variance (Figure 8a and Figure 8b) are separated by a very steep slope from the noise, which is characterized by much lower values and a mild slope and are in quadrature (Figure 8c). The distance of these two modes above the noise indicates that they are deterministic rather than stochastic. These facts and the corresponding reconstruction of Figure 8d suggests that the nonlinear oscillation associated with this mode is robust, persisting and can have possible connection to an efficient representation of harmonic limit cycles.

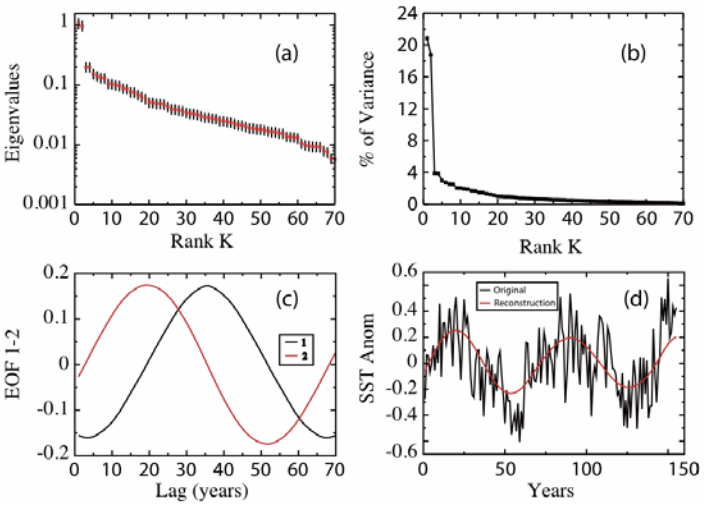

Figure 8 - a) SSA of SST time series, b) Percent of variance explained, c) First two EOFs)of the Mediterranean SST time series d) time evolution of the mean annual SST of the Mediterranean Sea from 1854 to 2008 (black line) and the reconstructed time series (red line) are shown, the latter is based on SSA with a 70-year window, which retains the first two modes

A diurnal cycle resolving sea surface temperature product for the tropical Atlantic

Recent findings indicate that resolving the SST diurnal cycle is important also for better simulation of climate related phenomena. We have suggested a possible way to fully exploit information contained in Meteosat Second Generation (MSG) satellite data to contribute to the diurnal variability research effort using the Tropical Atlantic as a test. We also used the Advanced Microwave Scanning Radiometer-EOS (AMSR-E) on board the Aqua platform launched in 2002 that measures SST and other geophysical parameters (e.g. wind speed, atmospheric water vapour) and Moderate Resolution Imaging Spectroradiometer (MODIS) aerosol products such as Aerosol optical thickness (AOT) and Angstrom exponent (AExp) at 0.55 μm and 0.55–0.85 μm, respectively. Validations were performed using data from the Pilot Research Moored Array in the Tropical Atlantic Mooring Array Temperatures (PIRATA) and the Coriolis SST dataset. The matchup SAF SSTs showed spatially and temporally varying bias (in situ minus satellite) relative to the PIRATA buoy SSTs, particularly at the more northerly stations (Figure 9). The average bias is < 0.5 K, but it can also reach several degrees at some location.

The analogous satellite-buoy comparison using AMSR, a MW-based polar-orbiting instrument, produces a small flat bias pattern. Thus, for our study, AMSR is chosen as a reference field to compute a night-time SAF adjustment. This adjustment needs to be performed daily due to the bias dependence on atmospheric factors that have short time scales.

To reconstruct the diurnal SST cycle in the Tropical Atlantic Ocean we used SEVIRI SST adjusted for mentioned bias using AMSR data and an optimal interpolation (OI) schema, originally developed for AVHRR in the Mediterranean Sea and then expanded for use with other sensors in the Tropical Atlantic.

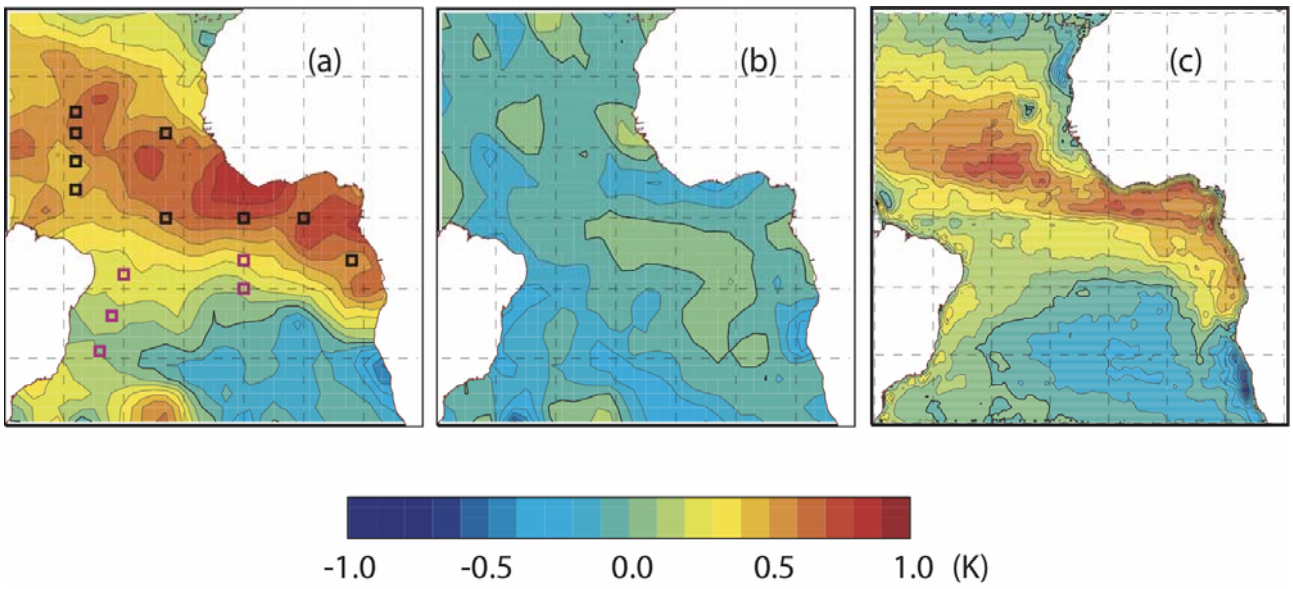

Figure 9 - ***Contoured SST bias: in situ (Coriolis) minus (a) SAF and (b) AMSR, averaged over the entire 2 year study period. (c) Contoured mean difference between nighttime AMSR and SAF (0400 UTC) SST over the same period. Rectangles show location of PIRATA buoys***

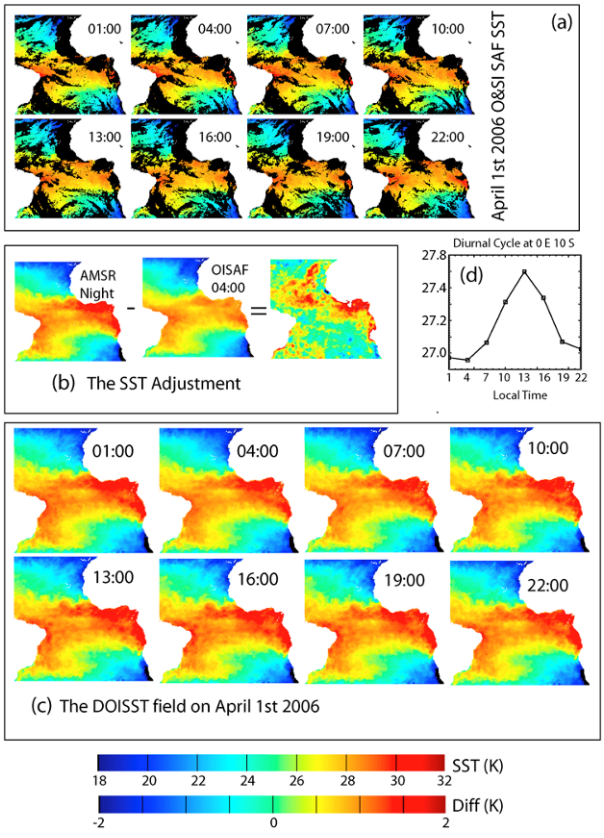

Figure 10 - ***Diurnal Optimally Interpolated SST (DOISST) processing. (a) Three-hourly uninterpolated SAF maps. (b) An adjustment field computed from interpolated night-time AMSR and SAF. (c) The adjusted and then interpolated 3-hourly SST fields. (d) Diurnal cycle at 0°E 10°S***

The possibility to extend the Tropical Atlantic DOISST to the Mediterranean Sea is actually under investigation. Starting from the OI schema proposed for the Tropical Atlantic we are developing a new approach based on a combined use of an operational Ocean General Circulation Model (OGCM) and optimal interpolation of SEVIRI data. In practice we interpolate anomalies respect to the modeled diurnal SST cycle avoiding the need to separately produce maps every three hours using only the data of the previous and following day take at the same time of the interpolation moment. This permits to reduce the searching window at ±1 day (instead of ±5 days used in the Tropical schema) improving the results of the interpolation.

1.2.6 The TYR01 oceanographic campaign

UTAPRAD-DIM Laboratory had participated, in collaboration with other Italian research institutions, to the TYR01 cruise (October 29th 2010 to November 22nd 2010), organized by the Istituto di Scienze dell'Atmosfera e del Clima (ISAC) on board of the R/V Urania of the Italian National Council of Research (CNR). The TYR-01 survey was devoted to the characterization of the bio-optical and hydrological properties of coastal and offshore waters in the Tyrrhenian Sea and to the study of the cross-shelf exchange dynamics, with particular focus on the advection/mixing mechanisms of river plumes offshore. The cruise rationale was the necessity to collect, to process and to analyze specific environmental data to be able to contribute to the understanding of the main mechanisms that drive the marine ecosystem functioning in the coastal areas of the central Tyrrhenian Sea. The data collected during TYR01 will help to get to a first evaluation of the natural and anthropogenic pressures and impacts on the ecosystem, focusing on terrigenous input (mostly from river discharge) and its effects on marine organisms (mainly phytoplankton) in autumn. The efficiency of the coastal dynamical processes in transporting and renewing the coastal waters has been investigated also by performing a Lagrangian In Situ Experiment (LISE).

The strategy adopted to achieve the cruise objectives included the acquisition of:

- hyperspectral radiation profile data

- marine biochemical and biological data through water sample collection and analysis, and specific experiments
- 292 standard hydrographical data (see figure 10)
- in situ LIDAR marine data

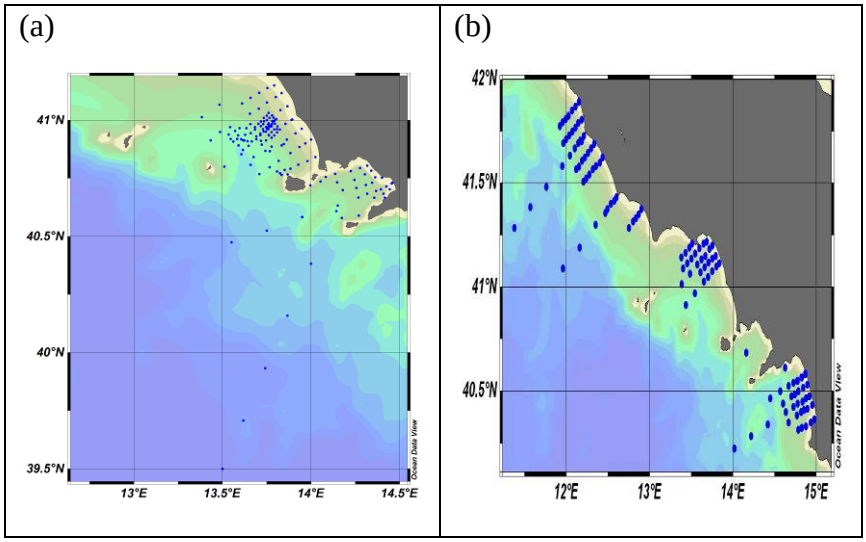

Figure 11 - Hydrographical stations during (a) leg I (10.29.2010 -11.09.2010) and (b) and leg II (11.10.2010 -11.22.2010)

During the cruises ENEA was involved in fluorosensor lidar measurements, acquisitions and filtering of water samples for subsequent laboratory analysis (Spectrophotometer, HPLC, and phytoplankton size classes determination by laser flow cytometry) and collaborated to the hydrographical activity.

Figure 12 - TYR01 campaign: filtration ramp for phytoplankton sampling inside the Urania vessel (left) and HPLC equipment for marine pigment analysis (right).

In particular, phytoplankton has been sampled on GF/F filters in coastal and oligotrophic areas at different depths (Figure 12). Filters have been stored in liquid nitrogen and then transferred in a -80°C freezer in the lab before analysis. The high performance liquid chromatography (HPLC) is the reference technique established by UNESCO for chlorophyll analysis and associated phytoplankton pigments. For this reason an HPLC method has been set up in our lab for chlorophyll-a and b analysis (Figure 12). The

method is a modified version of the protocol suggested by the Joint Global Ocean Flux Study (JGOFS) project and approved by UNESCO. During the TYR01 campaign samples for spectrophotometry and citometry analysis have also been collected. The analysis of the data acquired during the cruise is currently in progress and will likely be terminated during the next months.

1.3 Diagnostics for Security and Safety

1.3.1 Detection of drugs and precursors

UTAPRAD-DIM is a partner of the FP7 Security EC CUSTOM (Drugs And Precursors Sensing By Complementing Low Cost Multiple Techniques) project started in June 2010. CUSTOM has been conceived with the purpose to develop a portable device capable of detecting traces of drugs and chemical precursors used in the manufacture of the most dangerous drugs. To achieve this goal two technologies, based on spectroscopic measurements, were identified for their merits: namely fluorescence and photoacoustic spectrometry. Our task is the development of the Main Control Board (MCB) to operate the two instruments considering the main requirements:

- general: Electrical, Environmental and Physical Req.s;
- sensor: Operational Req.s;
- user: Human Interface Req.s;
- electronic: Control and Communication Req.s;

With special orientation to the selected sensor technologies used for drugs and precursors detection, we have outlined the general architecture of the CUSTOM analyzer with the purpose to elucidate the implications on the physical and electrical characteristics of the overall system, and to set the initial requirements for the board controlling the overall apparatus (Figure 13).

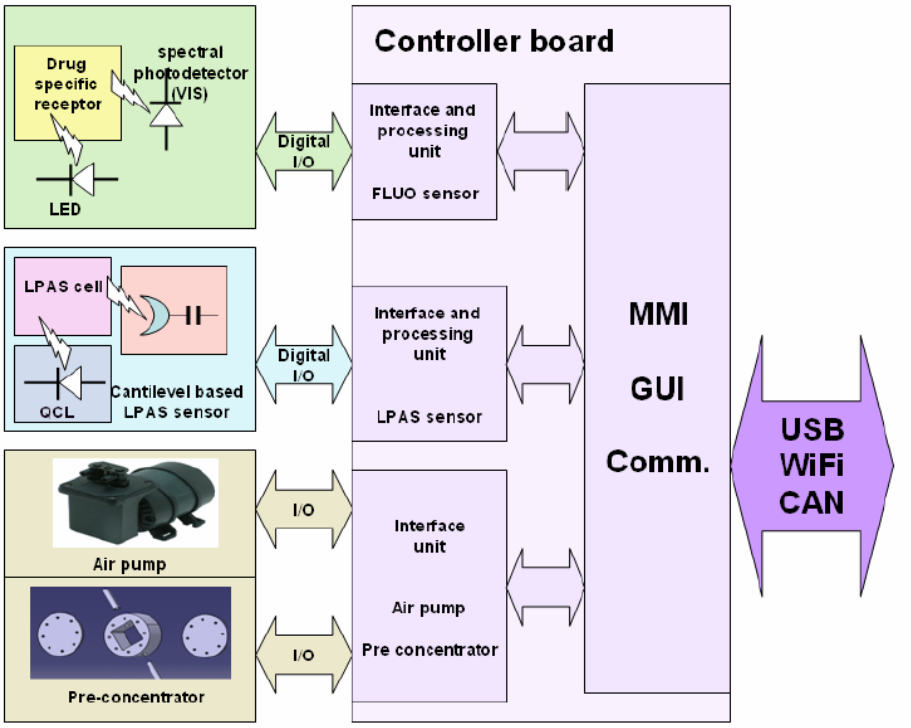

Figure 13 - Layout of the CUSTOM analyzer

The MCB must guarantee the sensors physical connection and functional operation under computer or manual control, therefore it dictates the definitions of the physical layer for communication

to which the sensors must conform. MCB has to have the capabilities of detecting (and eventually tolerating) the most common faults, i.e. misconnection, bus error, or single unit fault. The sensors must be supplied equipped with custom electronics driving specific functionality in predefined operational modes, so that an ordered sequence of tasks is negotiated with the MCB.

1.3.2 LIBS trace detection of energetic materials

One of the aims of the previous ISOTREX project (SEC6-PR-203600) was to realize a compact LIBS instrument for rapid detection of energetic materials at trace levels (<1 ng), in air surrounding. The experimental data, previously collected by the prototype LIBS system (IPAC) on not uniformly distributed organic residues, were further analyzed and this brought to some important conclusions and results:

- The detected plasma was not stochiometric and this is particularly evident from comparison between RDX and HMX, having the same atomic ratios in their molecular formula
- The emission intensity, temperature and electron density of the laser induced plasma strongly varies from one sampling point to another. This leads to changes in the laser induced fragmentation of the organic molecules and of the chemical reactions in the plasma.
- As a consequence of above, huge changes occur in the line intensities and their ratios (up to an order of magnitude) from one sampling point to another. Such drastic fluctuations exclude a possibility to obtain affordable LIBS identification of the organic residues by comparing directly the characteristic atomic line intensities, even when applying some chemometric tools.
- We observed an important anti-correlation between the line intensities belonging to atomic carbon and hydrogen from one side, and from oxygen and nitrogen on the other side. This anti-correlation is particularly severe for aromatic compounds at intermediate plasma intensities, where an increase of carbon emission corresponds to an increase of the plasma electron density.
- Once explained the sources of the LIBS signal behavior, it was possible to establish a data processing procedure, which leads to a very good linearization among the data sets (Figure 14). In this way, some real differences between the LIBS spectra from explosives and interferents were determined and correlated with their molecular formulas.
- We obtained correct classification of all the examined organic residues by applying some very simply algorithms, without using more complex, statistical methods (chemometrics). For some explosives, a correct classification was possible only in high temperature LIBS plasma, corresponding to a very small amount of an organic residue.
- A number of parameters extracted from the LIBS spectra, which distinguish the explosives from other organic materials, were also determined. It results that TNT is the easiest to classify by LIBS, differently from TATP and Nitroglycerine, for which we found only one parameter that clearly distinguishes them from the examined interferents.

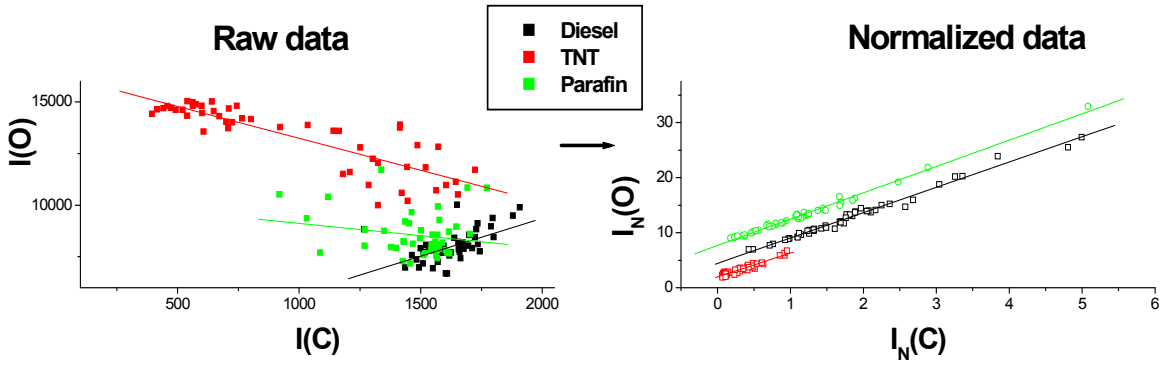

Figure 14 - Integrated line intensities from O and C before and after the data processing, for diesel, paraffin and TNT.

1.3.3 The Surface Enhanced Raman Spectroscopy: evaluation of substrate amplification factor on explosive compounds (*)

The Raman spectroscopy has the ability to distinguish between molecules with great similarity. However, due its intrinsic weakness, it can be used to trace level detection only if coupled to surface enhancement effect, where the Raman signal can be amplified by many orders of magnitude. This drastic enhancement, which occurs when the molecule is placed on, or is very close, to a metal nano-structure, is mostly related to a resonant coupling between the exciting laser light and the conduction electrons localised at the metallic surface. First SERS experiments demonstrated that several factors affect the signal enhancement, consequently extensive theoretical modeling is currently dedicated to study the field enhancement as function of nanoparticle aspect ratio and shape, interparticle spacing and dielectric environment. To use the SERS as analytical techniques it is necessary to develop surfaces or media which have and ordered and homogeneous nano-structure which guarantees the same amplification factor over the whole active zone. To this respect, accessible and reliable techniques are now disposable to tailor the surface enhancement levels and reproducibility required for the desired application. Our study was dedicated to evaluate the amplification factors of SERS substrates fabricated by vapor depositing a gold layer (100 nm) onto a silicon surface with a ordered nanostructure produced by microlitography (see Figure 15).

The limit of detection, also known as LOD or detection limit (DL), is the lowest amount of analyte that can be detected. The LOD can be calculated from the slope of a calibration curve having as ordinate the system response ad as abscissa the mass of analyte. As system response, in agreement with literature, we take the area of peak with highest intensity in the Raman spectra. Examples of calibration curves for RS and SERS are reported in Figure 16.

The LOD of RS performed with a compact plat form (Ocean Optics HR 3000) at an excitation wavelength of 785 nm, Φ=1J/cm^2/s, is 1µg, which corresponds to a density of 10 mg/cm^2 in the 100 µm diameter laser beam, whereas the limit of detection with surface enhancement effect is 5 pg (Figure 16), which corresponds to a surface density of 60

ng/cm^2. An enhancement factor of $2 \cdot 10^5$ of nano-scale textured substrate, to respect the conventional one, can be estimated by the ratio between the two detection limits.

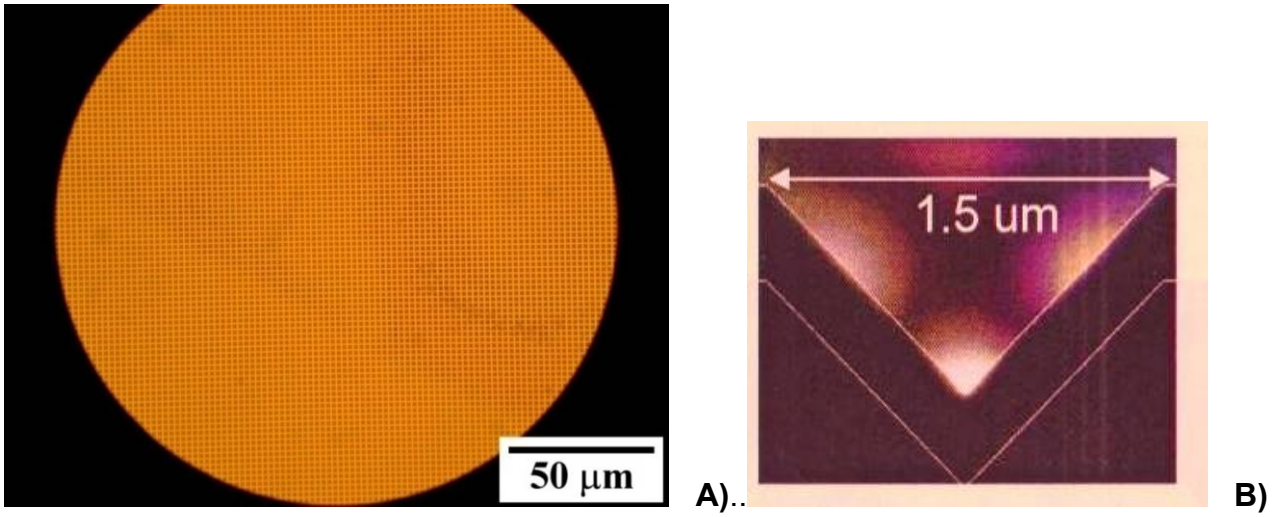

Figure 15 -*The SERS substrate structure: a) optical microscope; b) detail from the http://www.d3tech.net/*

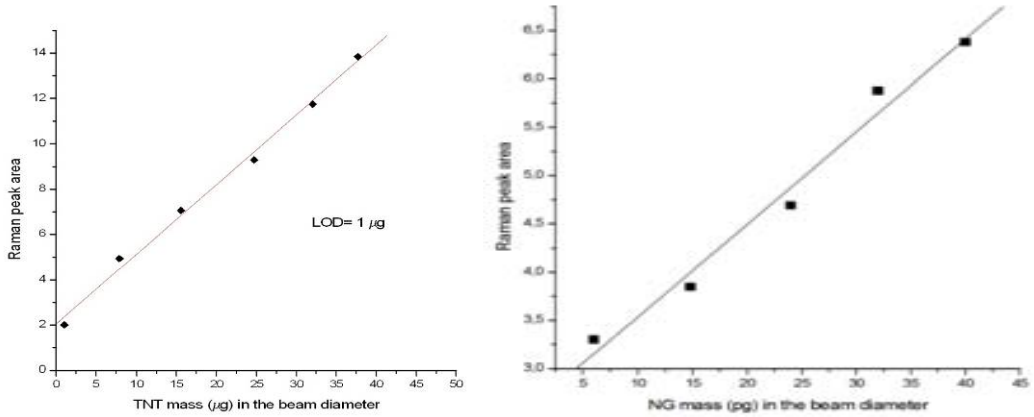

Figure 16 - On the left: calibration curve for trinitrotuoluene (TNT) without surface enhancement; on the right: calibration curve for nytroglicerin (NG) with surface enhancement.

(*) Activities relevant to Raman Spectroscopy are conducted in MNF Laboratory, they are here described in order to complete the innovative diagnostic description.

1.3.4 Agro-alimentary diagnostics to protect the "made in Italy" products

Security issues applied to environmental and agro food chain are deeply considered also at the UTAPRAD-DIM Biology laboratory, where spectral images captured by means PAM (Pulsed Amplitude Mudulated fluorescence) instrument had the goal to investigate the phytoremediation effect of *Zn on poplar plant* and the health risk of different salad products (ready to eat). The PAM technique allows to estimate, rapidly and non-invasively, the photochemical parameters and related images: the quantum efficiency of PSII (Fv/Fm),

electron transport (ETR), photochemical (qP) and non-photochemical quenching (NPQ) related to CO_2 assimilation.
Several processes as well as industrial and agricultural in the last years have increased the flow of heavy metals, as well as Zn, that can be transported to the plants. The physiological levels of Zn in leaves is 15-50 mg kg^{-1} dry weight and an accumulation of high concentrations may interfere the metabolism of Fe and to induce chlorosis.
In order to detect changes, induced by Zn on photochemical metabolism and then to characterize the response of plants, leaves of Populus x euramericana clone I-214 were examined at different time of treatment. The plants were grown in the presence of two concentrations of Zn 500 and 1000ppm. The fluorescence images of the main parameters as well as Fv/Fm, ETR, qP and NPQ were carried out by PAM images. At T2 the ETR decreased significantly by 9.0% at 500 ppm and 14.1% in 1000 ppm compared to T1. Even if among the treated plants were not observed significant differences the significant interaction T x Zn, (F = 5.72 **) confirmed the effect on the electron transport chain by the presence of heavy metals.

Comparison between treated and untreated poplar leaves at different Zn content are presented in Figure 17. The NPQ parameter point up the activity in the light of the antenna pigments involved in the non photochemical quenching, the result highlight the ability to dissipate light energy in the plant control that appears more heterogeneous than leaves of the plant treated with 500 to 1000 ppm of Zn. The photochemical response of the poplar plants by means PAM imaging, known as a plants model for the study of mechanisms of accumulation of heavy metals, shows the possible protective role of the photosynthetic pigments and allowed to assume their active involvement in mechanisms of tolerance in response to the presence of toxic levels of the Zn.

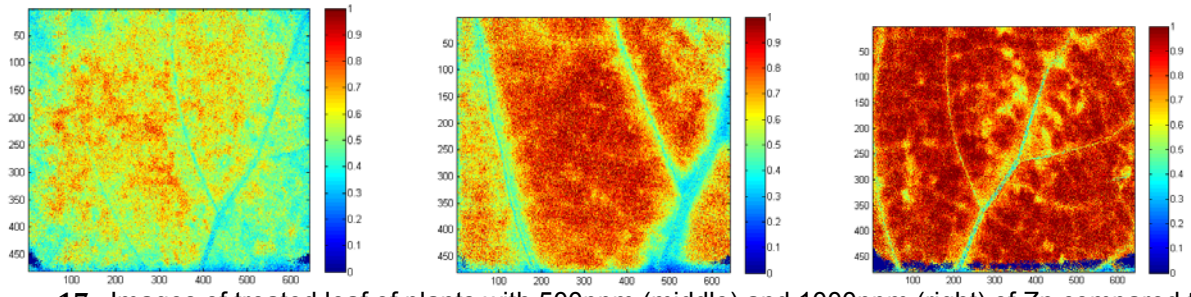

Figure 17 - Images of treated leaf of plants with 500ppm (middle) and 1000ppm (right) of Zn compared to not treated plant (Left) (PAR 600 µmol m^{-2} s^{-1}). The elaborated images are in false color between 0 (blue) minimum and 1 (red) maximum fluorescence .

Also in salad products of IV gamma (ready to eat), the PAM imaging fluorescence has been applied to the analysis of rucola leaf salad at different days after packing, for the security of food and to protect “made in Italy” (SAL@CQO Project). All photochemical parameters collected are reported in Figure 18. A spatial heterogeneity of each leaf, due to the physiological variability related of each environmental conditions, is clearly evident. Five hours after packing the Y(II) of samples showed an increase probably due to accumulation of CO_2 that reached photosynthesis metabolism. Fv/Fm, accepted as sensitive indicator of membrane damaging processes, in this case it appears to be less reliable as an indicator of senescence. Although senescing tissue deteriorates relatively slowly, it tends to maintain its photosynthetic capacity until near the end of its storage life.

The adulteration of the olive oil with lower-priced oils is a serious problem in the olive oil market and a fast on-site screening method is needed to be developed. In the past years

the suitability of spectroscopic techniques to discriminate between chemical similar oils was demonstrated, encouraging the development of these techniques to study the adulteration of olive oils with polyunsaturated vegetable soils. At the beginning, the use of Raman spectroscopy was limited due to the fluorescence of samples, but the relatively recent instrumental advances have made possible the accurate collection of Raman spectra by dispersive–based Raman spectrometer. Within preparatory activities of SAL@CQO Project, we investigated as the Raman and IR spectra of extra virgin olive oils are affected by the mixing with a chemically very similar adulterant as the sunflower oil. The investigated concentration range is between 0 and 50%. Due to its noninvasive and non-destructive detection, high throughput, real time, no consumable chemical disposals and portable instrument, the sensor based on spectroscopic techniques has potential to be employed for on-site rapid discrimination of the virgin olive oil adulteration with vegetable oils containing percentages of unsaturated fatty acids.

The extra virgin olive and sunflower oil samples that we tested are of different Italian brands and were purchased as commercial products in supermarkets. We tested also three samples of extra-virgin olive oil traditionally produced by cold press. All the samples were stored at room temperature until the time of analysis. To study the adulteration, we prepared binary mixtures of extra-virgin olive and sunflower oil. The percentage of sunflower oil varied from 0% to 50% (v/v). As adulterant, we used sunflower oil, because, among all vegetable oils, its spectroscopic characteristics are the closest to the olive oil, moreover, due its quasi transparent color, it is the most widely used for olive oil fraud.

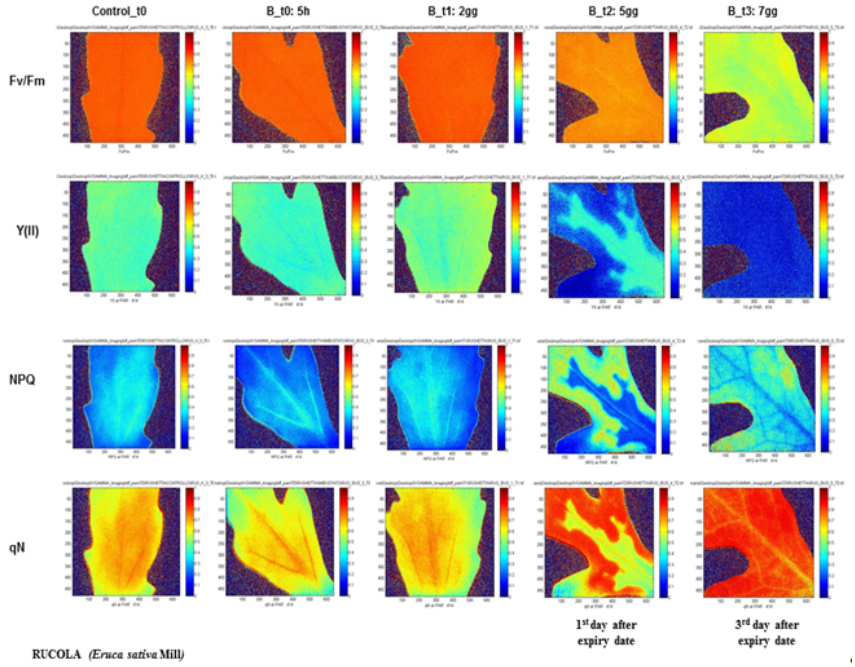

Figure 18 - Photochemicals parameter of different leaflets of rucola ready to eat

The Raman spectra were acquired with an integrated Raman system (Ocean Optics HR-3000) with a 500 mW solid state laser operating at 785 nm as excitation light source.

The main feature of unsaturated fatty acids is their content of double bonds, to this respect Raman scattering is of great value because non polar groups as C=C give intense Raman scattered bands. Although the near-IR excitation eliminates most of sources of sample fluorescence, in the Raman signal of each oil sample the contribution of fluorescence is still present. The fluorescence signal was approximated with a polynomial which was subtracted to the raw data resulting in a flat baseline spectrum. All the spectra were normalised to the highest peak which for olive and vegetable oils is at 1440 cm^{-1}.

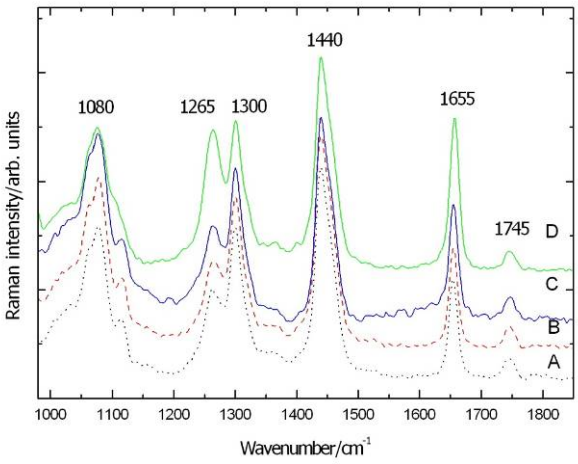

Figure 19 - Raman spectra of pure extra-virgin olive oils: sample A and B traditionally produced in a farm, sample C commercial brand; sunflower oil: sample D commercial brand.

Figure 19 shows the normalised Raman spectra of olive and sunflower oil. Each spectrum is the average of four scans, data smoothing was not necessary. The observed bands and their corresponding vibration modes are mainly due to vibrations of chemical bonds of triglycerides: 1080 cm^{-1} (C-C stretching in the –(CH2)n– group), 1265 cm^{-1} (=C-H bending in cis RHC=CHR group), 1300 cm^{-1} (C-H twisting in –CH2 group), 1440 cm^{-1} (C-H scissoring in –CH2 group), 1655 cm^{-1} (C=C stretching in cis RHC=CHR group) and 1745 cm^{-1} (C=O stretching in RC=OOR group). At a first look, the Raman spectra are similar as expected due to the chemical similarity of sunflower and olive oil. For this reason, as already discussed, we selected sunflower oil as adulterant of olive oil. However, the Raman bands at 1265 cm^{-1} and 1655 cm^{-1} due to cis =C-H and cis -C=C vibrations, respectively, have weaker intensities in olive oils to respect to sunflower oils. Olive oil mainly consists of monounsaturated oleic acid (i.e. with only one C=C double bond), whereas the other vegetable oils show a high content of linoleic acid, which has the same chain length of oleic acid, but contains one more C=C double bond. Consequently, the Raman intensity of the vibration at 1265 cm^{-1} and 1655 cm^{-1}, which are correlated with the double carbon bonds, increase as the degree of unsaturation (i.e the number of C=C bonds) decreases. This finding can be used to discriminate between olive and the other edible oils.

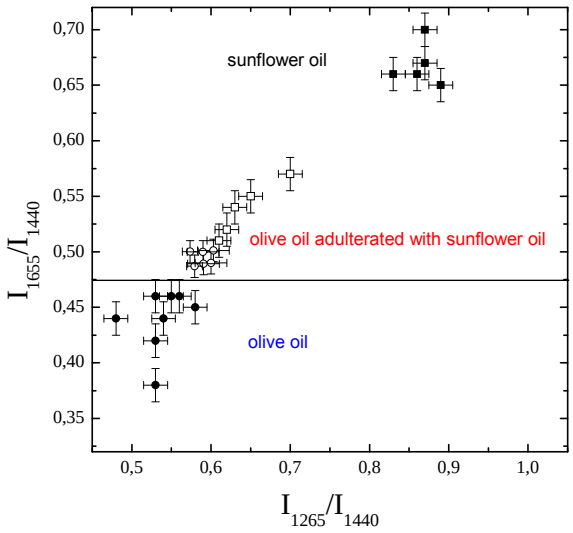

Figure 20 - Distribution chart of extra-virgin olive oil (solid circle), sunflower oil (solid square) and olive oil blended with sunflower oil in different volume percentages: 1%, 2%, 4%, 5%, 5%, 7%, 9% (open square), 10%, 15%, 20%, 25%, 30%, 40%, 50% (open diamond).

Figure 20 shows a distribution chart of olive and sunflower oil where, as horizontal coordinated was used the ratio I1265 to I1300, and as vertical coordinate the ratio of I1655 to I1440. In this way, each Raman measurement is represented by a dot with a unique x, y coordinate. The olive oil can be easily distinguished from sunflower oil by the different distribution region in this chart. The olive oil sample mixed with sunflower oil are

represented by dots with horizontal and vertical coordinates which increase with the content of unsaturated fatty acid in the mixture, moving toward the top of the right side of the chart. Samples with sunflower content smaller than 4% are represented by dots near the edge of olive oil region, however they are separated from olive oil dots, even taking into account the uncertainty.

The IR spectra of Extra Virgin Olive Oil (EVOO) and of SunFlower Oil (SFO), obtained through the FTIR apparatus, are shown in Figure 21. All of them are characterized by the same well evident peaks at 2800-3100 cm^{-1}, at 1700-1800 cm^{-1} and at 900-1400 cm^{-1}. The similarity of the spectra reflects the similarity in the chemical composition of the oils. Nevertheless minor differences appear at a more detailed analysis in term of small band shifts and of small changes in the relative intensity. The quantification of these minor differences served as basis for the oils classification. The spectral structure of the edible oils is mainly due to lipid molecules containing fatty acids. This determines the presence of characteristic absorption bands in the mid infrared region of electromagnetic spectrum. The specific frequency of a given vibration mode depends on the specific arrangement of the carbonyl groups and of the lipid hydrocarbon backbone, while the intensity of the specific vibration mode depends on the relative concentration of the related functional group. Because the fatty acids composition of a given edible oil is closely related to the vegetable variety from which the oil is obtained, this allows the spectral characterization of the oil's vegetable variety.

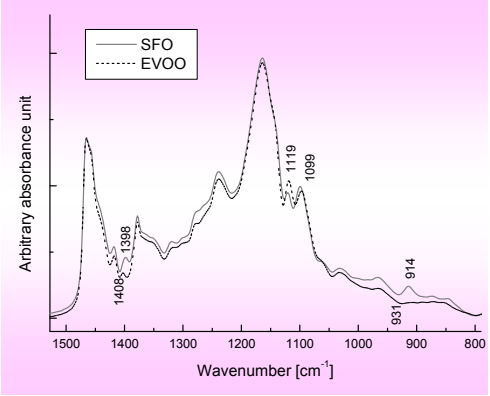

Figure 21 - FTIR spectra of EVOO (dashed line) and SFO (solid line) in the 800-1500 cm^{-1} spectral range.

At a closer inspection of the infrared spectra, some differences between oils located around 900, 1100 and 1400 cm^{-1} become clear. From the literature it can be inferred that: the band at 1400 cm^{-1} is due to the bending vibration of the =C-H group; the bands occurring in the region between 1300 and 1000 cm^{-1} are due to stretching vibrations of the C-O bonds present in triglycerides molecule; the band at 914 cm^{-1} are related to the bending vibration of -HC=CH- groups.

As in case of Raman spectra, the method of intensity ratio was adopted to classify the IR spectra. To quantify the discrepancy, the signal recorded at the modified wavelengths was compared to the signal recorded at a nearby non modified one. Each spectrum was evaluated on the base of the following ratios between signal values: I1099/I1119 and I914/I931. The ratios of I1099 to I1119 and of I914 to I931 were graphed for a given EVOO versus the adulterant sunflower content in the oil blend. The spectral parameter I1099/I1119 resulted to be linearly correlated to the percentage content of adulterant oil in all the examined binary blends. The same happened for the I914/I931 ratio. The obtained results were applied in realizing a distribution chart in which each dot corresponds to a couple of the spectral parameters. In the distribution chart shown in the in Figure 22 the value of the I1099/I1119 ratio was reported on the y-axis, while the value of the I914/I931 ratio was reported on the x-axis.

Each oil blend is represented by a dot. Each dot represents the average of 3 samples. From these data it is well evident that the adopted spectral parameters are dependent on the sunflower oil content in the oil blend. The EVOO and the SFO are located in well separated regions of the distribution chart, and the binary mixtures of the two oils occupy intermediate positions depending on the percentage content of the adulterant oil in the EVOO. Samples with smaller SFO content are represented by dots located nearby the pure EVOO location. The distance from the pure EVOO increases with the SFO content. In particular the EVOO is identified by x coordinate lower than 1.01; SFO is identified by x coordinate higher than 1.24; finally the oil blends with 2-30% SFO show x coordinates falling in the 1.02-1.09 interval, the value increasing with the SFO percentage content. This allows the discrimination between EVOO and SFO, and to give an estimation of the EVOO adulteration with SFO.

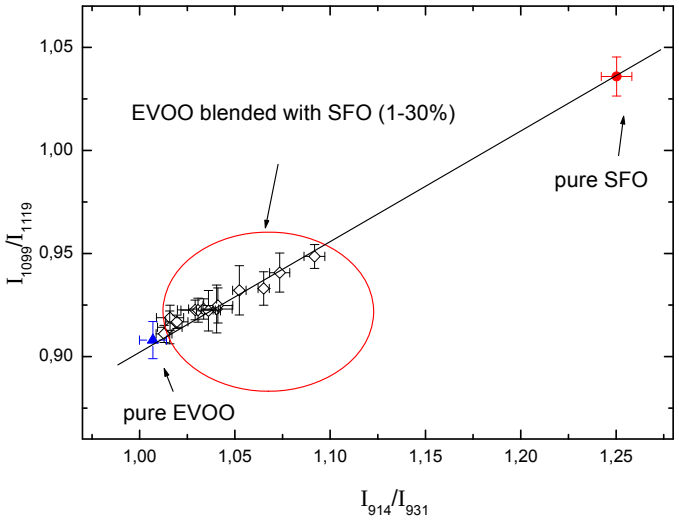

Figure 22 - IR distribution chart of extra-virgin olive oil (solid triangle), sunflower oil (solid circle) and olive oil blended with sunflower oil in different volume percentages: 1%, 2%, 3%, 4%, 5%, 6%, 7%, 8%, 9%, 10%, 15%, 20%, 25%, 30% (open diamond).

1.3.5 Extremely Low Frequency (ELF) weak electromagnetic fields as diagnostic tool for livings

The hypothesis of the existence of an effect of weak magnetic fields on livings has been supported by an extensive literature, there are many controversial findings even though a considerable number of peer-reviewed publications show that electromagnetic fields can result in physiologically effects in vivo and in vitro. The influence of weak magnetic fields on Glutamic acid solutions in water have been studied through FTIR-ATR spectra (

Figure **23**). After the exposure to the magnetic field (Figure 24), the solutions at pH lower than the isoelectric point show a shift toward the de-protonation of the carboxylic group and at the highest values of pH the same effect is observed on the amine group. Summarizing the results, published by Bioelectromagnetics, we have observed that the effect of the field is to weaken the OH bond and increase the population of de-protonated species at every value of pH. The effect is reversible within 1 hour after the exposure.

The most striking characteristic of this effect is the evidence of the existence of a long living state induced by the perturbation, i.e. the effect induced survive to the removal of the perturbation for very long times compared to the characteristic relaxation times of the molecular excited states. Because of the paramount importance of the Glutamic acid in the vertebrate physiology, the present study can stimulate an applicative research on therapeutic techniques. In fact, Glutamic acid, plays a fundamental role in the plasticity of the neural synapses linked to cognitive functions and it is responsible for cerebral damages in case of its anomalous storage outside the cellular barrier.

Further studies on the effect of ELF (Extremely Low Frequency) fields on solutions include a detailed knowledge about the water structure. In order to have a clear picture of the solute-solvent dynamics we have studied the IR structure of a mixture H_2O-D_2O. It can be shown that water can be described as a complex of two separate populations with respect to the dynamics of solubility and that the interface between the two populations behaves as the real active site of the chemical reactions.

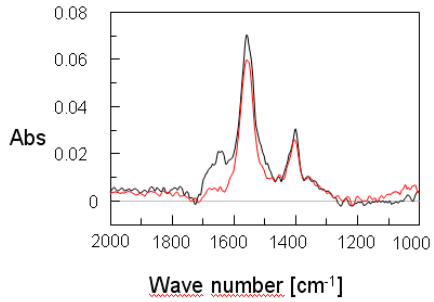

Figure 23 - IR spectra of glutamic acid at pH=11.86; comparison among unperturbed (black line) and exposed 20 min (red line) to the magnetic field.

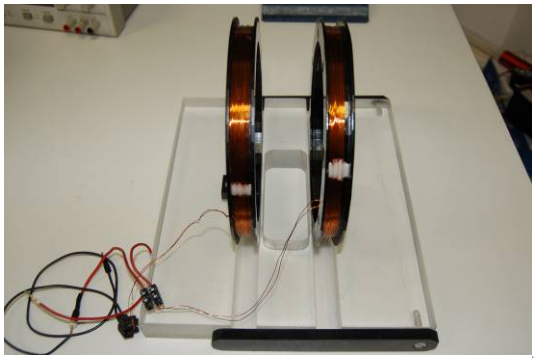

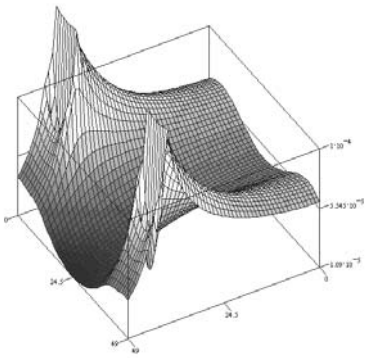

Figure 24 - Left Helmoltz coils used to produce the magnetic field. Samples were placed in the space between the coils; Right magnetic field inside the coils: the simulation was carried out using a finite element code in a 50X50 mesh and shows the magnetic field strength B in the half space that was symmetrical with respect to the axis of the coils.

1.4 Diagnostics for Cultural Heritage preservation and fruition

1.4.1 RGB-ITR – the form and the color

After over a decade spent in developing monochromatic 3D laser imagers, in recent years the ENEA Artificial Vision laboratory realized and patented the RGB-ITR (Red Green Blue Imaging Topological Radar), the first amplitude-modulated (AM) 3D scanner in the world that can natively acquire color information.

The RGB-ITR incorporates three AM laser sources at optical wavelengths of 450 nm (blue), 532 nm (green) and 650 nm (red) respectively, combined into a single “white” ray by means of a dichroic optical component. The beam is swept onto the target by a passive optical head, including lenses and a motorized mirror, and the collected backscattered light is then split again into the three original components. Each component is separately detected and analyzed by means of a lock-in amplifier unit, also used to modulate the correspondent launch beam component. Typical modulation frequencies are 190 MHz for red, 1-10 MHz for blue and 25 kHz for green.

Color information, converted in standard RGB format, is subject to a calibration procedure carried out by using certified diffusive targets. Specifically developed, copyrighted software applications are eventually used to process range and calibrated RGB data, yielding highly realistic 3D digital models, which can possibly be further post-processed and exported into the most common 3D file formats.

In 2009 the RGB-ITR was utilized in a 3D digitization campaign, carried out in the Oratorio di San Pietro Martire (Rieti, Italy), a 15th century oratory currently hosted in a military complex entitled to “Attilio Verdirosi”. The campaign was aimed at realizing an accurate color 3D model of the interiors of the oratory, to be used for monitoring and cataloguing purposes (Figure 25). The frescoes, painted in 1552 by the Veronese artists Lorenzo and Bartolomeo Torresani, represent the Last Judgment, and are often referred to as the “small Sistine Chapel”. They almost completely cover the walls and vault of the 10x6x8h meters oratory. Their 3D digitization by means of the RGB-ITR required 3 days, for a total of 4 scans and almost 13 GB data collected in 72 recording hours. During this campaign a new high-speed ADC was utilized, which enabled the recording of data at the rate of 3000 sample points per second, to be compared with the previous rate of 128 points/s.

During 2010 the processing of the enormous amount of data recorded in Rieti required the implementation of brand new software programs, specifically designed to handle the huge high-resolution, color 3D datasets produced by the RGB-ITR. A novel color calibration algorithm was also devised and is currently under advanced implementation. Some color calibration preliminary results are shown in Figure 26.

Figure 25 - 3D color model of Lorenzo and Bartolomeo Torresani’s Last Judgment (Oratorio di San Pietro Martire, Rieti, Italy).

Figure 26 - Preliminary results obtained by applying a new color calibration algorithm – currently under development - to the raw color data acquired by the RGB-ITR. The upper and lower parts of the figure show original and calibrated data respectively.

1.4.2 Laser Scanner for 3D digitalization of targets in underwater environment

Three-dimensional (3D) digitalization of submersed targets by means of 3D laser imagers is of interest to several areas, ranging from subsea archaeology to offshore oil and gas industry. The computer-aided inspection of 3D models of submersed objects obtained by high-resolution laser scanning may help identify faults in submersed industrial infrastructures, or enable marine archaeologists to spot fine details on shipwrecks.

Whatever the application, the added value of underwater 3D laser monitoring can hardly be underestimated, also considering the recent costly disasters that seriously endangered the safety of workers and the environment.

Several laser systems for underwater 3D imaging, operating on different techniques, are presently under study in various laboratories all over the world. Within the BLUARCHEOSYS project, the ENEA Artificial Vision laboratory is giving its contribution to the efforts spent worldwide in order to take these devices out of laboratories to the real world. In the last quarter of 2010 ENEA has completed the development of RE-VUE (REmote Viewing in Underwater Environment – formerly named UW-ITR), a 3D imaging system based on an amplitude-modulated laser at the wavelength of 405nm. At relatively turbid water conditions (total attenuation coefficient $0.3m^{-1}$) the device can provide high-resolution (~1mm) 3D models up to a distance of 9 meters from the target. The system's horizontal and vertical angular field of view is of 40° and several tenths of degree respectively. RE-VUE (Figure 27) is fully remotely operated by means of custom software, and is qualified to operate at a maximum depth of 200m.

RE-VUE is the result of five years of both experimental and theoretical investigations carried out by the laboratory staff. In particular, several experiments have been performed in order to identify efficient techniques for rejecting the disturbance signal due to light scattered off the water column between the sensor and the target. Investigated experimental techniques include modulation/demodulation, direct cancellation and polarimetry. Theoretical investigations have been focused on the definition and analytic resolution of a full-fledged radiative transfer problem mimicking the operation of the RE-VUE system in realistic conditions. The laboratory boasts several national and international collaborations and is steadily committed to widen the areas of application of this technology.

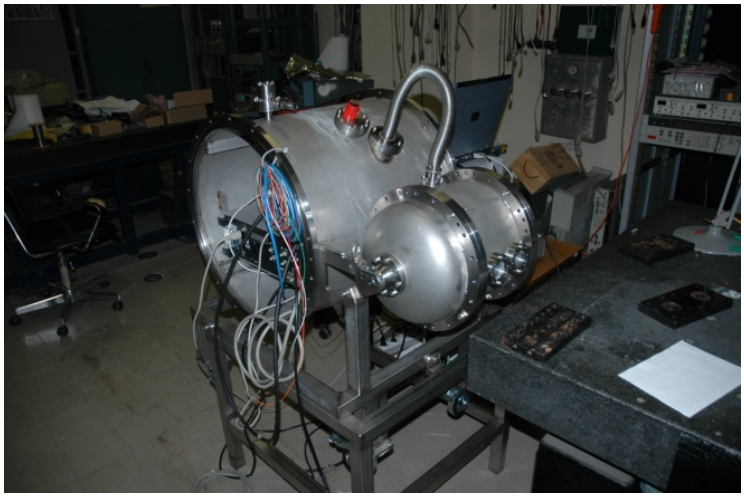

Figure 27 - RE-VUE during the operations of maintenance in the laboratory. The small cylinder hosts the laser, the scanning system and the receiving optics. The big cylinder contains the electronic modules

1.4.3 LIBS for undersea archaeological sites

Project AQUALAS, in which ENEA participates together with University of Malaga (UMA), has the aim to develop a LIBS system for in-situ characterization of the archaeological materials on sunken ancient ships close to Andalucia coast.

A commercial LIBS system was properly modified and tested for this application. The system contains a nanosecond-pulse Nd:YAG laser operated at 1064 nm with energy of 30 mJ, a chord 50 meters long with a fiber and air flushing (5 bar pressure), a compact spectrometer, optical components, and controlling electronics with PC. The computer screen for the divers is also included. The power is supplied through a standard electrical generator. The system was tested during summer in Malaga bay, up to depth of 30 meters, and on different kind of samples of archaeological interest. It was possible to measure both major and minor sample constituents also at the maximum depth. By increasing the underwater depth, a penetration of water into the plasma was observed, which lowers the optical signal. Further work regards the laboratory tests on an extended set of samples, and final measuring campaigns inside the underwater archaeological sites.

Within the collaboration contract with University of Malaga, Department of Analytical Chemistry, an experiment was performed (in Malaga), regarding LIBS analysis in presence of liquid coverage. The role of this coverage was to increase the material ablation rate before sending the second, analytical laser pulse. This application is particularly important for rapid measurements on moving samples, as for example, during depth profiling on-line in steel industry (galvanized steel), where laser pulses are not sufficient to remove a thick coating at the fixed point.

To this aim, laboratory measurements were performed on different metals in dry conditions, in presence of water droplets with volume from 1 to 20 μL, and in presence of water aerosol (average droplet diameter is 1-4 μm). The laser pulse energies were moderate, 80 mJ maximum for the first pulse and 40 mJ for the second one.

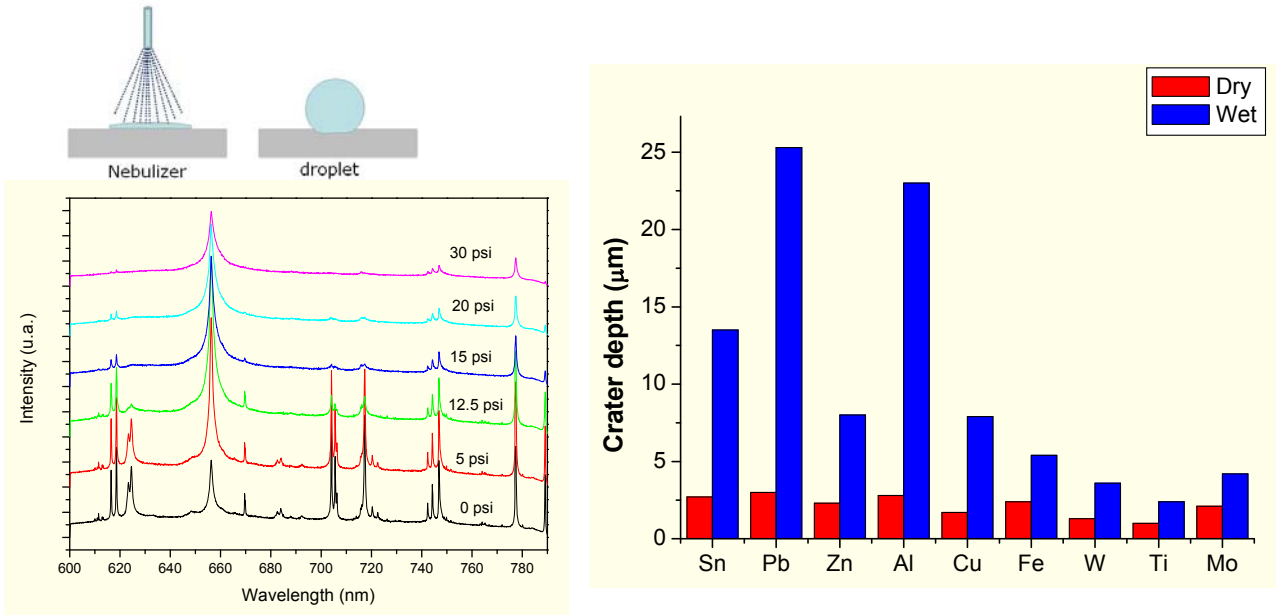

Figure 28 - Surface coverage with water, LIBS spectra at different aerosol flow rates, and enhancement of the laser ablation rate in presence of droplets of 15 μL

Already 1 μL of water on the surface increases the ablation rate more than 10 times on the aluminum sample. This effect can be explained by a strong mechanical effect of the hot vapor and the corresponding shock waves, which remove the molten material. Increase in the ablation rate, together with improved RSD (Relative Standard Deviation) of the crater

depth, was observed on different metals (Figure 28). LIBS signal after the second laser pulse (interpulse delay in order of 10 μs) is lower than on the dry surface, but still sufficient for the analysis of deep material layers. With the aerosol coverage, the enhancement of the ablation is less pronounced (2-3 times on the aluminum), but the LIBS signal after the second laser pulse is comparable to the case of dry sample.

1.4.4 LIF analysis of biofilms from Roman catacombs and marbles

The formation of biofilms from microorganisms under favourable conditions of humidity and temperature is well known and their detection and identification are very important to prevent the deterioration processes of monuments. Some biofilm samples from Roman catacombs have been analyzed by Laser Induced Fluorescence (LIF) technique, while Principal Component Analysis (PCA) has been applied to identify the origin of the different contributions to the resulting emission spectra and to discriminate among the developed microbial communities.

The studied biofilms were collected in Roman catacombs sited along the ancient via Appia, where the relative humidity is higher than 90%, the temperature is constant in the range 15.6–18 °C. The samples were maintained in wet and completely dark conditions in order to reproduce hypogea environment and, thus, to preserve their features. Also the temperature was controlled at appropriate values. LIF spectra of the biofilms have been measured with our scanning hyperspectral lidar fluorosensor.

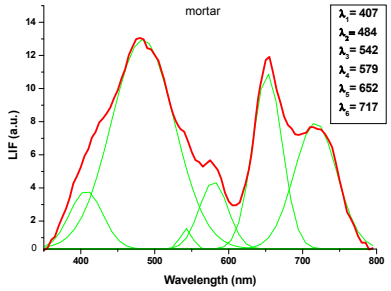

Figure 29 - LIF spectra of biofilms on mortar and respective band deconvolution.

LIF spectra depend on the particular area under study and appear, as can be observed in Figure 29, as the superposition of several contributions, due to the presence of complex microbial colonies in the same sample. Each resulting component, resulting from the deconvolution of the spectra, can be ascribed to the pigments characterizing the present microorganisms. Distinct biofilms sampled on mortar present very different emission bands. Differences on these spectra may depend on the stage (age and morphology) of the biofilms evolution. On the contrary, biofilms on tufa show very similar spectra suggesting that on this kind of substrate colony structure are more homogenous. As can be observed in Figure 30, PCA is able to distinguish among samples characterized by very similar spectra.

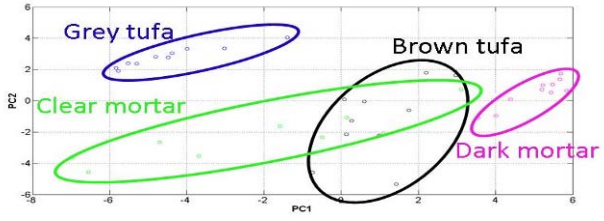

Figure 30 - Projection of the fluorescence spectra on the first (PC1) and second component (PC2).

1.4.5 LIF scanning field Campaign at the Padua Baptistery

The LIF scanning system developed at the UTAPRAD-DIM (patented in 2010 in its latter version) is capable to collect hyperspectral fluorescence images scanning large areas for applications to cultural heritage surfaces (e.g. frescos, decorated facades etc.). A new compact set up has been built aimed to increase the performances in terms of space resolution, time resolved capabilities and data acquisition speed. Major achievements have been reached by a critical review of the optical design and consequently of the detector utilized.

This arrangement is characterized by having the spatial and spectral information on two mutually orthogonal directions imaged on the detector, with submillimetric spatial resolution and a spectral resolution better than 2nm. Additionally it is possible to implement time resolved measurements on the ns scale by gating the spectral detector.

The overall current system performances are horizontal resolution 640 pixel, 0.1 mrad angular resolution, minimum acquisition time per line 200ms, field of view (FOV) aperture 5.7° (corresponding to a scanned line of 2.5m at 25m distance). With the latter optics an image of 1.5×5m^2 is scanned in less than 2 minute at 25 m. The compact arrangement of the experimental apparatus is shown in Figure 31a.

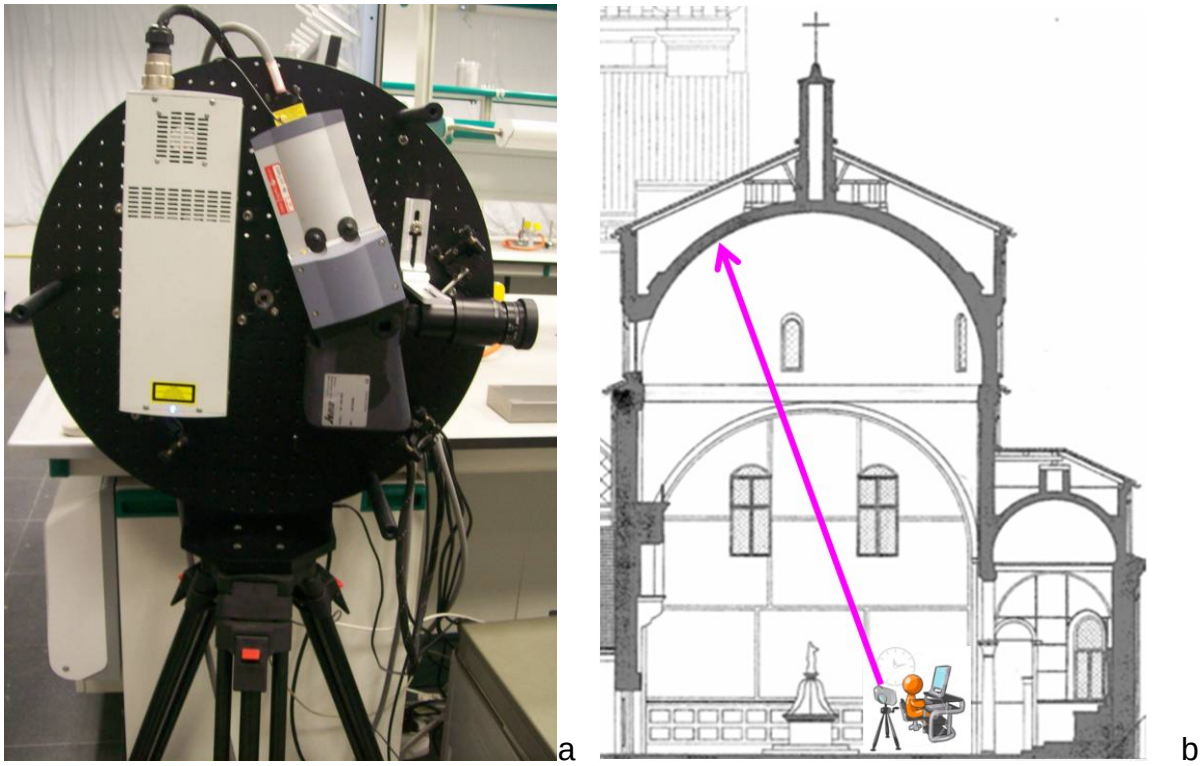

a b

Figure 31 – A) Compact LIF line scanning, the vertical optical bench is mounted on a tripod, vertical scanning is performed by mean of an accurate stepping motor on the back side. Transmitting and receiving optics are in the front, the CCD and the laser on the rear; B) the experimental set up inside the Padua Baptistery during the measurement campaign.

The performances of the LIF scanner are designed to fully exploit the information contained in spectral signature characteristic for each chemical compound laying on the

examined surface. The detection of the emitted fluorescence radiation allows to identify different materials utilized, mostly desired in view of a planned restoration. Indeed this system reveals with high spatial resolution the occurrence of retouches, traces of former restorations and consolidants not otherwise reported in the documentation relevant to the artwork. The system has also the chance to identify extraneous materials onto the surface (degraded substances, pollutant, waxes, and some kinds of biological attack such as microalgae and fungi).

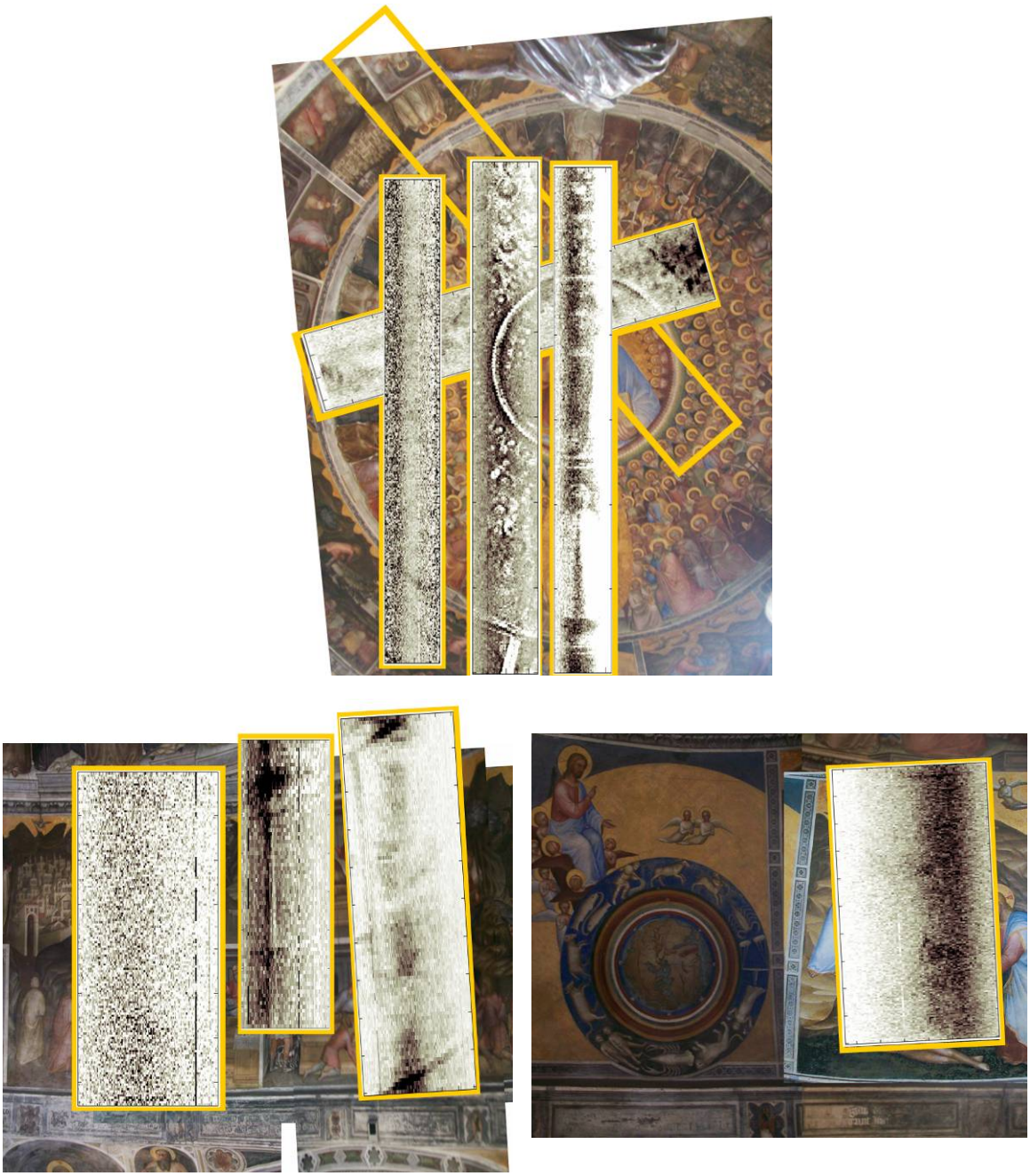

Figure 32 - Composite of conventional photographs and images relative to the spectral amplitude at 293nm, corresponding to MOVILITH/PRIMAL AC33. The top composite is from the dome, the bottom images are from the tambour. The grey scale corresponds to the concentration of this consolidant.

The LIF-based optical radar has been deployed during a field campaign conducted in June 2010 on frescos by Giusto de' Menabuoi in the Padua Baptistery (Figure 31b). Remote

laser sensing was performed from the floor, at about 20 m from the frescos. Consolidants have been identified on the fresco surfaces: an example is given in Figure 32.

1.5 Technologies for energy

1.5.1 LIBS characterization of ITER-like tiles superficial layers

The occurrence of several plasma-wall interaction processes, eventually affecting the overall system performances, is expected in a working fusion reactor chamber. Suitable diagnostic techniques have been developed able to perform depth profiling analysis and to monitor the erosion of the superficial layers of the vacuum vessel tiles or the release and accumulation of pollutant elements. Due to the constraints commonly found in fusion reactors, the measuring apparatus must be non invasive, remote and sensitive to light elements. These requirements make LIBS (Laser Induced Breakdown Spectroscopy) an ideal candidate for on-line monitoring the walls of current and of next generation (as ITER) fusion reactors. In this work, LIBS depth profiling capability has been verified for the determination of the composition of multilayer structures simulating the tiles of a plasma facing component either clean or covered with deposited impurity layers. A new experimental setup has been designed and realized in order to optimize the characteristics of a LIBS system working at low pressure and remotely. The system layout is shown in Figure 33.

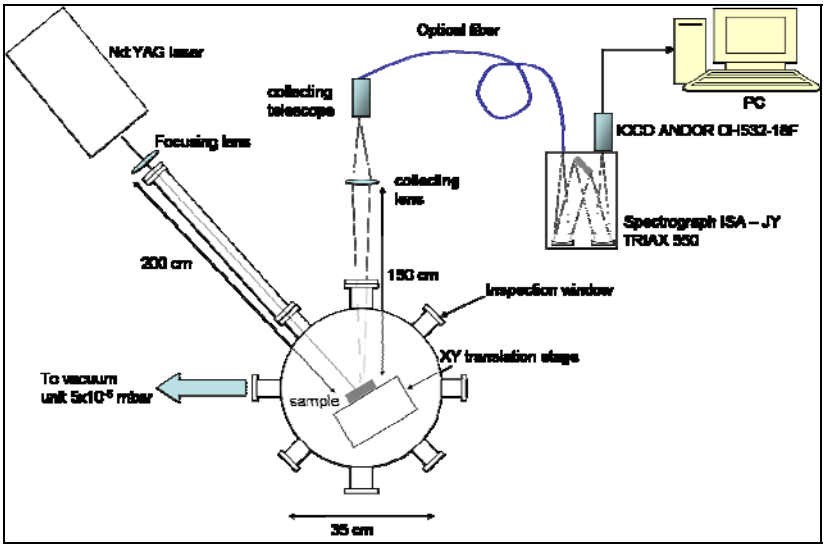

Figure 33 - Experimental set-up for low pressure measurements.

Some preliminary tests were performed to infer the critical plasma parameters in the adopted low pressure conditions. Samples of metallic substrate of pure Ti have been deposited with metallic coatings of fusionistic interest for PFCs of two different kinds: the first is a W coating, 12.8 μm thick with an inner 2.4 thick Mo layer as the one to be used as marker of W erosion in JET divertor; the second is a C-W coating, 8.5 μm and 12.2 μm thick with different atomic concentration.

The elemental composition and the stratigraphic structure of the micrometric coatings have been studied recording the emission intensity of the W, Mo, Ti lines as a function of the laser shots number. The intensities of the monitored lines are shown as a function of laser shots at different laser fluencies in Figure 34. From the nominal thickness of the layers we estimated the ablation rate at various laser fluencies for each sample, as reported in Table I. Submicrometric values were found in each case, demonstrating the good depth profiling capabilities of the apparatus. The results show that thin interfaces of different materials have been clearly detected and a resolution better than 0.5 μm in depth profiling has been obtained for our set-up.

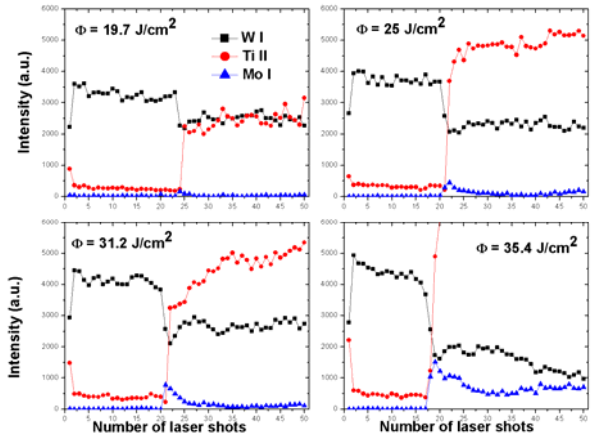

Figure 34 - LIBS intensity of W I at 434.7 nm, Mo I at 438.16 nm, Ti II at 439.5 nm lines at different laser flu encies.

Table I - Ablation rates for different coatings at different laser fluencies

Laser fluence (J/cm²)	Ablation rate (μm/shot) Sample 1 (W coating)	Ablation rate (μm/shot) Sample 2 (C-W coating)	Ablation rate (μm/shot) Sample 3 (C-W coating)
15.2		0.293	0.3
18.2		0.315	0.343
19.7	0.454	0.34	0.375
25	0.526	0.37	0.4
31.2	0.556	0.37	0.429
35.4	0.625	0.404	0.444

1.5.2 Laser In Vessel Viewing and ranging System (IVVS)

Machines for thermonuclear fusion research like JET and ITER need periodic inspections to check for damage on the in-vessel components. A prototype of Laser In Vessel Viewing&Ranging System (IVVS) based on an AM laser radar scheme has been developed at UTAPRAD–DIM laboratories under EFDA task agreements in cooperation

with UTFUS-ING. In the AM laser radar, the laser beam amplitude is modulated (up to 500MHz), both intensity and phase shifting of the reflected beam (compared with the launched one) are simultaneously detected. A highly spatial resolution picture of the scene is obtained from the intensity signal, while target ranging can be performed with good accuracy using the phase shifting (1mm@ 10m and pixel integration time 1ms). A laboratory prototype has been formerly produced and up-graded.

A Grant with F4E started in spring 2009, relevant to the design of the IVVS for **ITER**, including all the environmental conditions (pressure 10^{-3} Pa, operating temperature ≤120°C, gamma rays radiation dose up to 5 KGy/hour, total neutron fluence $5 \cdot 10^{13}$ n/cm^2, magnetic field up to 8 Tesla) and the mechanical constraints. The main activities in 2010, have concerned the assessment of the expected viewing/metrology capability of the probe and the conceptual design of the IVVS prototype (the probe is schematized in figure 35) and related test bed, in preparation of the future procurement and testing activities.

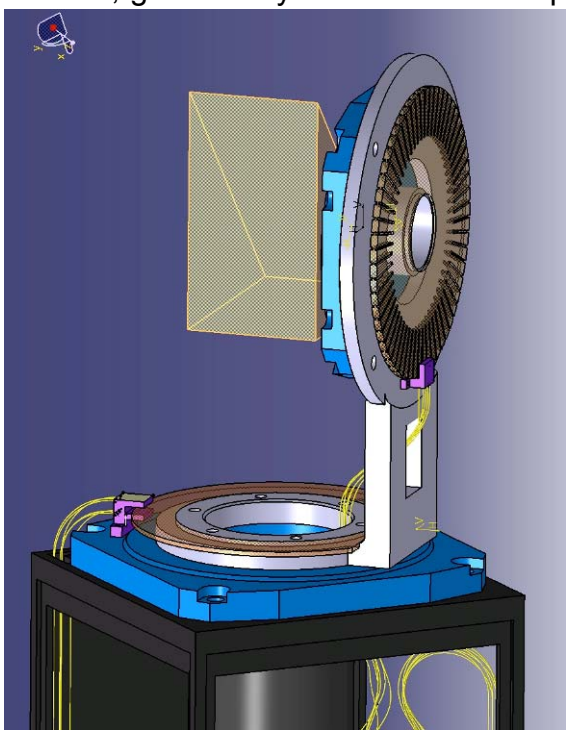

Figure 35 – IVVS scanning probe: the tilt and pan movements are obtained by using rotative ultrasonic piezomotors and it also includes 2 incremental optical fibers encoders. The width of the fused silica right angle prism is 55mm.

2. Mathematical Modelling Laboratory

2.1 Mission and infrastructures

Advanced mathematical methods for the study of the classical and quantum optics, and for modeling the transport of charged particle beams, to study and modeling of complex systems, including biological systems.

Competences available in the Laboratory are originated from expertise in different scientific disciplines as charged beam dynamics and transport, accelerators, RF structures, lasers, free electron lasers, optics and resonators, mathematical modeling

Facilities developed by UTAPRAD-MAT and utilized for current activities include:

- Laboratory for magnetic measurements and characterization
- The SPARC free electron laser test facility

2.1.1 Funding and projects

The research activities of the UTAPRAD-MAT Laboratory are mainly funded in the frame of National research programs (MIUR) as partner of collaborations (SPARX)

2.2 SPARC and SPARX FEL sources: development of innovative laser sources

2.2.1 Overview of SPARC

The acronym SPARC stands for Sorgente Pulsata Amplificata Radiazione Coerente FEL (Free Electron Laser). We will review different aspects of the activity, including the experiments, the technical and theoretical work and the design effort. In Figures 36-39 we report different views of the SPARC layout.

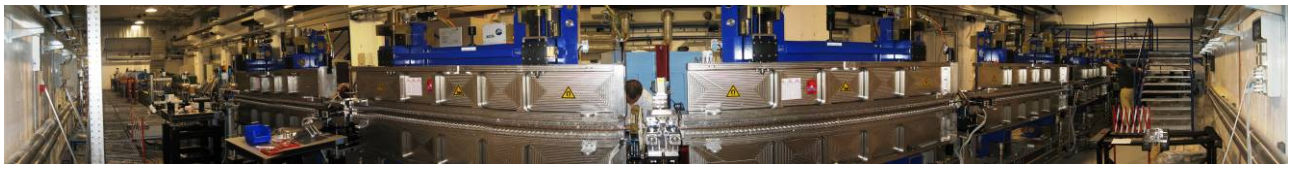

Figure 36 SPARC side view

The SPARC project has been conceived with the following objectives:

- Test whether the e-beam qualities are adequate to drive a FEL SASE up to the saturation;
- Show the possibility of extending the tunability of the system by means of the non linear harmonic generation mechanism which represents a natural tool to generate coherent radiation at higher harmonics
- Check the so called external seeding mechanism, necessary to improve the coherence properties of the laser and to induce a higher efficiency in the generation of harmonics.

The path towards the commissioning of the SPARC experiment has gone through different steps, starting from the improvement of the injector performances, the observation of the Self Amplified Spontaneous Emission (SASE) at 500 nm obtained in 2009, and finally the study of specific SASE configurations and the seeding mechanism together with the generation of high order harmonics (2010). ENEA, as partner of the collaboration with INFN and CNR, has contributed to all the three steps. In this context we will concentrate our analysis to the SASE experiments and the seeding experiments carried out during the year 2010, which where under the direct ENEA responsibility. In seeded mode the main goal was to study and test the amplification and the FEL harmonic generation process of an input seed signal such as higher order harmonics generated both in crystals and in gases.

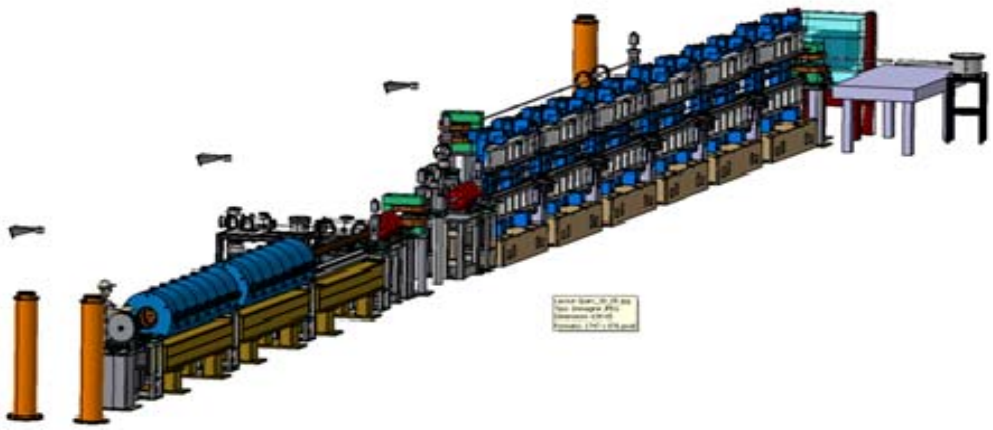

Figure 37 SPARC Layout

The SPARC FEL can be configured to test several seeded and cascaded FEL configurations. In SASE mode the FEL has been recently operated in fully saturated conditions by combining the technique of velocity bunching for increasing the peak current, with the idea of tapering the undulator gaps to mitigate the effect of the residual chirp and correlated energy spread resulting from the compression process.

2.2.2 Single Pass Seeded Amplifier

The SPARC FEL is driven by a high brightness accelerator providing a high quality beam at energies between 150 and 200 MeV (See Figure 38). The undulator beam line is composed of six, variable gap, undulator sections (See Figure 37). The SPARC undulators are variable gap modules of 75 periods each, with a period length of 2.8cm and a maximum K=2.2. Magnetic maps and undulator strength K vs. gap were measured before the undulator installation with a Hall probe mounted on a translation stage. These values were formerly verified with the spontaneous emission spectra measured with a test electron beam, showing a good agreement.

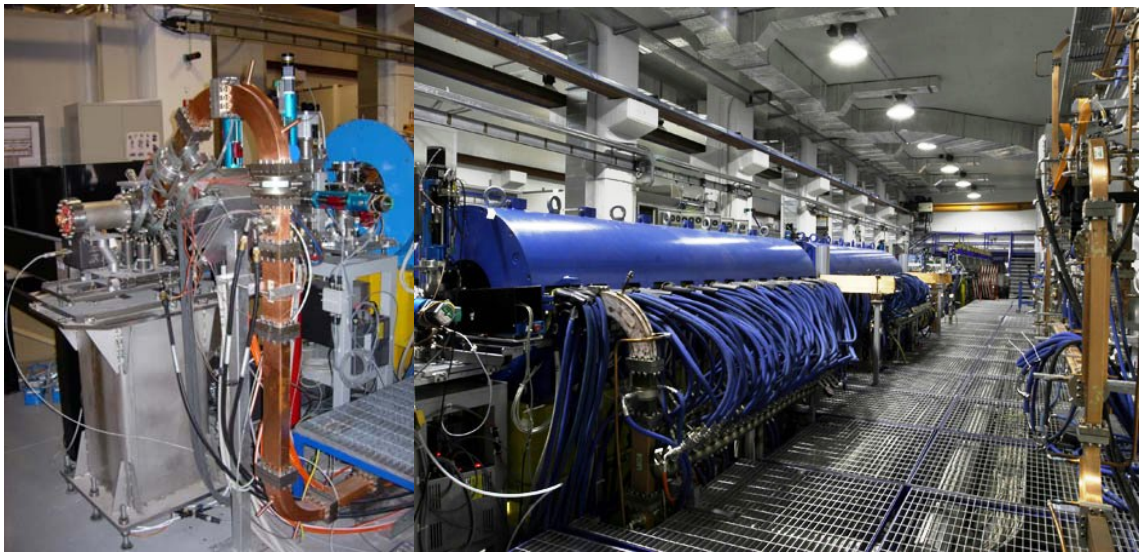

Figure 38. View of the SPARC injector (left) and linac (right)

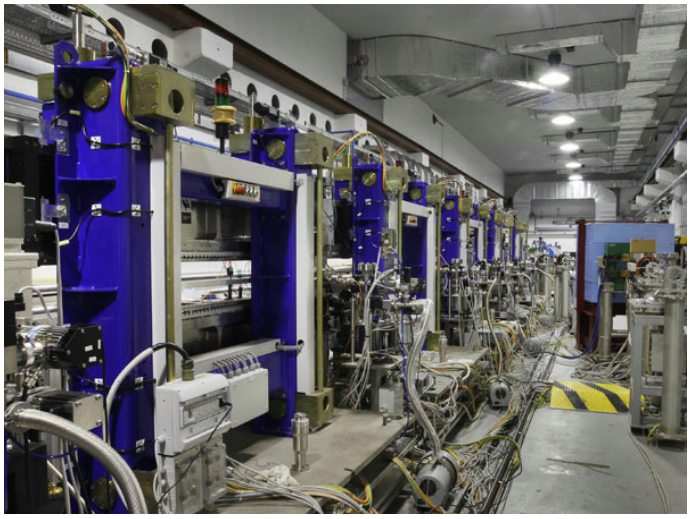

Figure 39. View of the SPARC six undulator modules

The beam transport is obtained with a FODO lattice where quadrupoles in the undulator intersections provide the horizontal focusing and the undulator field provides the vertical focusing. In this condition the matching Twiss β parameter depends on the resonant frequency which sets the undulator field strength. The mean beam energy measured with a magnetic spectrometer installed on the transfer line leading the beam to the undulator is 177.2 MeV. A RF deflector cavity installed on the transfer line before the magnetic spectrometer allows the measure of the beam parameters as a function of the longitudinal coordinate. The seed used in this experiment is the second harmonics of the Ti:Sa laser, i.e. λ= 401 nm, 120fs FWHM. The seed energy may be increased up to 150μJ but energies below 10μJ were sufficient for the experiments described hereafter. With the undulators tuned at the seed wavelength we match the orbit minimizing the transverse beam size and imposing that the transverse average Twiss β coefficients are the same in the two directions $\left(\langle\beta_x\rangle = \langle\beta_y\rangle\right)$.

With these conditions we have $\langle\beta_x\rangle = \langle\beta_y\rangle \cong 1.5m$. The analysis of the images acquired with the combined use of the deflector cavity and the spectrometer magnet allows the determination of mean energy, energy spread (slice and projected), energy chirp, bunch length and, knowing the bunch charge, measured independently, the longitudinal profile of the bunch current. A list of these parameters is presented in Table II. An in vacuum spectrometer designed and built by the LUXOR laboratory in Padova is the main radiation diagnostic.

Table II – Summary of the Main Beam Parameters

Beam energy (MeV)	177.2
Energy Spread (proj., %)	0.13
Energy Spread (slice, %)	0.05
Length (ps - rms)	2.64
Peak current (A)	54
Emittance X (mm mrad)	2.9
Emittance Y (mm mrad)	2.5

The spectrometer gratings and the CCD detector have been calibrated in efficiency and yield to allow the simultaneous determination of spectral properties of the observed radiation and of the single shot pulse energy. The spectra shown in Fig.40 were acquired with all the undulators tuned at 400 nm, after ensuring temporal and spatial superposition between the seed and the electron beam.

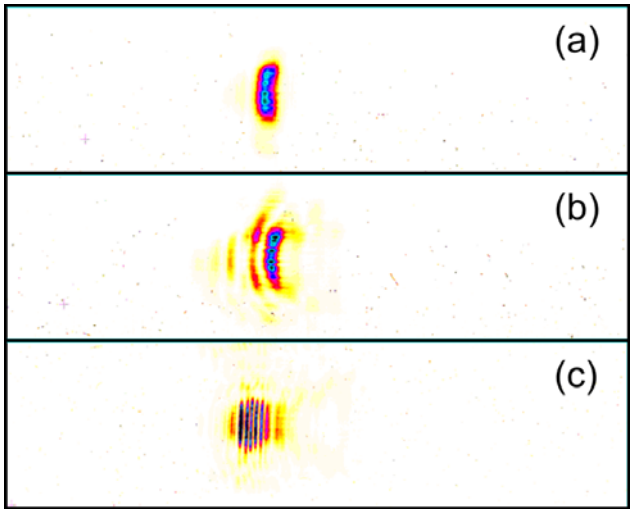

Figure 40: Spectrum of the seeded amplifier. The horizontal axis represents the wavelength, the window range is 45 nm and the central wavelength is 400 nm. The vertical axis indicates the position on the (vertical) entrance slit of the spectrometer. The images with labels (a), (b) and (c) have been obtained with different seed energy: (a) E<0.5μJ , (b) E~3μJ, (c) E~9μJ.

The vertical axis on the image represents the vertical position on the input spectrometer slit, while the horizontal axis represents the wavelength. The window is centred at 400 nm and the represented wavelength range is about 45nm. The figures Fig.40,a to Fig.40,c represent spectra obtained at different seed energy as indicated in the figure caption. The multi-peak structure, corresponding to the presence of various spectral lines, slightly red-shifted compared to the unseeded and HHG is about a factor two larger than the expected SASE bandwidth. The Pierce parameter should be $\rho = 3.2\,10^{-3}$, corresponding to a bandwidth of the order of 1.3 nm, while the spectrum in Fig.40.c is larger than 2 nm. The observed pattern, appearing at high seed energy, is completely different both in shape and in intensity from the typical SASE spiking where the number of peaks and their position change from shot to shot. The sidebands structure which appears in the spectrum at high seed energy only, is a saturation effect. This structure may be interpreted as the effect of a saturated pulse slipping forward along the electron pulse, with the radiation emitted by fresh electrons in the pulse front, interfering with radiation out of phase produced by overbunched electrons in the rear part of the pulse. Numerical simulations have been carried out with the GENESIS 1.3, implemented with harmonics and with PERSEO Time Dependent code (PTD), taking into account the spectral overlap and three-dimensional effects, such as the transverse mismatch. An amplification of the seed in the exponential regime in the first two sections of the undulator, and superradiance in the other four ones

is observed in the simulations. In order to compare the spectra with the simulations the field data generated by GENESIS have been post processed through a numerical procedure resembling the slit/grating/CCD of the spectra detection system.

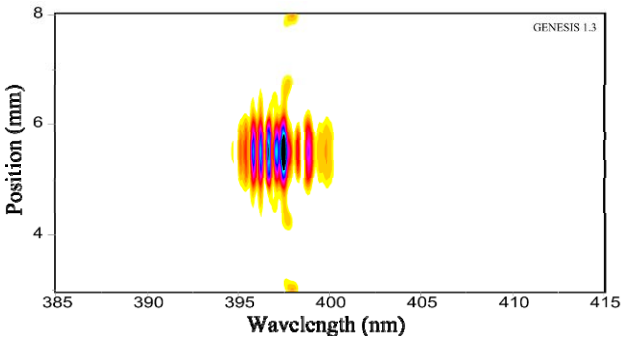

Figure 41: GENESIS 1.3 data, obtained with the following data: I=65A , εx=2.9 mm-mrad, εy=2.5 mm-mrad (norm.).

One of the results obtained is shown in Fig. 41 where the spectrum has been deduced from GENESIS 1.3, obtained with the following simulation data: I=65A , ε_x=2.9 mm mrad, ε_y=2.5 mm mrad (normalized). The energy per pulse is E =50μJ, to be compared with the energy observed in the experiment E=20μJ with a standard deviation of 6μJ. The energy measured in a sequence of 100 consecutive shots is shown in Fig.42.

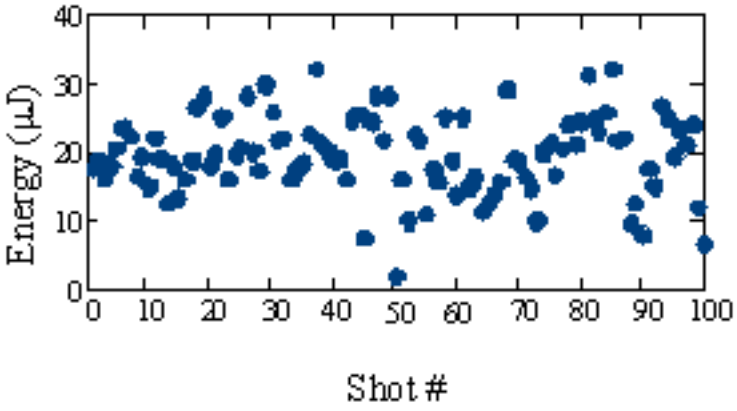

Figure 42: Energy measured in a sequence of 100 consecutive shots.

Harmonics of the fundamental frequency have been observed up to n=11. The spectral emission on the harmonics presents regular Gaussian shape pulse to pulse. In fig. 43 the spectrum from 32 up to 115 nm is shown with the presence of eight harmonics from 11th up to 4th from left (in sequence: 36.18 nm, 39.8nm, 44.2 nm, 49.75 nm, 58.6 nm, 66.3 nm, 79.6 nm, 99.5 nm). Both even and odd harmonics are visible, with the odd ones slightly more intense. In Fig. 44 the spectral band from 115 up to 205.85 is shown with the presence of the second and the third harmonics (132.66 nm and 199 nm). The spatial shape seems to be similar to the unseeded emission.

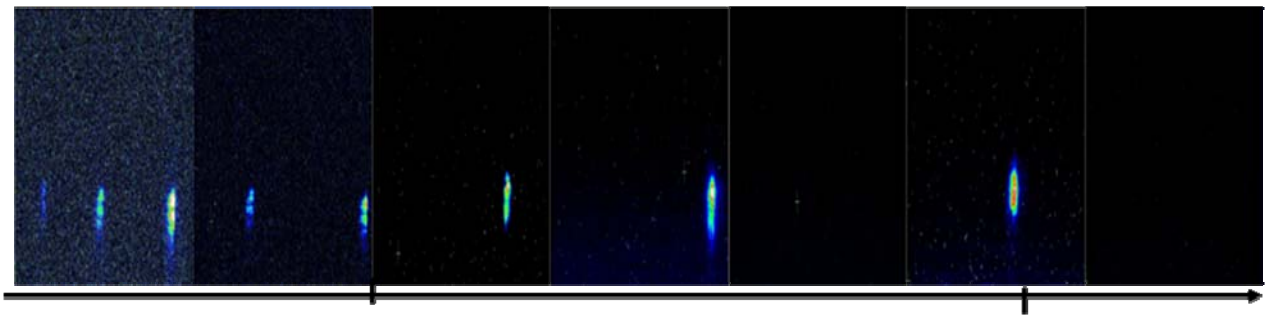

Figure 43: Spectrum from 32 up to 115 nm is shown with the presence of eight harmonics from 11th up to 4th from left (in sequence: 36.18 nm, 39.8nm, 44.2 nm, 49.75 nm, 58.6 nm, 66.3 nm, 79.6 nm, 99.5 nm).

The process of coherent higher order harmonics generation in this regime of operation, i.e. with a seed pulse shorter then the e-bunch length was studied in [13]. The regime,

formerly analysed and explored in a single pass FEL amplification experiment, is characterized by a self similar pulse amplified while it propagates through the undulator. The main reason of the expected intense harmonics emission can be found in the structure of the front side of the pulse and in the interaction with the co-propagating electron beam. In Fig. 45a it is shown a plot of the short radiation pulse shifting from left to right because of slippage. In Fig. 45b the expanded view of the electron beam phase space in the pulse front side (colored region in Fig.44a) and the bunching coefficients for the first harmonics, are represented.

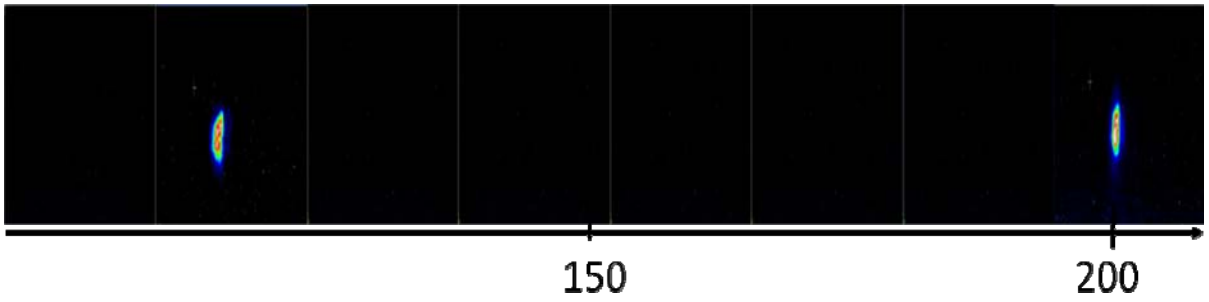

Figure 44: Spectral range from 115 up to 205.85 nm is shown with the presence of the second and the third harmonics (132.66 nm and 199 nm).

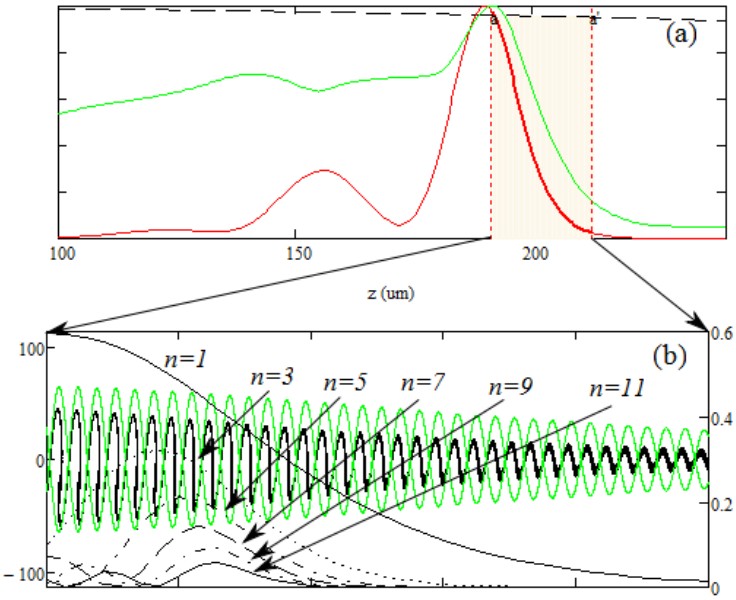

Figure 45: Graphical representation of the radiation pulse slipping from left to right in the e-beam frame (red) and of the induced energy spread (green) (Fig.44a). Longitudinal e-beam phase space in the front part of the pulse (Fig.44b). In Fig.10b the square moduli of the bunching coefficients for the first eleven (odd) harmonics are plotted. The green line represents the motion separatrix whose envelope is proportional to the square root of the laser field (simulation with PERSEO TD).

The pulse advances over fresh electrons on the right side inducing an increasing modulation and bunching. The bunching factor at the fundamental grows from right to left until reaches the maximum value approximately at the peak of the pulse. Bunching factors at the higher order harmonics follow a similar behaviour, reaching the maximum value in a position in the pulse front side with a length scaling as 1/n. Simulations predict extremely narrow pulses at the highest harmonics. Several aspects of this dynamical regime suggest an intense high harmonics emission. Saturation dynamics is governed by the slippage process. At a given position along the bunch the field grows because of slippage and not because of exponential gain. Fresh electrons are “seeded” by the propagating wave and the faster dynamics in phase space causes the peaks in the bunching coefficients to be narrower with a more effective modulation. The bunching at a given harmonic reaches a maximum value determined by the inhomogeneous dispersion associated to the beam quality. The self similar behaviour

of this particular solution of the FEL dynamics causes the fact that the bunching distribution is “preserved” along the undulator. In steady state regime (or in the long pulse regime), bunching at a given harmonic may be induced over a limited undulator length, because interaction with the laser field and dispersion combined with the induced energy spread, cause debunching. In this particular condition there is a region of the beam phase space, drifting over the electron current where bunching is preserved along the undulator. There is no de-bunching due to dynamics. The experimental observation confirms the predicted behaviour.

2.2.3 Superradiant Cascade

Intense short seed pulses allow to test the super-radiant cascade concept, where the seed laser power is sufficient to bring the radiation pulse close to saturation in the modulator. The pulse generated in these conditions propagates with the typical signature of superradiance in the next radiators. The six SPARC undulators may be configured in order to set up a single stage cascaded FEL based on a modulator-radiator configuration, similar to the one originally tested at BNL. The layout of this configuration is shown in Fig.46.

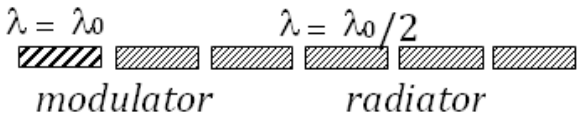

Figure 46: Undulator layout of a single stage cascade at SPARC.

The number of sections playing the role of modulator and radiator may be adjusted to the intensity of the available seed. In conditions similar to the one analysed in the previous section, we have tested the configuration in Fig. 46 composed by a single undulator tuned at 400nm and playing the role of modulator and five undulators tuned at 200 nm as radiators. In Fig. 47 it is shown a plot of the pulse energy measured at 200nm while changing the optical path length of the seed laser. The average, maximum and minimum energy observed in a sequence of 30 shots at each position are plotted. The large difference between the minimum and maximum value of the intensity at a given position was due to a phase jitter of the beam energy which was bringing the seed out of resonance in the modulator.

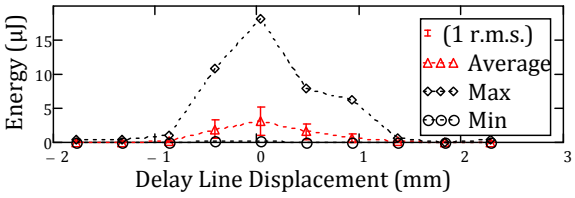

Figure 47: Energy at the exit of the radiator as a function of the relative delay δ between the seed and the electrons in the modulator. The zero position is set to the maximum energy. Error bars represent one standard deviation.

The spectrum at δ=0 corresponding to the shot characterized by the maximum energy is displayed in Fig. 48 (left). The spectrum shows a structure suggesting that saturation is reached at this wavelength as well. As in the previous case a significant harmonic emission is expected. The spectrum of the third harmonic of the radiator is shown in Fig. 48 (right) while in Fig. 49 the distribution of energy per pulse and relative linewidth of the third harmonic for a sequence of 30 consecutive spectra is shown. Several shots show energy at the 0.1 μJ level. The large fluctuation of the observed energy is associated to the beam energy jitter which affected the beam during the shift.

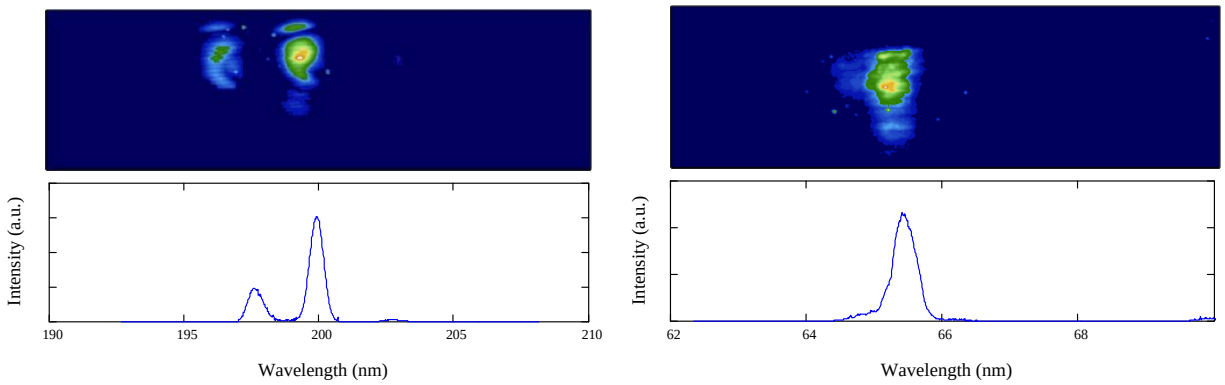

Figure 48: Spectrum of the radiation emitted by the radiator tuned a 200nm (left) and of the third harmonic of the radiator (right).

Figure 49: Energy per pulse vs spectral width for a sequence of 30 consecutive spectra.

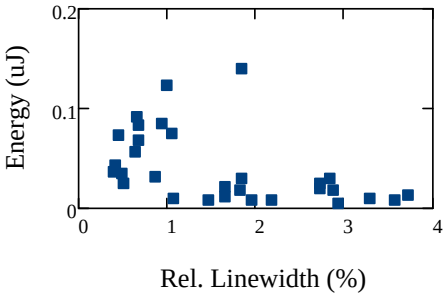

2.2.4 Seeding with harmonics generated in gas

In the framework of the DS4 EUROFEL collaboration, a research work plan, aiming at the study and test of the amplification and the FEL harmonic generation process of an input seed signal, obtained as higher order harmonics generated in gases. In Fig.50, the gas interaction chamber, developed at CEA and installed to inject radiation in the transfer line between the linac and the undulator beamline, is shown.

Figure 50. Harmonic generation chamber realized at CEA. The laser enters from the left side and is optically matched to the undulator by two spherical mirrors located in the chamber on the right. The differential pumping ensures vacuum at 10^{-7} mbar in the electron beamline.

The radiation seed at 266nm, as observed on a screen at about 15 m from the source, is shown in Fig.51. While the radiation transverse intensity showed a reasonably regular profile (Fig. 51), the spectrum of the seed presented a double peak structure, as shown in Fig.52.

Figure 51. Spot of the 266nm radiation seed generated in gas as observed on a screen at about 15 m from the interaction point.

The spectrum at 266nm was registered by the spectrometer at the end of the undulator. The energy on higher order harmonics (160nm and 114nm) was not sufficient to detect a signal above the camera background noise. The double peak structure was observed only during this shift, and was not registered on the IR laser radiation before conversion at 800 nm. These preliminary experiments were performed with the double peak structure in the spectrum.

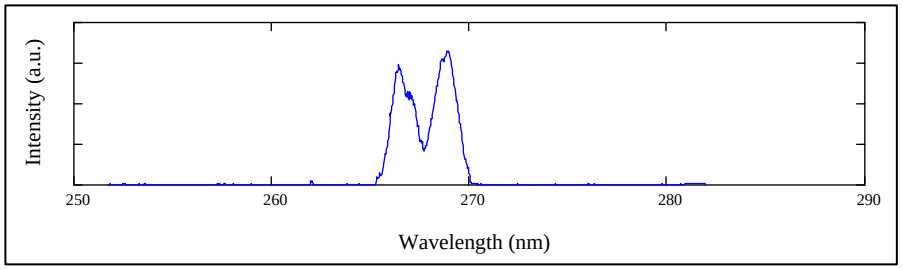

Figure 52. Seed spectrum at 266 nm.

An in vacuum optical system is used to match the transverse optical mode of the harmonic to that of the e-beam in the first undulator section. The UV pulse is injected into the SPARC undulator by means of a periscope and a magnetic chicane deflecting the e-beam from the straight path. High-order odd harmonics of the Ti:Sa laser may be generated at the wavelengths 266nm, 160nm, and 114nm.

The FEL amplifier has been seeded with the radiation generated in a gas cell at 266nm. The seed energy was about 50 nJ. After ensuring a transverse spatial overlap in the first undulator module, we have scanned the seed delay to ensure a proper synchronization between electrons and radiation. The output energy vs. delay is plotted in Fig. 53 together with the e-beam current, measured with the RF-Deflector at the entrance of the undulator. An arbitrary delay has been added to the trace to superimpose the two curves. A large energy jitter was the main reason of the large standard deviation observed in the figure.

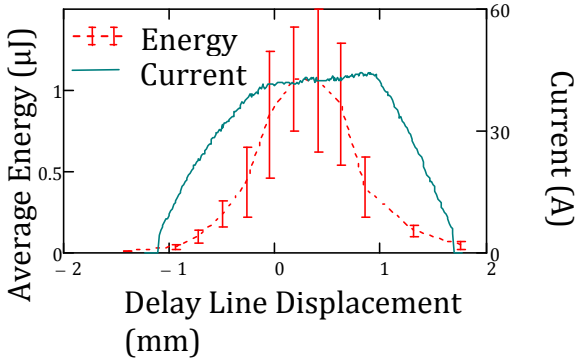

Figure 53. Average energy (± 1 std. dev.) from the seeded FEL compared to the e-bunch current measured via RF deflector.

The corresponding linewidth is shown in Fig. 54. The SPARC undulator may be operated as an undulator cascade, where the first modules are tuned at the seed wavelength 266nm in this case, and the last modules are tuned at the second harmonic (133nm). We have explored this configuration varying the number of modulators/radiators (with six total modules). The optimized number of undulator modules operating as radiator and modulator depends on the input seed energy.

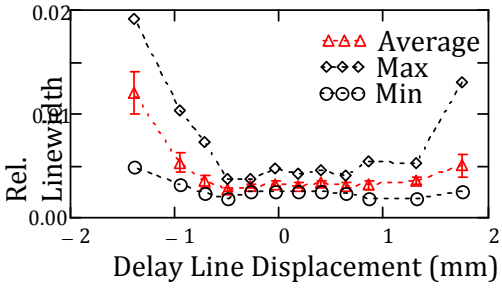

Figure 54. Relative linewidth vs. delay line displacement.

The higher output energy E=1μJ at 133nm was obtained with four undulators as modulators and two radiators (Fig.55). A typical spectrum, obtained in single shot mode in this configuration, is shown in Fig. 56.

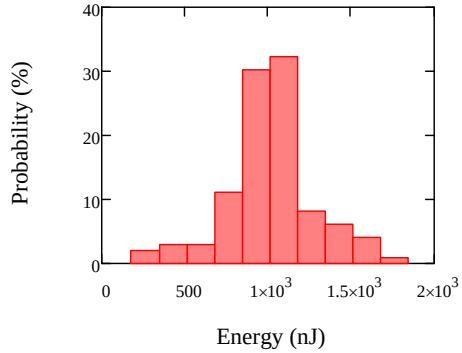

Figure 55. Histogram of the output pulse energy at 133nm in a sequence of 100 shots.

Figure 56. Single shot spectrum of the FEL cascade seeded with radiation at 266nm generated in gas. The horizontal axis represent the wavelength, the vertical axis represents the position at the spectrometer slit.

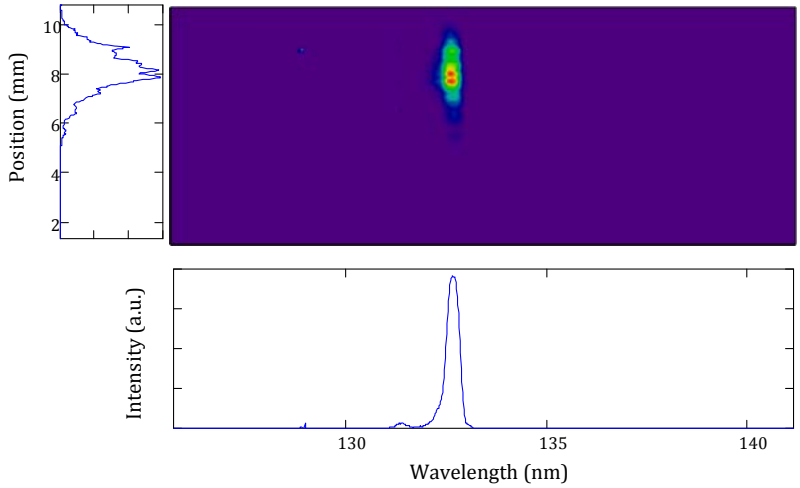

2.2.5 SASE with a chirped beam

The SPARC layout, shown in Fig. 37, does not include a magnetic compressor. When the linac is operated in velocity bunching mode, the first linac section is tuned off crest, close to the zero crossing phase. The result is a strong chirp in the longitudinal phase space which leads to an increase of the peak current. This condition has already been extensively studied at SPARC. Compression factors up to 17 and compensation of the emittance growth with the superposition of a magnetic field on the first linac section have been demonstrated. The correlated energy spread associated to the chirp would be mitigated in a long linac by longitudinal wakes and by acceleration itself. In the SPARC case the linac is composed of three SLAC type sections only, allowing a maximum energy of about 180MeV. In compression mode, the first section operated out of phase is not optimized for acceleration and the final energy is about 120MeV. The linac structure, typical of an injector, is not sufficient for compensating the correlated energy spread. The phase space at the linac exit still contains a strong residual chirp and despite the high peak current which can be obtained, the detrimental effect of the chirp on the gain prevents the FEL from reaching full saturation.

The effect of the chirp on the gain can be compensated by tapering the undulator. The compensation mechanism can be explained analysing the diagrams shown in Fig.57. The pictures represent the propagation of a field spike (green) developing on the rear part of a chirped e-beam (light blue). The vertical axis represent the resonant condition which depends on the relative position between the beam and the radiation. The upper diagram is relative to the un-tapered case. When the beam propagates through the undulator, the

slippage process leads the spike out of resonance. When the chirp is combined with an appropriate undulator taper (lower diagram), the resonance condition can be preserved.

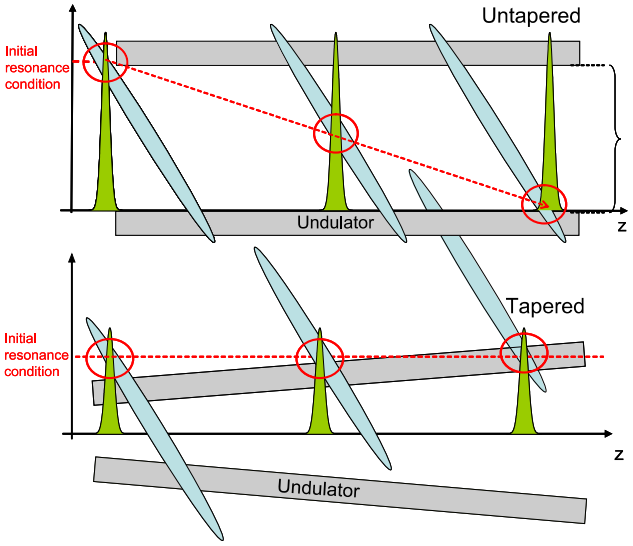

Figure 57. The pictures represent the propagation of a field spike (green) developing on the rear part of a chirped e-beam (light blue). The upper diagram is relevant to the un-tapered case, the lower one to the tapered case.

In a chirped beam the resonant frequency

$$\omega_0 = \frac{2\gamma^2}{1+\frac{K^2}{2}}\omega_u, \qquad \omega_u = 2\pi c/\lambda_u \qquad (1)$$

where λ_u is the undulator period, K is the undulator strength and $\gamma = E/m_0c^2$ the beam energy, is a function of the position along the electron bunch. We may define the mean "local" energy as (linear chirp)

$$\gamma(s) = \gamma_0 + \alpha(s - s_0) \qquad (2)$$

where *s* corresponds to the longitudinal coordinate along the electron bunch centred in s_0 in a reference frame drifting at the velocity $\beta_z = 1-(1+K^2/2)/2\gamma^2$. The parameter α defines the slope of the average slice energy vs. the coordinate *s*. The different velocity of the light with respect to the electrons brings a radiation spike building up in a given position, out of resonance when it slips of a distance of the order of $\delta s \approx \rho\gamma m_0c^2/2\alpha$. For this reason an inhomogeneous gain broadening associated to energy spread, is expected even with a negligible local energy spread because of slippage. The field in presence of gain propagates at a velocity lower than *c*, the peak of a spike in the exponential gain regime is expected to move at a velocity given by [16]

$$v_L = \frac{3c\beta_z}{2+\beta_z} \qquad (3)$$

Above saturation the front side of the pulse drifts at the velocity of light c. Approaching saturation the radiation peak shifts at a different velocity than (3), closer or even higher than c because of the pulse shortening associated to the electron synchrotron oscillation. A taper of the undulator may be used to compensate the effect of energy dispersion associated to the pulse slippage on the chirped beam. The energy change caused by the chirp and observed at the peak of the radiation pulse may be expressed as

$$\gamma(z) = \gamma_s + \alpha\, z\eta\frac{\omega_u}{\omega_0} \qquad (4)$$

where z is the coordinate along the undulator, γ_s is the beam energy at the undulator entrance (z=0), at the position along the bunch where the spike will grow, and where η is a coefficient accounting for an arbitrary propagation velocity of the radiation v_L . For $v_L = c$

we have $\eta = 1$, for v_L given by (3) we have $\eta = 1/3$. Inserting eq.(4) in the resonant condition (3) and expliciting for the undulator K we obtain a taper scaling which preserves the resonance condition during propagation.

$$K(z) = \sqrt{2\left[\left(\frac{2}{\omega_0}\left(\gamma_s + \alpha\, z\eta\frac{\omega_u}{\omega_0}\right)^2 - 1\right)\right]} \qquad (5)$$

The correct scaling of the taper depends then on the parameter η, which can be deduced in the more general case of exponential growth in presence of a given taper and energy chirp. The chirped beam evolution has been also studied with the code PROMETEO.

We have tested the effect of the tapered undulator with the SPARC FEL operating in velocity bunching mode. The central wavelength used in the experiment is 540 nm and the corresponding β Twiss coefficient is about 1.5m. The mean beam energy measured with the magnetic spectrometer is 116MeV and the emittances measured with the quadrupole scan technique in the transfer line between the linac and the undulator beamline are 2.7/3.0 mm-mrad (x/y). The longitudinal phase space measured with the RF deflector cavity used in combination with the dipole spectrometer is shown in Fig. 58.

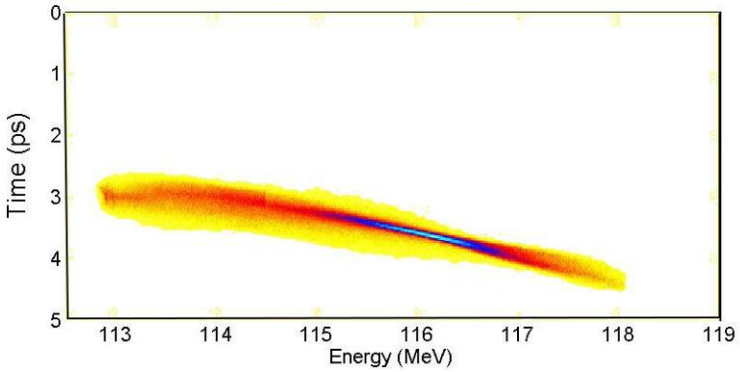

Figure 58. Longitudinal phase space reconstruction at the exit of the linear accelerator.

A list of the beam parameters measured before the injection of the beam in the undulator is presented in Table III. The operation in compression mode, i.e. with the first linac section at a phase close to zero crossing, is very sensitive to phase drift and jitter. This is the main reason in the large uncertainty factor in the chirp figure.

Tab. III – Summary of the main beam parameters

Beam energy (MeV)	115.2
Energy Spread (proj., %)	1.15
Energy Spread (slice, %)	0.6
Chirp keV/μm	6±1.5
Length (ps - rms)	0.42
Peak current (A)	380

The radiation diagnostic was the same used in the experiments presented in the previous sections and it is based on the in vacuum spectrometer. In Fig. 59 it is shown a typical spectrum collected with three undulator gaps set to the resonant wavelength of 540nm (at the mean beam energy).

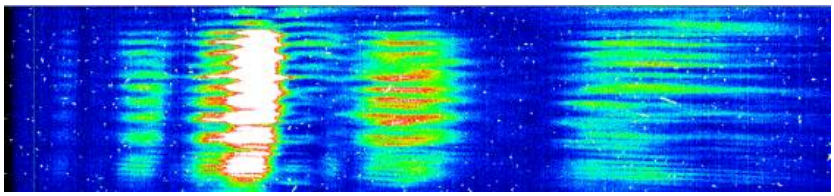

Figure 59.: Single shot spectrum acquired with three undulator closed. The vertical axis represents the vertical position at the spectrometer entrance slit. The window is centred at 540nm and the window width is 45nm.

The vertical structure in the spectrum image is due to the radiation diffraction caused by the vacuum pipe. With the first three undulator set at resonance and the last three undulators opened, the radiation has to propagate through about 8 m of vacuum pipe without gain guiding. The structure disappears in Fig. 60, obtained with six sections tuned at the resonance of 540nm (un-tapered undulator).

Figure 60.: As the previous figure, single shot spectrum acquired with six undulators set at the resonance of 540nm.

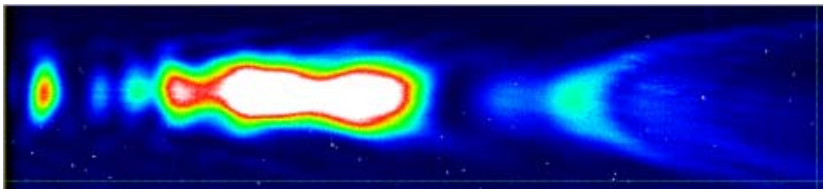

The strong chirp in the electron bunch shows up as a broadband spectrum filling up the wavelength acceptance window of the spectrometer. A statistical analysis of the collection of 100 spectra acquired in this condition provided the histograms shown in Fig.s 61.

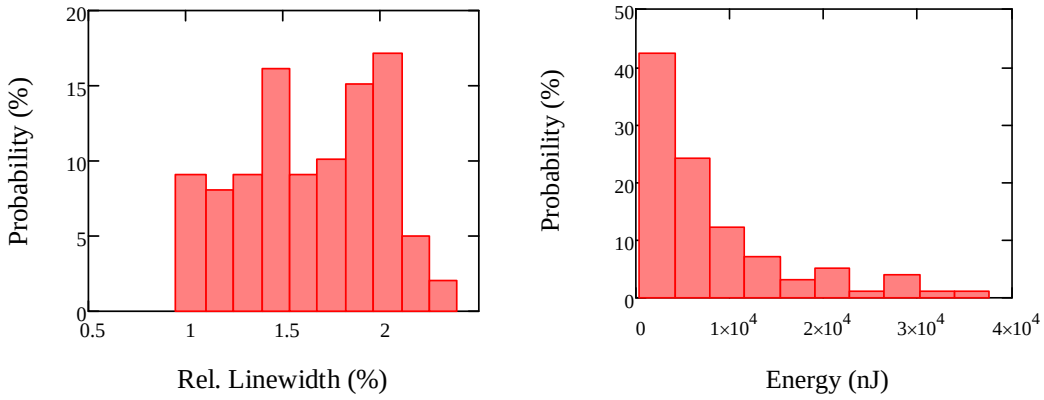

Figure 61. Histogram of the spectral width (left) and the pulse energy(right) obtained with the untapered undulator, with the resonance set at 540nm.

The average pulse energy obtained in these conditions is 7.8μJ. The r.m.s. of the distribution is comparable to the mean value (8 μJ).

The technique used to compensate the chirp with the taper was that of progressively closing the gaps one module at the time, starting from the first one while observing the emitted spectrum. For each module we found the gap minimizing the spectral width. This procedure lead to the set of gaps corresponding to the resonance frequencies (at 115 MeV) shown in Fig. 62.

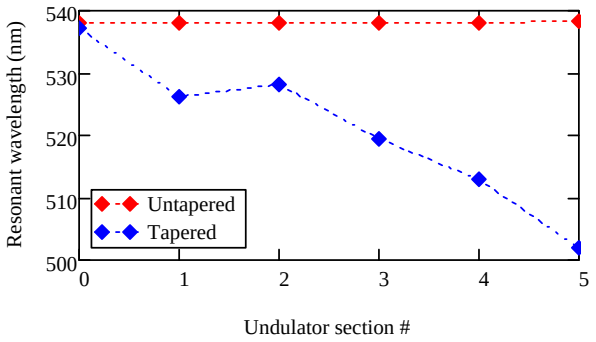

Figure 62: Resonant frequency in the six undulators in the untapered and tapered case.

After the procedure, with the resonant frequency per undulator as shown in Fig.62, we have obtained a substantial increase of the pulse energy which reached 140μJ with a standard deviation of about 100μJ and a reduction of the average linewidth which was $8x10^{-3}$ averaged over 100 pulses. In Fig.s 63 the histograms relevant to the statistics of the pulse relative linewidth and energy for the 100 shots are shown. Several spectra in the acquired set were characterized by a spectral pattern similar to the one shown in Fig. 64, constituted by a single coherence region (no SASE spikes). The pulse energy in the spectrum of Fig.64 is about 260μJ. The red dashed line corresponds to a Gaussian profile fitting the main structure in the spectrum with a spectral width of 1.65nm. A Fourier limited pulse would have a rms length of 46fs and a peak power of about 900MW.

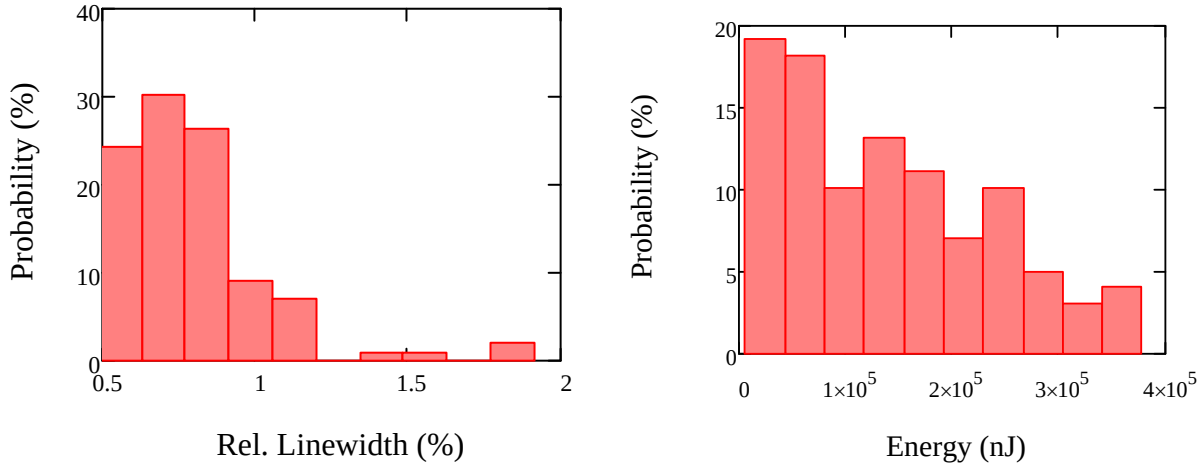

Figure 63: Histogram of the relative linewidth (left) and pulse energy (right) obtained with the tapered undulator.

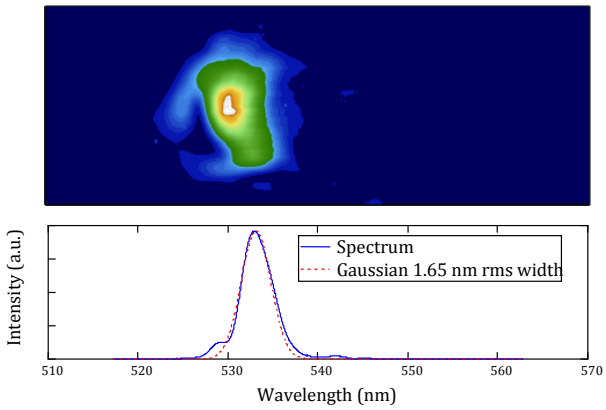

Figure 64: Typical spectrum showing a single coherence region (single spike).

The SPARC scientific activity encompasses FEL physics and beam dynamics experiments. We have summarized three of the main achievements of 2010 consisting in the observation of high harmonics emission from a single pass FEL amplifier seeded at saturation levels with an external laser, in the realization of a cascaded FEL operating above saturation with the observation of the third harmonic in the radiator and finally in the operation in SASE mode with a chirped beam compensated by the undulator taper. This is a promising way to obtain short Fourier

limited radiation pulses and we have confirmed for the first time the observation of spectra without any typical SASE spiking structure.

2.3 Modeling and design

A significant part of the theoretical and design activity has been devoted to the modelling of the FEL SASE dynamics. The codes developed for such a purpose are reported at the end of this report along with some guide Booklets conceived as reference design manual for FEL's and Linacs dedicated to the FEL operation. In the following we will briefly discuss one of the by products of this activity. The concepts of slice and projected emittances have emerged in the past years, and have modified the criteria for the design and the optimization of the electron beam transport.

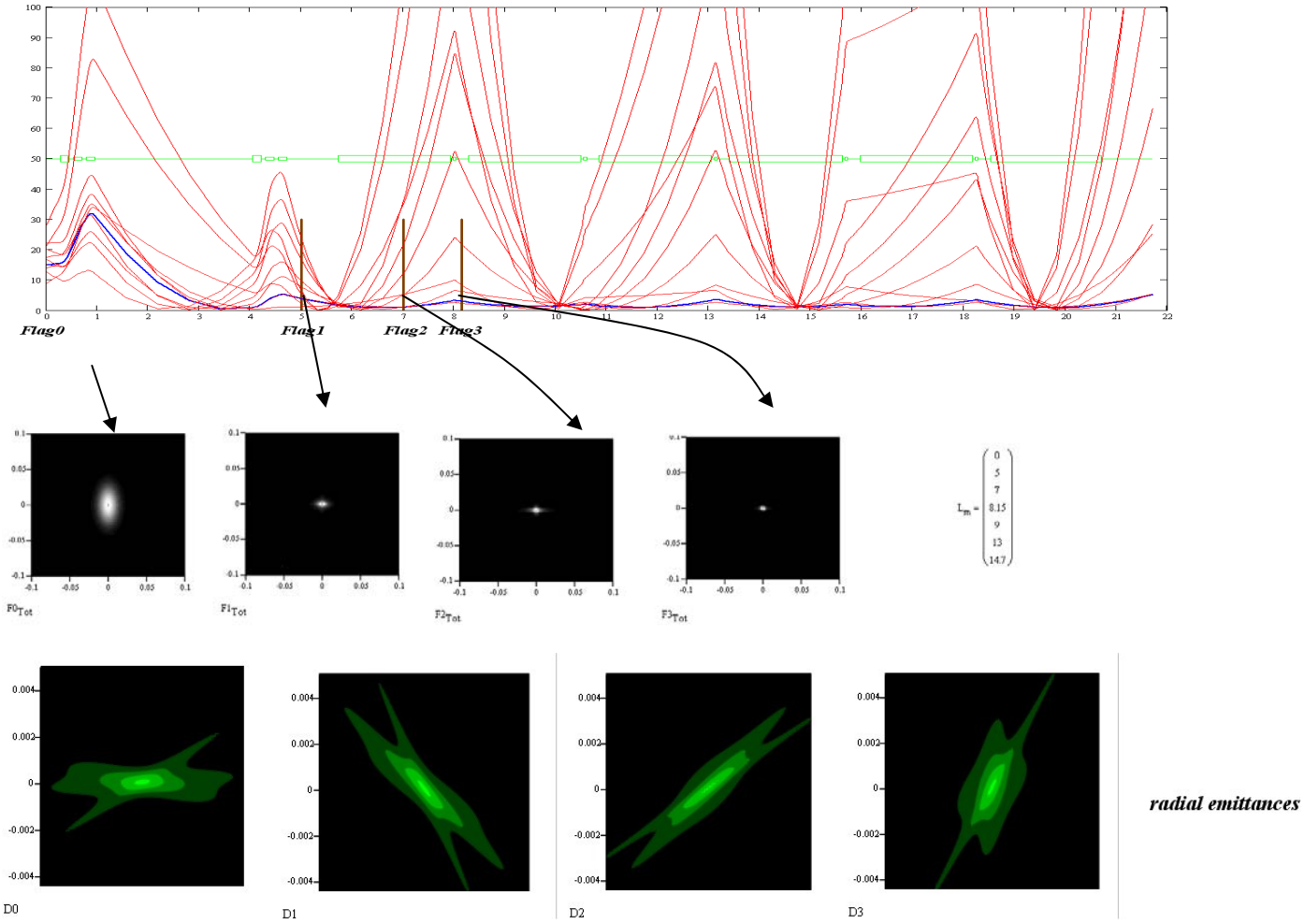

Figure 65: Slice transport along the SPARC magnetic channel, the Twiss parameters and the emittances of each slice have been generated randomly and the matching has been provided for the central slice denoted by a blue curve in the upper figure, where we have repo reported the (radial) beta function evolution of each slice. The lower curves, referring to the beam diagnostic flags along the channel, provide the beam section and the radial phase space evolution.

The idea of slice emittance is a by product SASE FEL Physics, as a consequence of the fact that the output laser field is the result of the competition between different bursts of

radiation emitted by different longitudinal portions (the slices) of the bunch. The longitudinal dimension of the slice is associated with the so called coherence length, given by $l_c = \frac{\lambda}{4\pi\sqrt{3}\rho}$ where λ is the wavelength of the emitted radiation and ρ is the gain parameter. From the physical point of view, the coherence length corresponds to the length spanned by the radiation, in one undulator passage, during its slipping over the electron bunch. This fact ensures that the radiation, emitted by one slice, is coherent, furthermore a kind of chaotic competition occurs between the radiation, emitted at different position, in the bunch, which, being not locked in phase, grow independently.The contribution to the FEL SASE dynamics of the SLICE quality is crucial. Any slice is indeed characterized by a specific brightness. It cannot be therefore excluded that only few slices, or even just one, reach the saturation and not the full bunch.The first problem, emerging when dealing with the slice structure of the phase space, is the e-beam matching. We have indeed different choices: matching with respect to the projected emittances or to the slices with larger brightness. An example of transport is given in Fig. 65 where we show the evolution along the SPARC channel of the Twiss coefficients of the individual slices, of the e-beam transverse section and of the Courant Snyder ellipses on the successive diagnostic flags. The matching has been done with reference to the projected emittance and the result in terms of phase space distribution is not particularly encouraging. One of the main problems is that some slices may be completely out of control and their mismatch may create a significant reduction of the output power and of the transverse coherence of the FEL radiation, as we will stress later in this report.

The method we have developed either uses concepts from elementary analytical geometry, we stress again the importance of the geometrical interpretation of the Courant Snyder ellipse. The beam matching protocol is illustrated below

- We determine two average slices with opposite α
- We individuate the radical ellipse as that emerging from the intersection of these two slices phase space areas and the projected ellipse
- We transport the beam along the undulator (6 sections) with matching conditions: on projected emittance on central slice, on radical ellipse (Fig. 66)

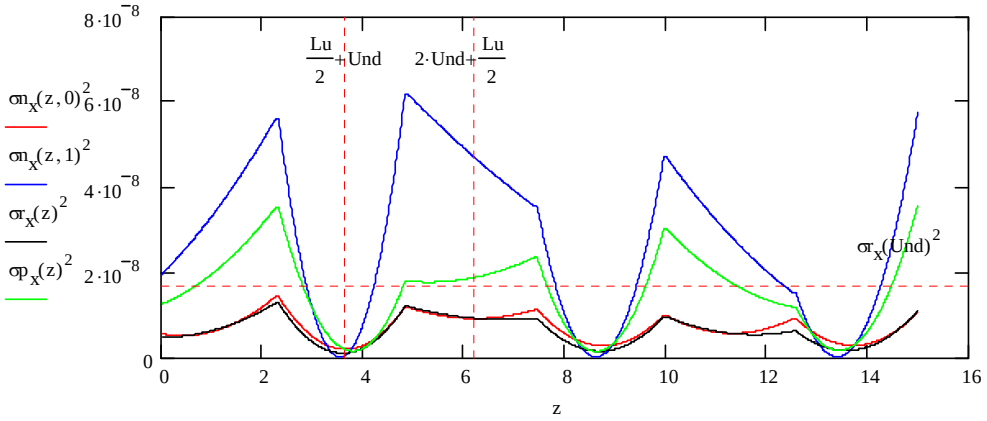

Figure 66: Blue: mismatched slice Red : central slice, best Twiss parameter Green: projected ellipse - Black: radical ellipse

The radical ellipse seems to exhibit the best transport characteristics.

2.4 SPARX progress

The situation of funding for SPARX has been clarified and the conclusion is that after the constitution of the Consortium Luce, the partners will be able to negotiate with the funding agencies (Regione Lazio and MUR) 25 milllion €, 10 of which for civil engineering and 10 for the hardware.

This is not sufficient to build a facility operating in the hard X-ray region, we have therefore studied different solutions for the realization of a source operating in the VUV soft X-ray region based on a single pass amplifier or oscillator configurations. A diagram of the radiation source in the amplifier configuration is shown in Fig.67.

Table IV: Undulator parameters

Undulator parameters (Br=1.21T)					
	Period(mm)	Min gap (mm)	K (max)	# periods	Length(m)
Modulator	44	9	4.643	45 (47)	2.068
SPARC	28	7.2	2.540	77 (75)	2.156
Radiator	17	6	1.140	150 (148)	2.550

The electron beam is injected in a sequence of undulators with parameters listed in Table IV, where the first two operate as modulating sections, eight modules with the same characteristics of the SPARC undulators constitute the amplifying sections and a final radiator with shorter period may be tuned at the same resonant frequency of the previous one or at one of the higher harmonics to extend the spectral range of operation. This configuration may also operate in seeded mode where the seed may be externally injected in the first modulating sections, or self generated, superimposing an optical cavity to these two modules.

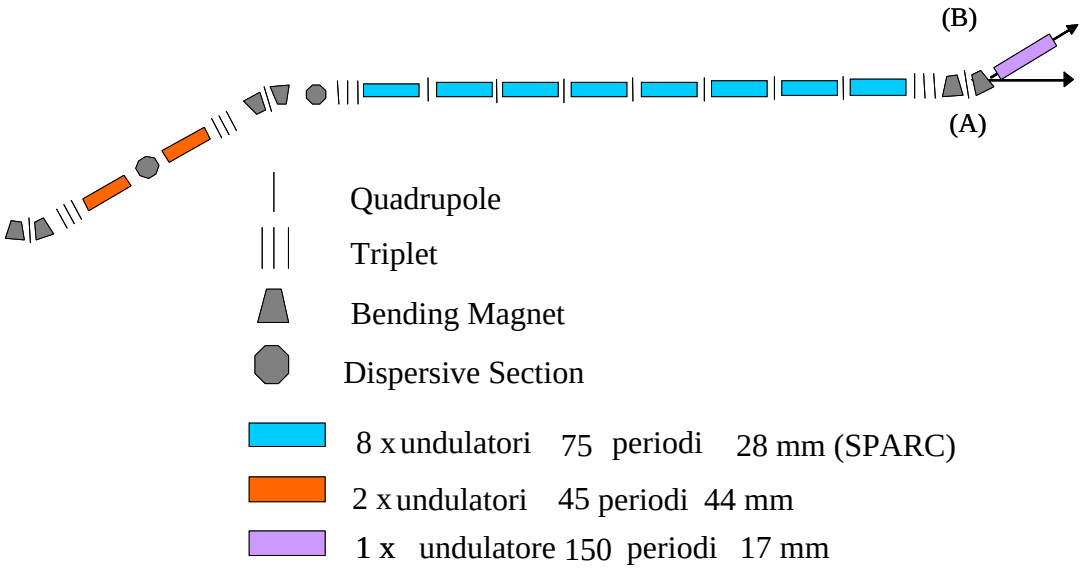

Figure 67: Layout of the SPARX FEL in the single pass configuration

The pure oscillator configuration designed by ENEA exploits a LINAC of moderate energy providing an e-beam of moderate brightness.

According to the above parameters (Table V), the FEL could operate at a wavelength of $121.5\,nm$, a spectral region where reliable mirrors exist. In Tab. VI we have reported the LASER intensity at the fundamental and the power associated with the higher order harmonics. As shown in Fig. 68 the rise time, necessary to reach these power levels is around 60 round trips, corresponding to $3\,\mu s$, if a 6 m long cavity is used.

Table V. SPARC-X FEL OSCILLATOR PARAMETERS

E	**500 MeV**	σ_τ	$1\,ps\,(fwhm)$
I	**600 A**	λ_u	**0.056 m**
Q	**0.6 nC**	**K**	**2.5**
σ_ε	$5\cdot 10^{-4}$	**N**	**50**
$\varepsilon_n^{x,y}$	$2\,mm\cdot mrad$	μ_c	0.2

Table VI Fundamental and higher order harmonic intensities

$n=1, \lambda \cong 120nm,\ \hat{P} \cong 2.310^6\ \frac{MW}{cm^2}$
$n=3, \lambda \cong 40nm, \hat{P} \cong 10^4\ \frac{MW}{cm^2}$
$n=5, \lambda \cong 24nm,\ \hat{P} \cong 2\cdot 10^3\ \frac{MW}{cm^2}$

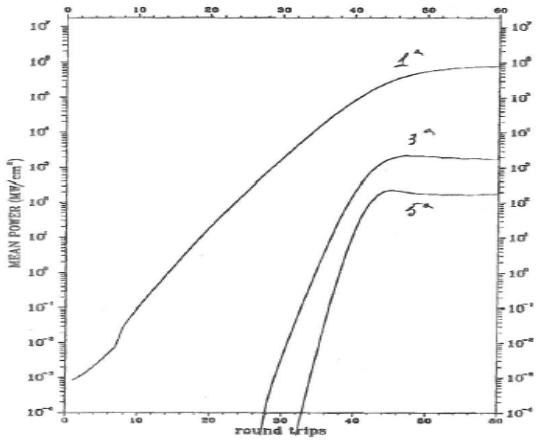

Figure 68: Intracavity evolution of fundamental and higher order harmonics, for the cavity adjusted at the maximum gain of the fundamental

We believe that the FEL-oscillator-amplifier configuration along with other solutions, involving seeding may be very flexible and offer an interesting source of radiation, which may be exploited for other interesting purposes illustrated below.

2.5 Futher developments

The intracavity backscattering of FEL photons may provide a very intense flux of gamma rays, which can be exploited for research in nuclear physics and for the production of polarized positron, which is an issue of paramount importance for the design of

experiments involving high energy collision of $e^{\pm}$ beams. The dominant processes in these experiment are (see Fig. 69) Annihilation (s-channel) and Scattering (t-channel)

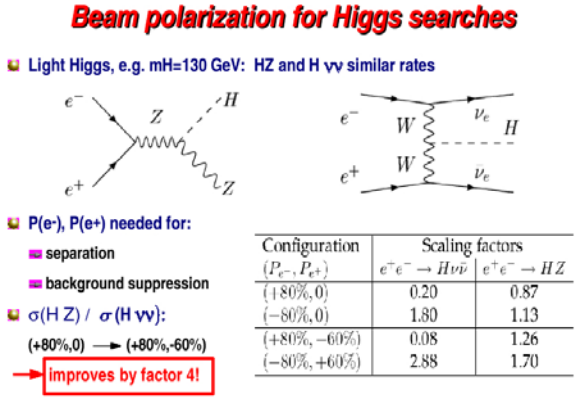

Figure 69: Annihilation and scattering of polarized electrons and positrons

In the first case the beam helicities are coupled to each other by the spin of the exchanged particle in the s-channel, in the standard model $J=1$ only is possible. The detection of a different spin state could be a proof of a violation of the SM. On the other side in the t-channel the helicities of the colliding beams are coupled to the chirality of the produced particles. The possibility of adjusting independently the polarization of both beams offers a unique opportunity of testing the properties of the produced particles. Polarized positrons can be produced from (A) conventional sources in which a high energy beam of electrons hit on a target and shower with positrons, which are eventually injected into a damping ring, or (B) with helical undulators, in which a high energy e-beam produces brehmsstrahlung gamma photons which are then converted into electron positron pairs. Compton backscattering of laser photons, the mechanism is essentially the same of, the only difference being that the laser beam replaces the static undulator. The use of the pulse stacking cavity shown in is foreseen as an element enhancing the rate of backscattered photons.We propose the use of the intracavity Compton backscattering of Free Electron Laser photon, with a natural pulse stacking. In Fig. 70 we report the scheme for the production of polarized positrons obtained via the conversion of gamma rays obtained through the Compton backscattering of a Nd:YAG laser pulse from 1.3 GeV electrons. The polarized electrons are then injected in a second linac section and brought to an energy of 2.4 GeV to be successively injected into a pre-damping- accumulator ring.

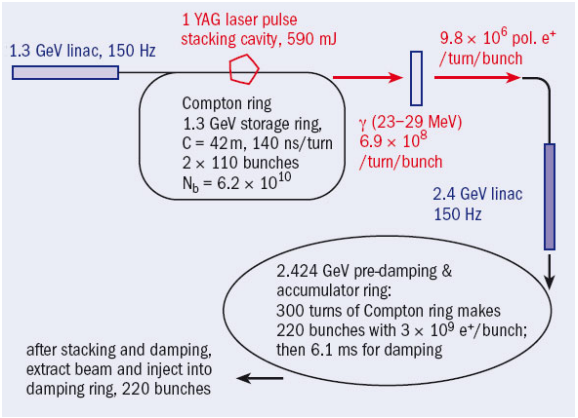

Figure 70: Scheme for the production of polarized positrons

The device leading to the production of polarized positrons consists in an integrated system which foresees

1. A FEL oscillator, which is exploited to produce intracavity photons in the range of 100 nm
2. An intracavity backscattering, with the production of gamma rays with energy around *40 MeV*
3. The separation of the electrons and positrons and the successive capture which in Linac sections, which bring the electrons at energy around 4-5 GeV
4. The injection of the accelerated beams into two damping accumulators rings
5. The extraction of the beams making to collide in a colliding section

The numbers we have obtained from our simulations yield the possibility of opening new fields of research.

3. Photonics Micro- and Nano-structures Laboratory

3.1 Mission and infrastructures

Photonics has been recognized by the European Commission as one of the key-enabling technologies for the future. The major challenges in the modern world, solution for health, energy, environment, information and communication technology (ICT), safety and security, are driven in their development by the production and manipulation of photons, the basic unit of light.
In the next years, photonics device miniaturization techniques based on functional combination of nano-structures will allow to meet these challenges.
The Photonics Micro- and Nano-structures Laboratory (UTAPRAD-MNF) is mainly focused on R&D of novel photonics micro-components, radiation detectors and nano-structures for scientific (high-energy physics, biomedical imaging diagnostics, aerospace, cultural heritage) and industrial (ICT, transport, infrastructures, seismic prevention) applications, as well as innovative energy production systems, including nuclear.

At MNF laboratory the experimental activities on the synthesis and functionalisation of nanomaterials and thin films together with high-level competences and instrumentation for advanced characterisation by optical and electronic spectroscopies are combined with consolidated expertise in applications of optical fibre sensors for structural monitoring and activities in seismological field.

The R&D activities are mainly focused on:

- **realization and optical characterization of photonics micro-components**: broad-band miniaturised solid-state light emitters, including laser and optical amplifiers in waveguide and micro-cavity configurations, based on point defects in insulating materials; broad-band miniaturised solid-state light emitters based on organic thin films, including OLEDs; optical fibre FBG (Fibre Bragg Grating) sensors;
- **development of innovative thin-film radiation detectors**: novel colour-centre based lithium fluoride thin film imaging detectors (for extreme-ultraviolet radiation, soft and hard X-rays, low-energy electrons and ions, gamma-rays, thermal neutrons, etc); novel photo-detectors based on organic thin films and plastic scintillating materials;
- **synthesis, functionalisation, and characterization of nanostructures:** synthesis and electronic characterization of semiconductor nanowires and carbon nanotubes, insulating and metallic nano-structured thin films and substrates; laser assisted synthesis and chemical functionalisation of semiconductor and insulating nanopowders;
- **development of structural monitoring systems and seismological activities**.

The reduction of energy consumption and the improvement of energy efficiency is based in many areas on “Green Photonics”. Cost-effective Organic Light Emitting Diodes – OLED’s, are one aspect. Highly efficient organic and conventional solar cells are another one. The search for novel production methods of sustainable energy is a crucial goal.
Novel optical diagnostic methods as well as imaging microscopy techniques, even in different spectral ranges, will lead to a better understanding and improvements of tools and instrumentation for life science progress.

The development of basic micro-components, like compact light-sources, detectors, optical fiber gratings make possible industrial innovation in optoelectronics- and photonics-related products as lasers, lighting, displays, and sensors.
On the basis of high-level competencies, the MNF staff carried out technical and professional training of researchers and students, with national and international universities and research institutions. Technical contacts are frequent and fruitful with several small and medium companies operating in the field of optical components, spectroscopy, microscopy, lasers, and vacuum evaporation systems.

Available infrastructures include well equipped laboratories for photonics material synthesis and characterization:

- evaporators for inorganic/organic films growth;
- optical spectroscopy and laser confocal microscopy laboratories;
- plants for laser assisted synthesis of nanopowders (LUCIFERO), nanowires and carbon nanotubes
- electron spectroscopy laboratory;
- Interferometry and fiber optical sensor laboratory.

3.1.1 Funding and projects

In 2010 MNF major funds came both from national project of industrial research supported by MIUR (such as TECVIM and MAMAS) and from European projects (Framework Programme in the NMP area, such as BONSAI and HENIX).

3.2 Organic thin films for OLED and photo-detectors

In last decades organic compounds brought a technological revolution in the field of light sources. The most studied low-molecular weight molecule is a metal-chelate, tris (8-hydroxy-quinoline) aluminum (Alq_3), commonly vacuum deposited as the active layer in green OLEDs, based on thin film technology. There has been a large interest in these new materials for flat and flexible panel displays and for low-consumption solid state illumination. In recent years, there has been a great deal of interest also in organic semiconductors for solar cells and radiation detectors.

Many efforts have been devoted to increase the lifetime of these encapsulated devices above the standard value of 10.000 h at initial display brightness (luminance) of 100 cd/m^2 by studying the effects of several degradation processes, primarily associated with degradation mechanisms of the electrode materials and electrode/organic interfaces, and exposure of transporting molecular layers to ambient factors, like moisture and oxygen.

Nowadays, their degradation is one of the challenging issues of basic and applied research in the field, and chemical and physical mechanisms of these complex phenomena are under study (ENEA patents) by optical spectroscopy techniques and advanced imaging microscopies in the framework of the activity “Organic thin films for OLEDs and related materials characterization” within the TECVIM (TEcnologie per la VIsualizzazione di IMmagini) project (MIUR FAR) led by CRF (Centro Ricerche FIAT) together with ENEA Frascati (UTAPRAD) and ENEA Portici (UTTP) under UTAPRAD coordination.

3.2.1 *Thermal evaporation and spectroscopic characterization of Alq_3 thin films for* OLED

At UTAPRAD-MNF, the solid state laboratories are equipped with thermal evaporation systems for organic-dielectric multi-layered films growth, a laser scanning confocal microscope and spectrometers for absorption and emission linear optical spectroscopy. The photo-bleaching effects caused by selective ultraviolet and blue-light illumination on the photoluminescence spectra of thermally evaporated Alq_3 thin films exposed in air were investigated by fluorescence spectroscopy and advanced optical imaging (Fig.71). The PL intensity time behavior observed in the Alq_3 films at different excitation powers allows to establish that Alq_3 molecules in their excited state are involved in these complex phenomena. The photo-bleaching processes were exploited for direct laser-patterning of the investigated Alq_3 thin films at micrometric levels in a confocal laser scanning microscope (Fig.71).

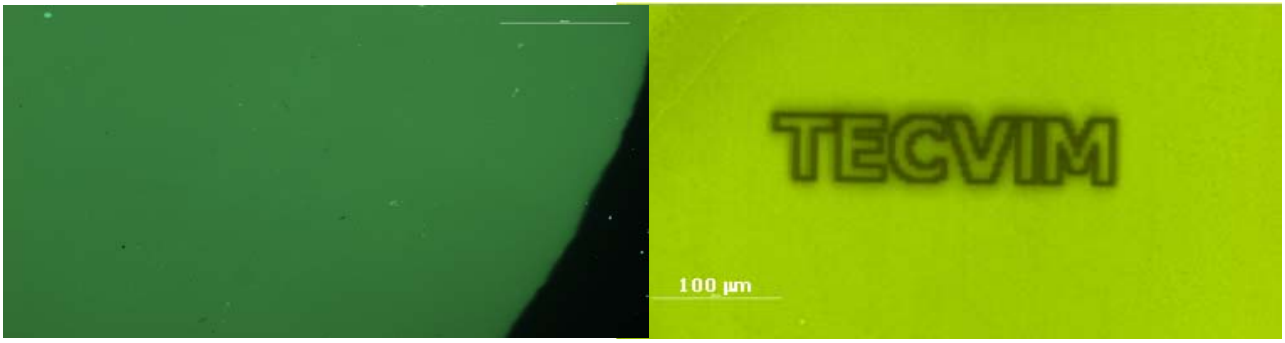

Fig.71. Fluorescence image, at low magnification under blue excitation, of an Alq_3 film, 50 nm thick, thermally evaporated on a glass substrate (left). Fluorescence image, observed under blue illumination, of a bleached pattern, the word TECVIM, directly written by the 457.9 nm line of an argon laser in the confocal microscope, on an Alq_3 thin film thermally evaporated on a glass substrate (right).

Conventional and confocal optical microscopies were successfully used for checking the quality of commercially available OLED displays (Fig.72).

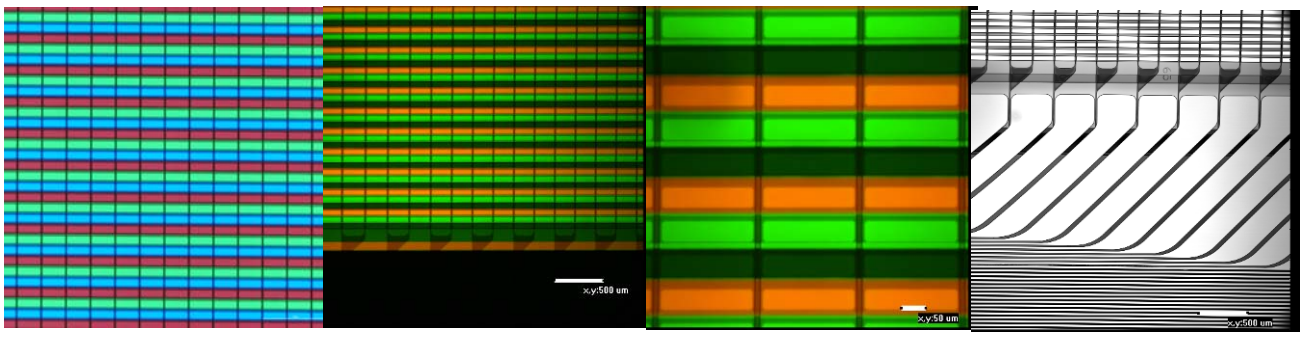

a) b) c) d)

Fig.72. Optical images of a commercial OLED display, 128x128 dots: wide-field conventional fluorescence under UV excitation, a); confocal fluorescence under argon laser excitation at 457.9 nm with two different magnification, b,c); confocal in reflection mode under the same laser illumination, d).

Laser Induced Breakdown Spectroscopy (LIBS) is a spectroscopic technique that allows the elemental composition of a sample to be determined by the analysis of the plasma produced by the interaction with a laser beam, in specific experimental conditions. Results obtained on an Alq3 and a LIF thin film are reported in Fig. 73.

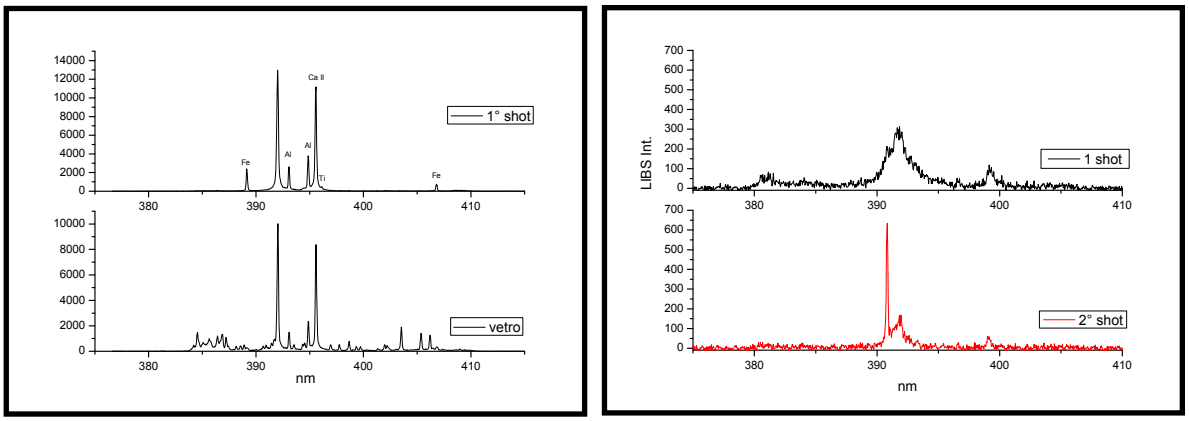

Fig.73. LIBS spectrum, in the wavelength range centered at 296 nm, of an Alq_3 thin film (thickness 300 nm) on glass substrate. LIBS spectrum of glass is reported for comparison (left). LIBS spectra of a LiF thin film (thickness 360 nm) on silicon substrate at 1st and 2nd laser shot (right).

3.1.2 Advanced optical spectroscopy of organic thin films for photo-detectors

The advanced optical (in collaboration with UTMAT-OTT, ENEA Casaccia) and spectroscopic characterization of organic thin films has been extended to TetraPhenil-Butadiene (TPB), which is the preferred material for the detection of ultraviolet (UV) radiation in modern particle detectors based on liquid Argon, especially for direct Dark Matter search. Like other organic substances, it exhibits an intense broad emission band in the visible spectral interval, peaked at around 430 nm, under light excitation at smaller wavelengths (Fig.74).

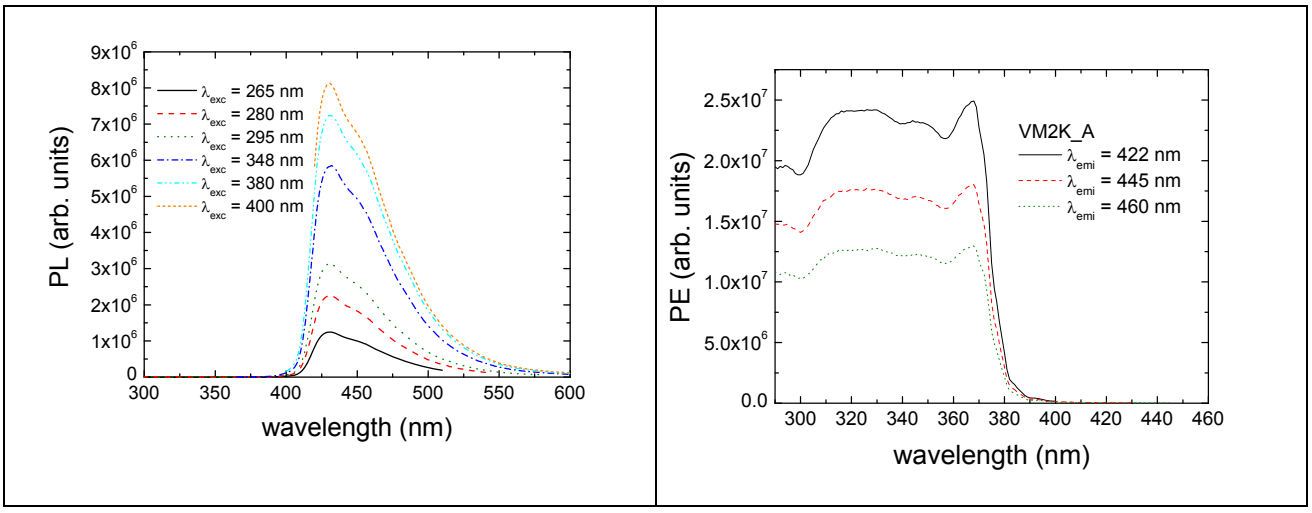

Fig.74. Photoluminescence (PL) spectra of a surface layer of TPB grown on a VM2000 foil (left). Photoexcitation (PE) spectra of the 3M VM2000 dielectric reflector foil used as substrate (right).

Although some measurements in the Vacuum UV (VUV) range were performed in the past in order to establish its conversion efficiency, a complete and systematic characterization in the optical spectral range is still missing. This activity was started under a Research Contract with INFN-LNGS, and it is going on in collaboration with the Physics Department of the Rome Tor Vergata University.

3.3 Nano-structured thin films for OLED and PV innovative cathodes

Organic Light-Emitting Devices (OLED) as well as photovoltaic (PV) devices require an easy charge injection and electron transfer to the cathode-organic interface. That is obtained for cathodes by using low work function and chemically stable materials.

3.3.1 XPS characterization of nano-structured LiF-based thin films for OLED

At UTAPRAD-MNF, the thin film growth and electron spectroscopy laboratory is equipped with a growth chamber for the synthesis of thin films and nano-structures connected with a Ultra-High Vacuum (UHV) system for in-situ electron spectroscopy of surfaces and interfaces (Fig.75). The growth techniques used are Physical Vapour Deposition (PVD), thermal and laser-assisted Chemical Vapour Deposition at low pressure (LPCVD) and Pulsed Laser Ablation (PLD) by using an excimer laser. The spectroscopy techniques available are X-Ray Photoelectron Spectroscopy (XPS) and X-Ray excited Auger Electron Spectroscopy (XAES) performed by means of a newly commissioned monochromatised Al K_α soft-X-Ray source and a hemispherical energy analyser.

The LiF/Al system has been indicated as an acceptable compromise between chemical stability and low work function cathode for OLED. A LiF thin film deposited on an Al surface allows the lowering of the metal work function. Therefore, it is crucial for the understanding of the underlying charge transfer mechanisms at the metal/insulator interface to investigate the electronic properties of LiF thin films. In this framework, LiF film grown by Xe-Ion Assisted Deposition (IAD) have been studied by XPS and compared with the XPS data obtained from LiF single crystals.

Fig.75. Detail of the UHV analysis chamber with the monochromator spot visible on a fluorescent sample.

Figure 76 shows the XPS Li1s core level (blue dots) measured on a LiF crystal and superimposed to the Li1s spectrum (red line) taken on a LiF thin film grown by 150eV IAD. The LiF IAD spectrum shows a clear broadening in comparison with the reference LiF crystal. Moreover, a new feature at about 6-7 eV towards higher binding energy is observed in the IAD XPS data. A quantitative analysis of the data has shown that the IAD LiF Li1s core-level lineshape can be explained by the presence of metallic Li at the surface. Thus, the observed broadening of the Li 1s core level as compared to the LiF single crystal is due to the contribution of an additional peak

on the lower binding energy side accounting for photoemission from metallic-like Li. Consequently, the metallic Li is causing the excitation of the correlated plasmon observed in accord with the literature at 6-7eV apart. The metallic Li contribution in the IAD LiF Li1s spectrum can be extracted by subtracting the LiF crystal Li 1s reference XPS data from the IAD LiF spectrum as shown by the data in the inset of Fig.76.

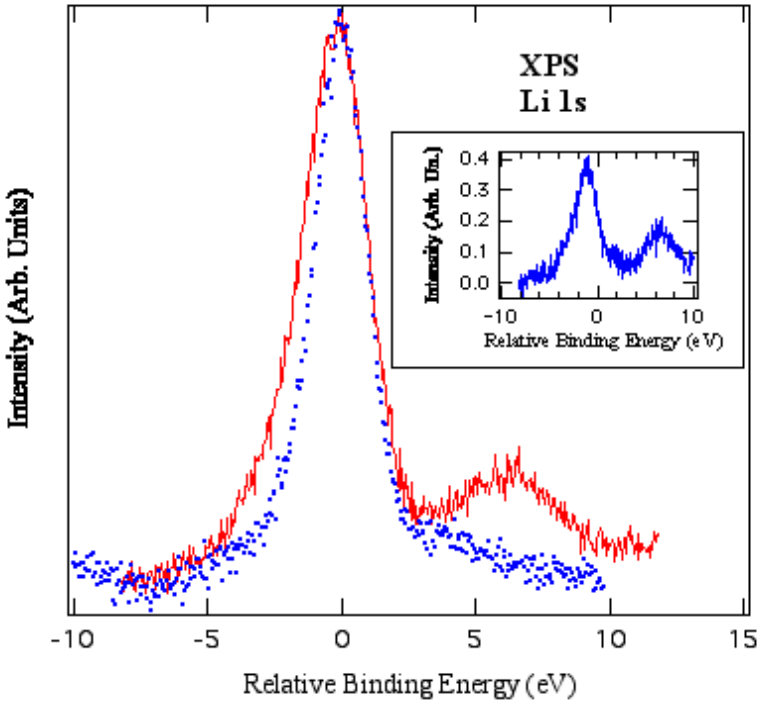

Fig.76. XPS Li 1s core-level spectra measured on a LiF single crystal (dotted line) and on a Xe-ion-assisted LiF sample thin film (continuous line). A constant background has been subtracted from the two spectra before normalization to the same height. The inset shows the difference spectrum obtained by subtracting the Li1s peak in LiF from the Li1s peak in the 150eV IAD LiF sample. The Li 1s intensity in LiF used in the subtraction has been scaled by a factor obtained from the results of a least-squares fitting analysis.

3.3.2 Silicon nanowires growth for photovoltaic applications

Nanowires and nanotubes are intensively studied because of their promising applications in the field of photonics, nanoelectronics and, recently, in photovoltaics.

Among a wealth of nano-structures being investigated, Si-based nanowires are the subject of enhanced research because they are easily integrable into the microchip technology cycles. Among the several ways to grow Si nanowires (SiNWs), the most common is the “seeding” of the substrate with a suitable metal: a thin metal layer is deposited in form of nanometric dots which turn out to be the origin of the nanowires. In fact, the metallic dots are preferential places for cracking the gas phase precursor molecules and subsequent accumulation of Si atoms during the Low-Pressure Chemical Vapour Deposition (LPCVD) growth process.

In order to study their growth and morphology, Si nanowires have been synthesized by LPCVD using disilane as the precursor on several types of Si substrates, e.g. atomically clean Si, SiO_2 and microcrystalline Si, the latter obtained by annealing of amorphous Si layers. The deposition steps were monitored by XPS. Au nanoislands are usually deposited on the substrates at room temperature by thermal evaporation with a following LPCVD growth for the nanowires’ synthesis. Figures 77 show an example of SiNWs obtained on an ordered and polycrystalline Si surface, respectively.

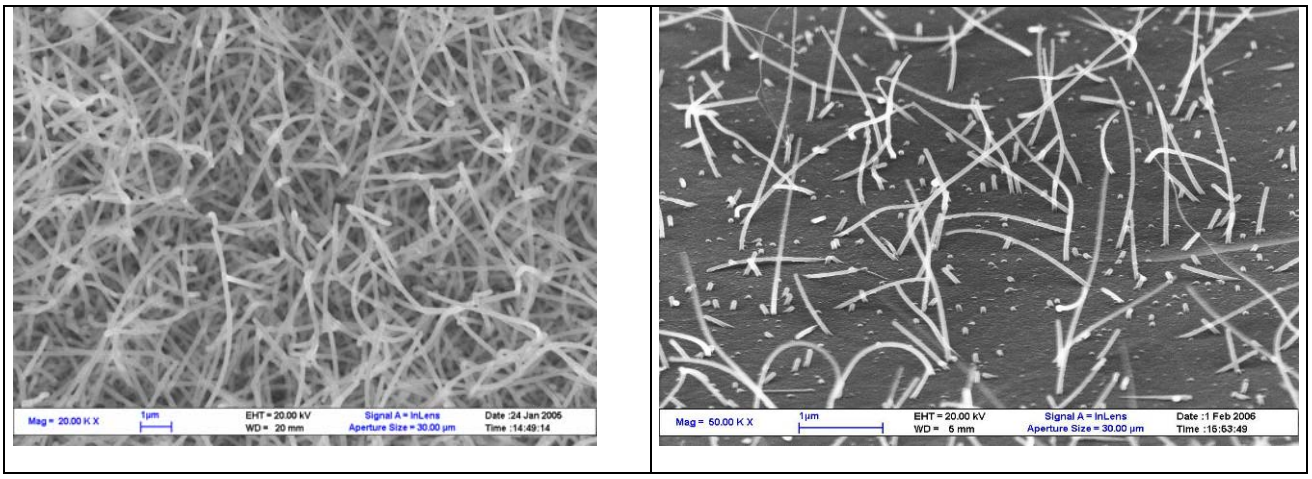

Fig. 77. SEM images of SiNW grown on a crystalline Si(100) surface after deposition of 2Å Au using Si_2H_6 as the precursor gas (right); SiNW obtained on a polycrystalline Si surface exposed to Si_2H_6 after deposition with 3Å Au (right).

Nowadays, most of commercial solar cell modules are based on crystalline Si. However, thin film solar cell technologies are developing quickly. Recent advances in thin film solar cell technology have shown that a promising evolution is represented by the addition of nanostructures to enhance the light conversion efficiency or, even, to use the nanostructures as the fundamental building blocks for the cell architecture. In order to study a possible light conversion behaviour, in collaboration with the Physics Department of the Rome Tor Vergata University, we have constructed prototype cells by adding ohmic contacts to our SiNW grown on Si substrates and measured the I-V (current-voltage) curves and the Incident Photon to electron Conversion Efficiency (IPCE) (not shown).

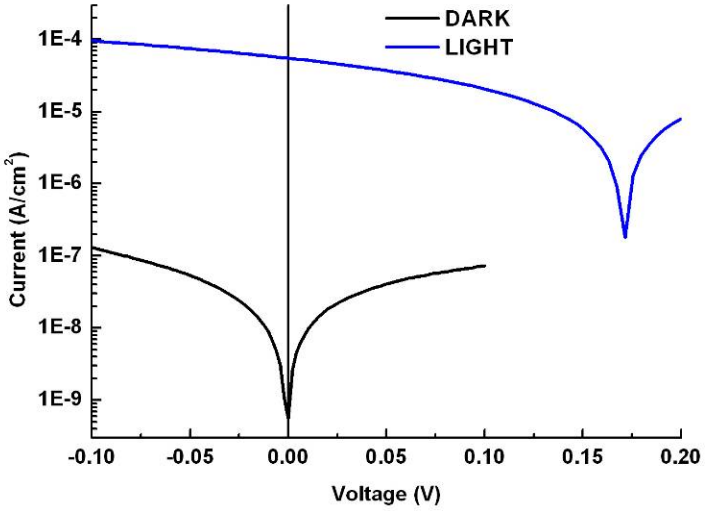

Fig.78. I-V curves of a prototype SiNW cell.

The black and the blue curves shows the I-V characteristics in absence and in presence of light, respectively.

As it can be seen in Fig.78, the I-V graph of the SiNW cell shows a clear change of the shortcut current I_{SC} and of the open circuit voltage V_{OC} when illuminated with light. Although this very basic cell configuration gives, as expected, low current and conversion efficiency values, it is a promising starting point for further developments.

3.4 Luminescent materials for miniaturised radiation detectors, novel light-emitting devices and bio-imaging

3.4.1 High resolution imaging radiation detectors based on luminescent colour centres in LiF thin films

Color Centers (CC) can be produced in LiF crystals and films by different kinds of ionizing radiation, like particles (high and low-energy electrons, ions, neutrons) as well as photons, like gamma, X-rays, short-duration femtosecond laser pulses. Optical spectroscopy and microscopy are fundamental tools for understanding the relations between point defects, light emission properties and material characteristics.

At UTAPRAD-MNF, in the solid state laboratories, novel LiF thin-film X-ray imaging detectors, based on the visible photoluminescence of F_2 and F_3^+ intrinsic electronic defects, have been realized and tested in the energy range from 20 eV to 10 keV. They show interesting peculiarities, like high spatial resolution on a large field of view, wide dynamic range, good sensitivity, versatility and simplicity of use, as it is insensitive to visible light and it does not need any development after exposure. These properties, combined with opportunities offered by different types of intense laboratory X-ray sources (table-top laser plasma produced sources, X-ray lasers, compact X-ray tubes, in collaboration with Rome Tor Vergata University, L'Aquila University, CNR-IFN Rome), as well as large scale facilities (synchrotrons, free electron lasers), makes their application very attractive in physics as well as in life sciences.

The intrinsic spatial resolution of the luminescent LiF-based imaging plates is related to the CC dimensions, of the order of the atomic scale (~ 1 nm), but in practice it is limited by the optical microscopes and techniques utilized as detection system. By using advanced optical microscopes as readout instruments, like Confocal Laser Scanning Microscope (CLSM) optical fluorescence images with sub-micrometric and nanometric spatial resolution can be obtained.

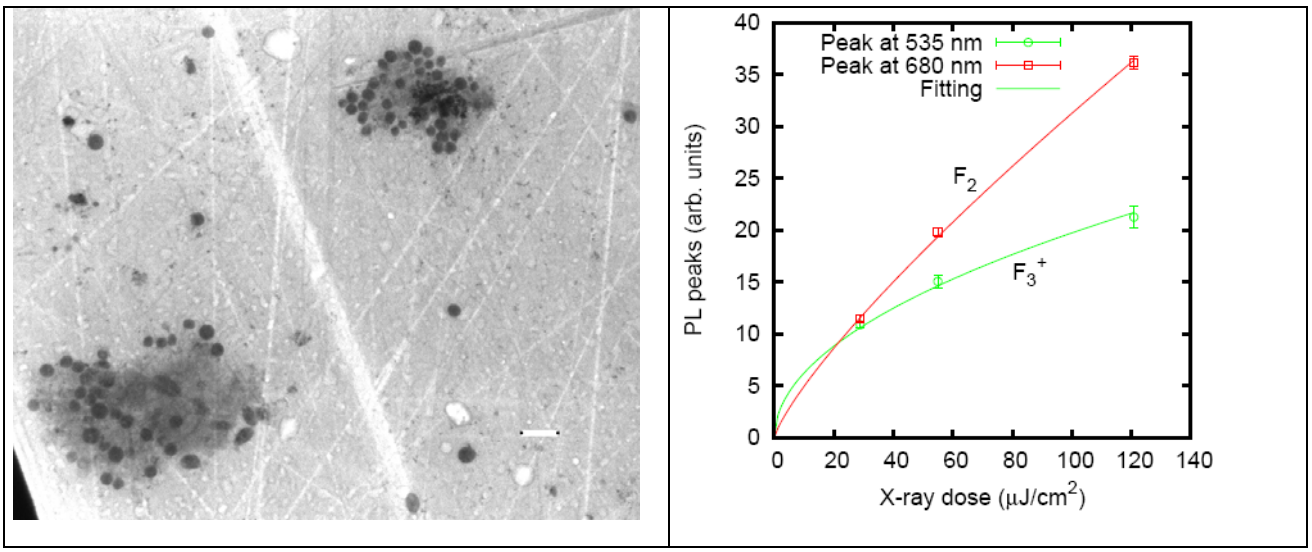

Fig.79. Confocal fluorescence image of a soft X-ray micro-radiography on a LiF crystal of *Chlorella* cells obtained *in vivo* in a contact single-shot experiment in the water window spectral range in a laser plasma source (collaboration Rome Tor Vergata University), (left). Intensities of PL spectra peaks at 535 nm (F_3^+) and 680 nm (F_2) of LiF films (thickness ~ 1 μm, glass substrates) irradiated at different doses by soft X-rays from a laser plasma source with a copper target, (right). The experimental data (points) were reported with the corresponding fitting curves (solid lines).

The improvements of the LiF-based detector sensitivity and response are particularly important in X-ray imaging experiments (Fig.79) for reducing the irradiation doses and consequently the sample damage due to the radiation exposure, especially for biological specimens (in collaboration with the DIM laboratory). The choice of polycrystalline LiF thin films grown on different substrates allows one to obtain high resolved images even when more penetrating X-rays are used (Fig.80), as the colour centres formation is limited in depth by the film total thickness.

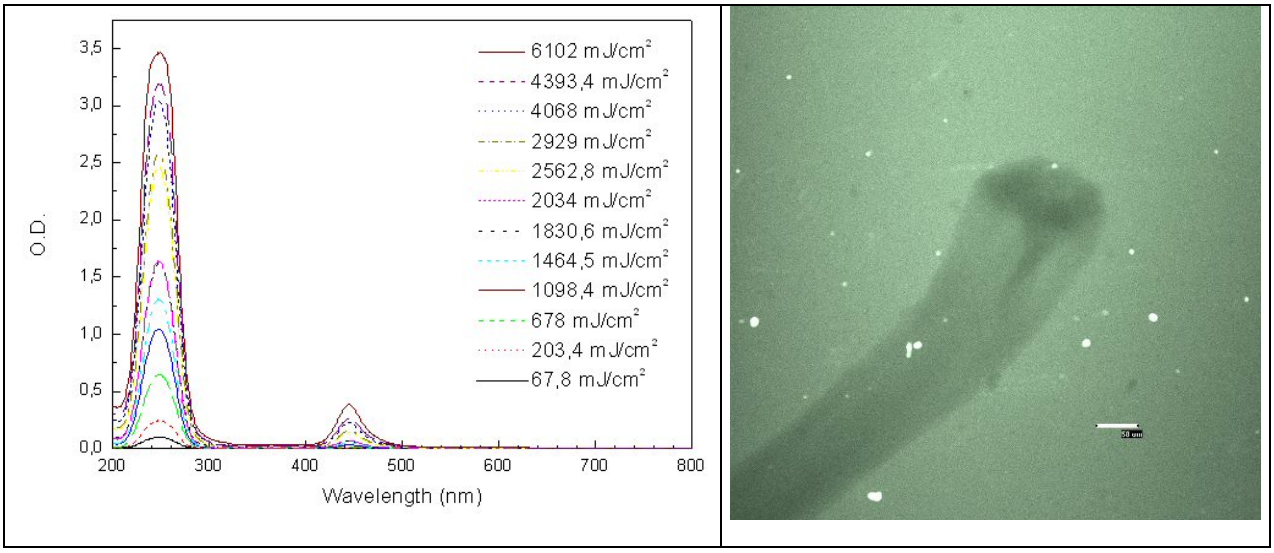

Fig.80. Room temperature optical absorption spectra of X-ray coloured LiF crystals irradiated at several doses in air by a laboratory X-ray tube with a Cu anode (collaboration Rome CNR-IFN). The blank crystal contribution has been subtracted (left). Confocal fluorescence image of a man-hair bulb X-ray microradiograph stored on a 1.4 μm thick LiF film grown on a silicon substrate, under laser excitation at 457.9 nm. The reference line is 50 μm.

The direct-writing of photoluminescent nanopatterns in LiF crystals and films by using an interferometric encoding technique based on a coherent soft X-ray laser (collaboration L'Aquila University) was achieved (Fig.81). CLSM operating in fluorescence mode results a very appropriate and efficient technique to investigate these optically active micro and nano-structures. The possibility to grow LiF thin films on different substrates with controlled thicknesses increases the versatility and the efficiency of the LiF-based photonics structures, that could be integrated in more complex photonics devices.

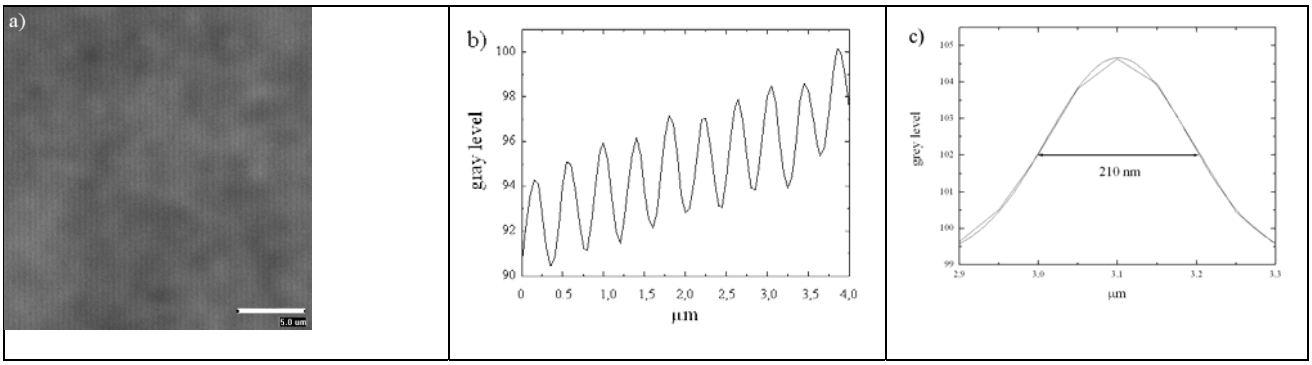

Fig.81. a) Confocal fluorescence image of a photoluminescent periodic pattern based on visible-emitting colour centres stored on a LiF film of thickness 600 nm on a glass substrate under argon laser excitation; b) grey level profile of a horizontal line of the photoluminescent pattern reported in a); c) grey level of a single line of the luminescent periodic structure with a best-fit Gaussian curve showing a FWHM of ~ 210 nm.

3.4.2 Luminescent materials: effect of heavy metals doping in LiF crystals

An important aspect in dosimetry applications is that LiF crystals can be doped with special impurities to enhance their sensitivity. The presence of some impurities modifies the structural and optical properties of the LiF crystals.
The evidence of the incorporation of Pb^{2+} ions in the LiF matrix and their stability during annealing procedure was investigated by optical spectroscopy (absorption and photoluminescence) and by X-ray Absorption Spectroscopy (XAS) measurements, performed at the European Synchrotron Radiation Facility, ESRF, Grenoble, in the framework of the international GILDA proposal N. 08-01-839, "Study of Pb dopants in Lithium Fluoride single crystals", coordinated by MNF and approved for 2010. This activity was inserted in the Collaboration Agreement between ENEA, the Dep. of Physics of Third University of Rome, and CNR-ISM Tor Vergata on "Realizzazione e caratterizzazione ottica avanzata di strutture mesoscopiche in film dielettrici per applicazioni nella fotonica e nanofotonica" (2007-2010), in collaboration with partners in Romania. Optical measurements performed on LiF:Pb crystals were able to reveal the incorporation of Pb ions in the LiF matrix, even in very low concentrations. X-ray absorption near-edge structures (XANES) data reveal that Pb is present as Pb^{2+} whereas EXAFS data show that it is incorporated in the crystal and not forming PbF_2 precipitates.

3.4.3 Luminescent nanomaterials: Si nanoparticles doped with Ytterbium

Silicon nanocrystals (SiNC) are being extensively investigated because of their widespread potential applications ranging from photonics to photovoltaics and even to biological imaging. Oxide-coated particles are well suited for biological imaging applications since they are stable, efficiently emitting, and moreover their surface can be easily functionalized for bioconjugation.

At UTAPRAD-MNF, the nanopowders laser synthesis laboratory was successful in preparing Si nanoparticles with controlled particle size and morphology as well as the surface properties, and, as a consequence, with different optical properties. It was a partner in two different projects: european project BONSAI "Bio-imaging with Smart Functional Nanoparticles" (FP6), and Italian national project TECVIM "Tecnologie per sistemi di visualizzazione immagine" (MIUR FAR), within which the task was to produce luminescent nanoparticles for bioimaging or luminescent inks, respectively.

Si nanocrystals were produced in the laser-assisted silane pyrolysis reactor "LUCIFERO" at the UTAPRAD-MNF Laboratory and their luminescence properties were optimized by varying laser synthesis parameters and by post synthesis treatment. Chemical processing and PL measurements were performed in collaboration with the UTTMAT-SUP laser spectroscopy laboratory. It was tried also an alternative route in order to tune the PL emission range from Si nanocrystals, *i.e.* the link of luminescent rare earths (RE) ions to the Si nanoparticle surface. In this system, the Si nanoparticles act as sensitizer (antenna) for the rare earth emission (Fig.82).

The selected rare earth ion is Ytterbium(III) because of its ($^2F_{5/2}$) - ($^2F_{7/2}$) luminescent transition at 980 nm that is commonly used in bioanalitycal

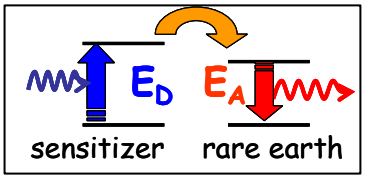

Fig. 82 – Mechanism of energy transfer from the sensitizer (Si) to the rare hearth (Yb).

applications. The f-f transitions are parity forbidden and, as a result, the absorption coefficients are very low and the emissive rates are slow, which results in long-lived and line-like emission bands. As a consequence, direct excitation of the lanthanide ions is unfavourable. A way to overcome the difficulties of low absorptivity and thermal relaxation is to incorporate lanthanide ions in a host matrix: the matrix is excited above the band-gap energy and, after energy transfer, the lanthanide ion emits.

Several methods have been developed for the preparation of discrete lanthanides-doped SiNC. At ENEA it was developed an innovative approach for Yb and SiNC, based on the aptitude of Yb to form complexes with amino groups. SiNC produced by laser pyrolysis with diameter equal to 8 nm and 6 nm, were first functionalised with aminopropyltriethoxysilane (APTES) and then doped with Yb(III) (Fig.83).

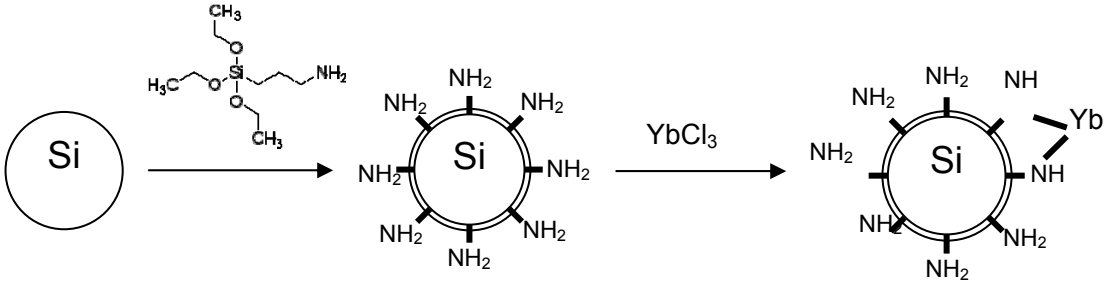

Fig.83. Schematic of the chemical route to dope Si nanocrystals with Yb-ions.

A thermal treatment is necessary in order to recover luminescence, as already reported in literature for sol-gel systems containing Si and Yb, but in the latter case a very high temperature is needed. On the other hand, our method is very convenient because the reaction takes place at room temperature and the thermal treatment occurs at a moderate temperature (300°C), so that the SiNC are not modified.
The Yb-doped SiNC showed sharp emission peaks at wavelengths around 1 μm (as shown in Fig.84). PL spectra are recorded by using laser excitation at 532 nm, where the Yb ions do not absorb, to ensure that the excitation of Yb ions occurs through energy transfer from SiNC. As expected, the intensity of the PL emission from SiNC-Yb prepared by using different SiNC/Yb ratios was found to increase as the quantity of Yb increases.

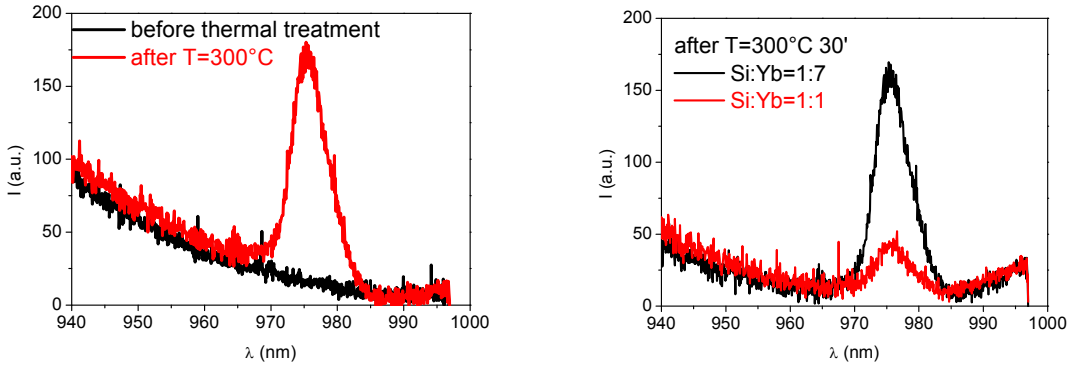

Fig.84. PL emission from Yb-doped Si NC before and after the thermal treatment at T=300°C (left). PL emission from Yb-doped Si NC prepared with different SiNC/Yb ratios (right).

In Fig.85 the excitation spectrum of SiNC-Yb is reported. The shape of the spectrum is compatible with that of SiNC absorption. The possibility of wide-band excitation, and particularly with near UV sources, is fairly evident.

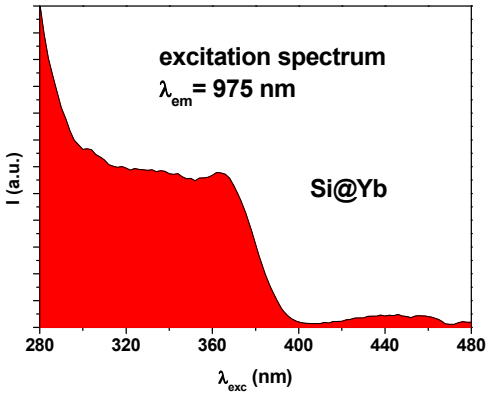

Fig.85. Excitation spectrum of Yb doped silicon nanoparticles

This methodology can be applied, in principle, to other RE (rare-earths)-Si-based nanocrystals, allowing to tune the PL emission in a wide range of wavelengths.

3.4.4 Broad-band light-emitting waveguides written in LiF crystals by femtosecond laser

Lithium fluoride containing colour centres represents a very interesting material to fabricate light-emitting devices. LiF-based colour-centre waveguides were produced in LiF crystals at different penetration depths by using direct-writing with femtosecond laser pulses (collaboration Brazilian Universities). The optical waveguides were characterized by optical microscopy (laser confocal imaging), near field profiling, optical emission spectroscopy, scattering and insertion loss measurements (collaboration Rome University "Sapienza").

The waveguides were preliminary characterized by an optical microscope NIKON Eclipse 80i equipped with an Argon laser at 458 nm operating in reflection and fluorescence mode. In the fluorescence operating mode, the photoluminescence signal is detected by a system of two photomultipliers. Figure 86 shows the confocal images of three channel waveguides in a LiF crystal obtained illuminating with the 457.9 nm line of the argon laser in the common absorption band of F_2 and F_3^+ CCs and detecting their emissions. Photoluminescence spectra of CCs permanently produced in the LiF waveguides during the writing process were measured under optical excitation in the M absorption band of F_2 and F_3^+ CCs through the top surface of the crystal and collecting the emission by using a fibre bundle at waveguides output facet.

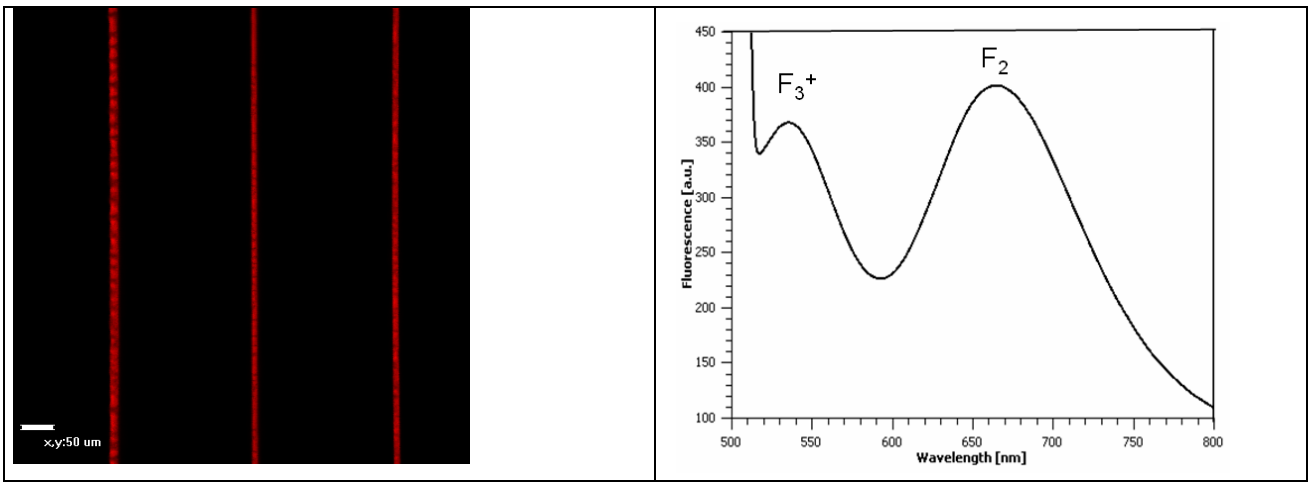

Fig.86. Confocal images in fluorescence mode of three active channel waveguides in a LiF crystal written by a fs laser (right). Photoluminescence spectra of CCs in a LiF waveguide (left).

The optical properties of these waveguides are promising for the development of LiF-colour centre waveguide lasers.

3.4.5 LiF thin films for thermal neutron detectors development

Measurement of thermal neutron flux is needed in several experimental and technological environments, in the field of nuclear applications as well as in the homeland security. Prompt detection would be advisable for instance in nuclear waste repositories, in order to provide signals from possible leaks of radioactive material from waste drums, or in the out-core zone of nuclear reactors in order to map the neutron field.

It is well known that the ^{6}Li isotope works as neutron to charged particles converter. The physical principle behind the technique is rather simple and well known: ^{6}Li, employed as neutron converter, has a capture cross section around 1000 barn for thermal neutrons that scales down as ≈1/v with increasing neutron energy. The excited ^{7}Li thus formed decays with 100% branching ratio into ^{3}H + ^{4}He, emitted back to back with a Q-value of 4.78 MeV, that is converted into kinetic energy, respectively 2.73 MeV to ^{3}H and 2.05 MeV to ^{4}He. The detection of these two decay products is at the basis of novel detectors development.

In the last years, at UTAPRAD-MNF, in the solid state laser laboratories, LiF films few μm thick, were directly evaporated starting from LiF material 94 % enriched in ^{6}Li, on the top Al electrode of artificial diamond neutron detectors, and successfully used to measure thermal neutrons in intense sources, like large experimental fusion devices (JET in UK) as well as in the TRIGA reactor at ENEA Casaccia, with very promising features (research collaboration with UTFUS-Frascati). Recently the feasibility of a compact and low-cost thermal neutron detector was investigated combining a neutron converter consisting of a circular thin film (5mm radius and 3μm thickness) of enriched LiF deposited on a 10x10x1mm^{3} glass plate with a bundle of nine plastic scintillating fibres coupled to two silicon photomultipliers (Fig.87).

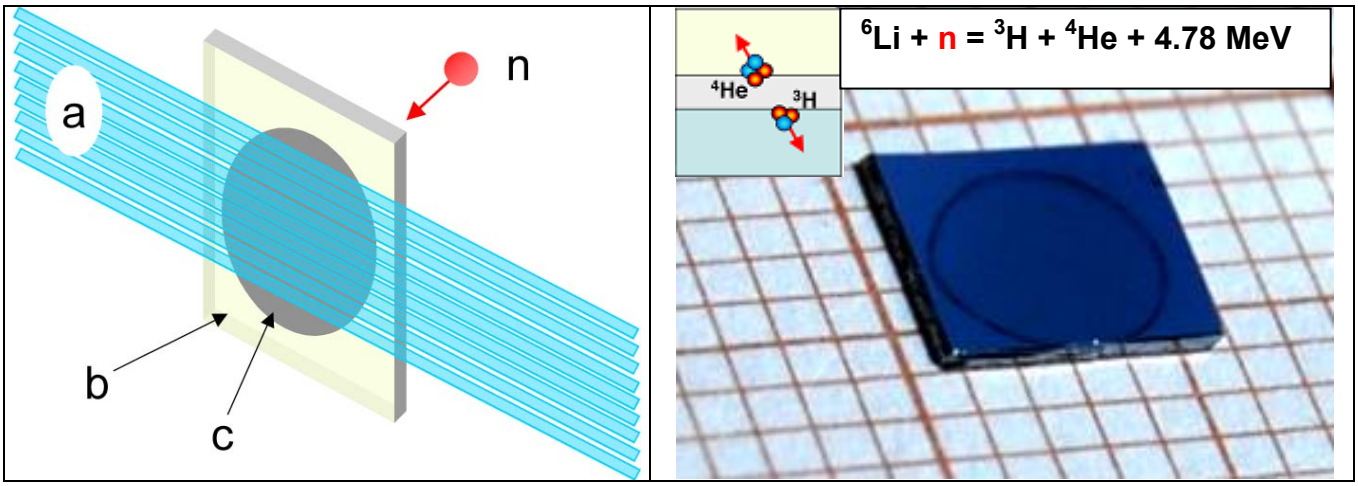

Fig.87. Sketch of the thermal neutron detector prototype. (a) scintillating fibre bundle; (b) glass substrate; (c) LiF film, 94% enriched in ^{6}Li; n is the incident thermal neutron (right). LiF film thermally evaporated on Si(100) substrate, thickness = 1.7 μm (left).

It proved capable of detecting thermal neutron capture events by means of the detection of the ^{3}H and ^{4}He decay products (collaboration INFN-LNS) and could allow to build cheap and compact detectors and dosimeters, opening new perspectives in terms of granular monitoring of neutron fluxes as well as space-resolved neutron detection.

3.5 Nanofluids from nanopowders for energy saving

Nanofluids have shown significantly enhanced thermal properties in comparison to traditional cooling fluids, by coupling significant technical benefit and commercial viability with environmental friendliness. The efficient removal of heat is one of the top challenges facing a number of industries, including microelectronics, transportation, manufacturing and power generation. With existing cooling technologies reaching their limit, innovative and more efficient cooling technologies are needed to support technological development and reduce the impact such technologies have on the environment.

At ENEA, UTAPRAD is participating in the Large Scale Integrated Project HENIX (Enhanced Nanofluids Heat-Exchange, FP7-NMP-2008), funded by the European Commission to produce high performance nanofluid coolants. In this Project, the task is the synthesis of nanopowders to be investigated as components for nanofluid production.

Nanopowders for the preparation of selected nanofluids are produced at UTAPRAD-MNF laboratory by CO_2 laser pyrolysis of gas-phase precursors. In particular, Si-based nanopowders are routinely prepared by silane in the presence of appropriate reactants (for example acetylene for the synthesis of SiC). Recently, the laser pyrolysis facility "LUCIFERO" was also equipped with an evaporator for using liquid precursors.
The characterization of the nanopowder samples was done in collaboration with UTTMAT-SUP, using the facilities for laser and optical spectroscopy of materials.

3.5.1 Preparation of TiO_2 nanopowders

The evaporating system was employed to produce nano-crystalline titanium dioxide, TiO_2, by laser pyrolysis of titanium tetraisopropoxide (TTIP). Ethylene or ammonia were used as sensitizer since TTIP does not absorb 10 μm radiation. Ammonia has, together with its good absorption of laser radiation to sustain the reaction, also the capability to dope titania nanoparticle with nitrogen atoms. Doping has the effect to move spectral absorption of titania toward visible range. It must be noted that the as-synthesized powders are contaminated by carbon coming from TTIP dissociation and from ethylene, if used. Thermogravimetric curves have shown that a thermal treatment in air at 450°C for 3 hours is suitable to remove completely the carbon contamination.

The first batch was produced by using NH_3 as sensitizer and the resulting nanopowder was N-doped, had an average crystallite size of about 12 nm and the crystalline phase was mostly anatase (Fig.88 left side). DLS (Dynamic Light Scattering) analysis was performed on annealed titania nanopowders dispersed in H_2O at concentration c=1g/l after US tip sonication for 70'. The resulting Z average was Z_{ave} = 153.5 +/- 1.6 nm with Polydispersity = 0.280 +/- 0.025
The process parameters were then changed to produce undoped TiO_2 and increase the productivity and a second type of nano-titania sample was prepared by using ethylene as sensitizer. It was found by XRD analysis that the average crystallite size is 10 nm and the

powder was composed by 30% of rutile and 70% of anatase as determined by Rietveld analysis and confirmed by TEM analysis (Fig.17 right side). DLS measurements were carried out on the sample dispersed in H_2O 1 g/l and treated with high power ultrasonic tip for 20'. The results are the following: after preparation: Z_{ave} = 183 ± 7, Polydispersity = 0.3; after 1 month: Z_{ave} = 167 ± 3, Polydispersity = 0.2.

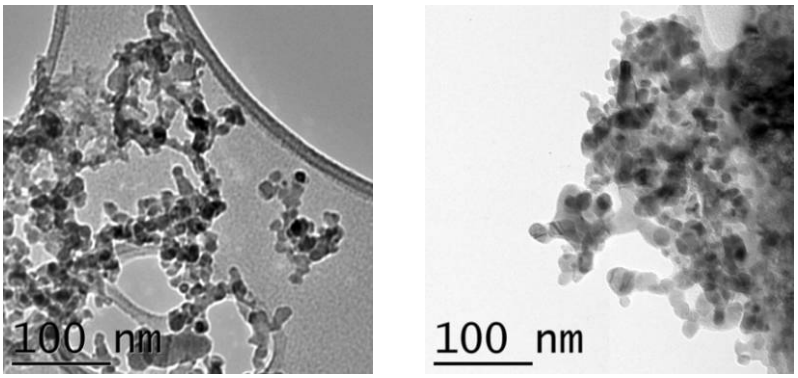

Fig.88. TEM images of N-doped TiO_2 (left) and undoped TiO_2 (right).

3.5.2 Preparation of SiO_2 nanopowders

SiO_2 nanopowders were first produced for HENIX by a two-step process, *i.e.* wet chemical oxidation of pyrolitic silicon nanopowders. Si nanoparticles were formed as a result of the laser induced dissociation of pure silane, that is a strong absorber of CO_2 laser radiation. The raw Si powders had a Si crystalline core of about 10-12 nm covered by native silicon oxide layer (1-2nm). Oxidation was performed by using water in alkaline ambient and the SiO_2 nanoparticles were obtained as white powder. DLS (Dynamic Light Scattering) analysis was performed on silica nanopowders dispersed in H_2O at c=1g/l after US tip sonication for 45'. The resulting Z average was: Z_{ave}=232 +/- 9nm with Polydispersity= 0.533 +/- 0.045.

On the other hand, it was also decided to try a completely different strategy, that is one-step preparation of silica by laser pyrolysis of tetraethoxysilane (TEOS), a liquid precursor. Ethylene was used as sensitizer. The as-prepared nano-silica sample was dark since it is contaminated with carbon. Thermogravimetric analysis revealed that removal of carbon contamination took place at 600°C for 6 hours. DLS analysis was performed on the sample before and after thermal treatment and showed that nanopowder was highly aggregate after thermal treatment. In fact after dispersion in H_2O at 1 g/l and treatment with US tip for 40', the resulting Z average was: Z_{ave} = 220 ± 5 nm with Polydispersity = 0.3 before thermal treatment and Z_{ave} > 1000 nm after thermal treatment.

The optimization of process parameters in order to minimize the carbon contamination is in progress.

3.5.3 Thermal conductivity measurements

Within HENIX project, nanofluids were realized by using nanoparticles synthesized at UTAPRAD-MNF and their thermal properties were tested by the other European partners.

Table VII Thermal conductivity enhancement measured in nanofluids upon nanoparticles addition

Nanofluids	weigth/weight %	T (°C)	Thermal conductivity enhancement
TiO_2 N- doped	2 2 2	20 30 40	0.80 % 0.40 % 1.70 %
TiO_2 undoped	2 2 3 6 9	20 30 20 20 20	1.80 % 2.10 % 0.70 % 1.00 % 1.80%
SiO_2 from Si	3 6	20 20	2.30 % 2.60 %
SiO_2 from TEOS before thermal treatment	3	20	-2.20 %
SiC	9 9 9	20 40 60	4.0% 2.5% 11.4%

Thermal conductivity enhancement, at different concentrations in H_2O and temperatures, of nanofluids produced using ENEA nanopowders are reported in the Table VII. It is evident a very promising enhancement in the SiC-based nanofluid, whereas the nanofluid based on SiO_2 prepared from TEOS is probably adversely affected by C contamination, thus pushing toward the optimization of a methodology to avoid/remove completely this contaminant.

3.6 Optical fibre sensors

FBG sensors are optical fibre sensors that allow the development of monitoring systems of various parameters, such as temperature, deformation, pressure, humidity. FBG sensors are well suited for permanent and long term applications, for both large scale industrial applications and R&D miniaturised systems. At UTAPRAD-MNF, in the holographic interferometry and fiber optic sensors, applications based on FBG technology are worked out in different fields.

3.6.1 Structural monitoring of large civil engineering works

FBG sensors allow the development of monitoring systems well suited for permanent and long term applications on civil engineering works.

A monitoring system based on FBG sensors has been developed for the sporting complex 'Città dello Sport' currently in construction in the city of Rome. The sporting complex is a very large civil engineering work composed of two independent pavilions, both with an elliptic base made by special reinforced concrete and an huge dome made by a metallic structure supporting glass tiles. The technology of FBG sensors was adopted because of its peculiar features, that allow the realisation of monitoring systems able to operate on long term with high accuracy and reliability for both static and dynamic measurements. Moreover, the technology of FBG sensors simplifies cabling of sensors, that can be connected in large number in series on one single cable.

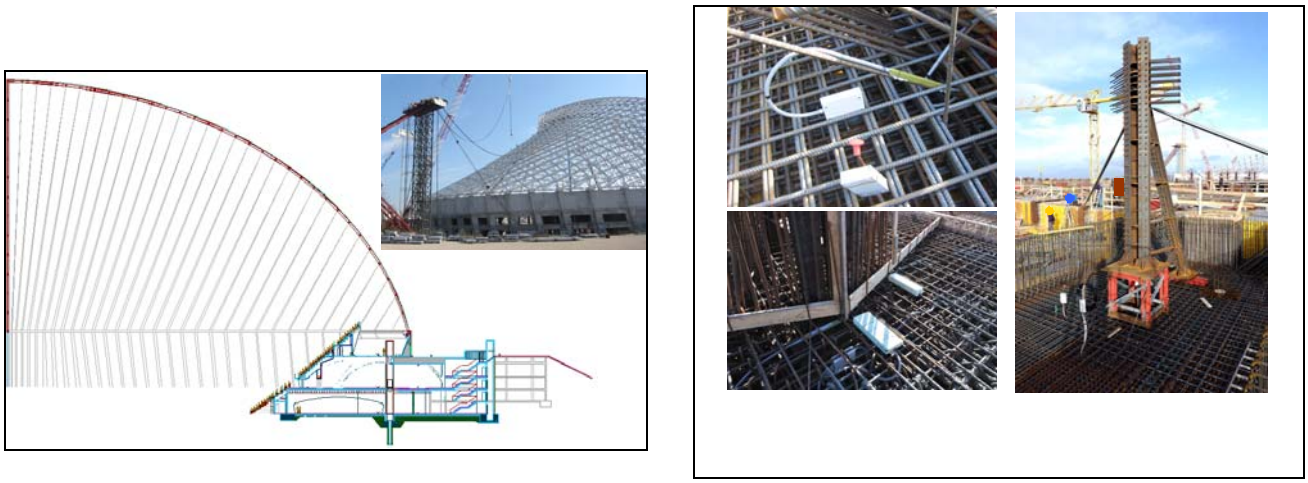

Fig.89. Cross section view drawing of one pavilion and a picture of the structure soon after completion of the dome frame (left). Phases of the installation of the FBG sensors on various structural components during construction works (right).

The developed monitoring system, provided with both structural and thermal sensors, has been installed during construction works, placing sensors on various critical structural components. Structural sensors are devoted to long term Structural Health Monitoring of the sporting complex during service life and are currently used to monitor static settlement of the structural components during construction works of upper levels. Moreover, structural sensors will provide additional information to the tests required to allow opening of the complex (Fig.89). Thermal sensors are used to monitor that the cure of thick in-situ cast concrete structures occurs with both the required temperature time-evolution and the required temperature gradient through their thickness. Figure 90 shows the temperature time history of concrete cure at four different sites: all sensors show steep temperature increase soon after concrete pouring and cure start, till first stage concrete cure completion that occurs after about two days; the sensors deep buried in the concrete cast (T04, T07) record the slow temperature decrease of concrete following cure completion; the sensor placed close to cast surface (T05) records the abrupt cooling due to thermal insulating panels removal and the subsequent night/day thermal cycling; the sensor placed at medium depth inside the cast (T06) records an abrupt cooling due to thermal insulating panels removal but is not affected by night/day thermal cycling.

For the time being, the monitoring system is composed of 58 sensors that can be accessed by a centralised optical patch-panel situated in one of the service rooms of the

sporting complex. The management of the existing monitoring system and its extension to structural components of the domes is planned in cooperation with the Department of Civil Engineering of Rome University Tor Vergata.

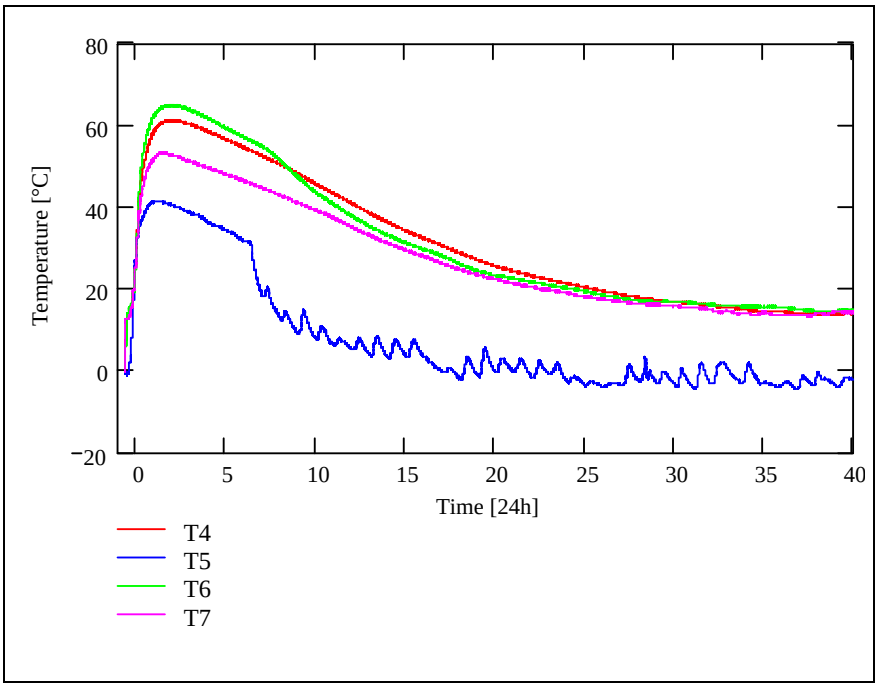

Fig.90. Temperature time history of concrete cure at four different sites

3.6.2 Structural monitoring of Cultural Heritage

FBG sensors can be effectively used for structural monitoring of architectural historical complex, taking specific advantage of the unrivalled low invasive character of FBG monitoring systems.

A monitoring system has been developed and installed on the historical complex of the Aurelian Walls of Rome, the actual remains of the line of walls around Rome started by the roman emperor Aurelian in the third century AD. The activity has took place in cooperation with the Supervising Department for Cultural Heritage of the Municipality of Rome, as a preliminary investigation prior to planned restoration works aimed to the reopening to visitors of part of communication trenches. The installed sensors perform continuous static monitoring of the opening of cracks and scheduled dynamic monitoring of masonry strengthening tendons (Fig.91).

Fig.91. View of the section of the Aurelian Walls subject to monitoring (left); view of one of the monitored tendon in the trench (middle); one of the monitored crack in the wall of a tower (right).

The installed monitoring system takes full advantage of the possibility to connect in series FBG sensors, being realised by one thin single optical cable running along the communication trench and interconnecting all the optical sensors. Monitoring so far performed has given significant results allowing the correlation between temperature at the masonry and cracks opening behaviour, pointing out crack opening cycles due to both day/night and seasonal temperature variations.

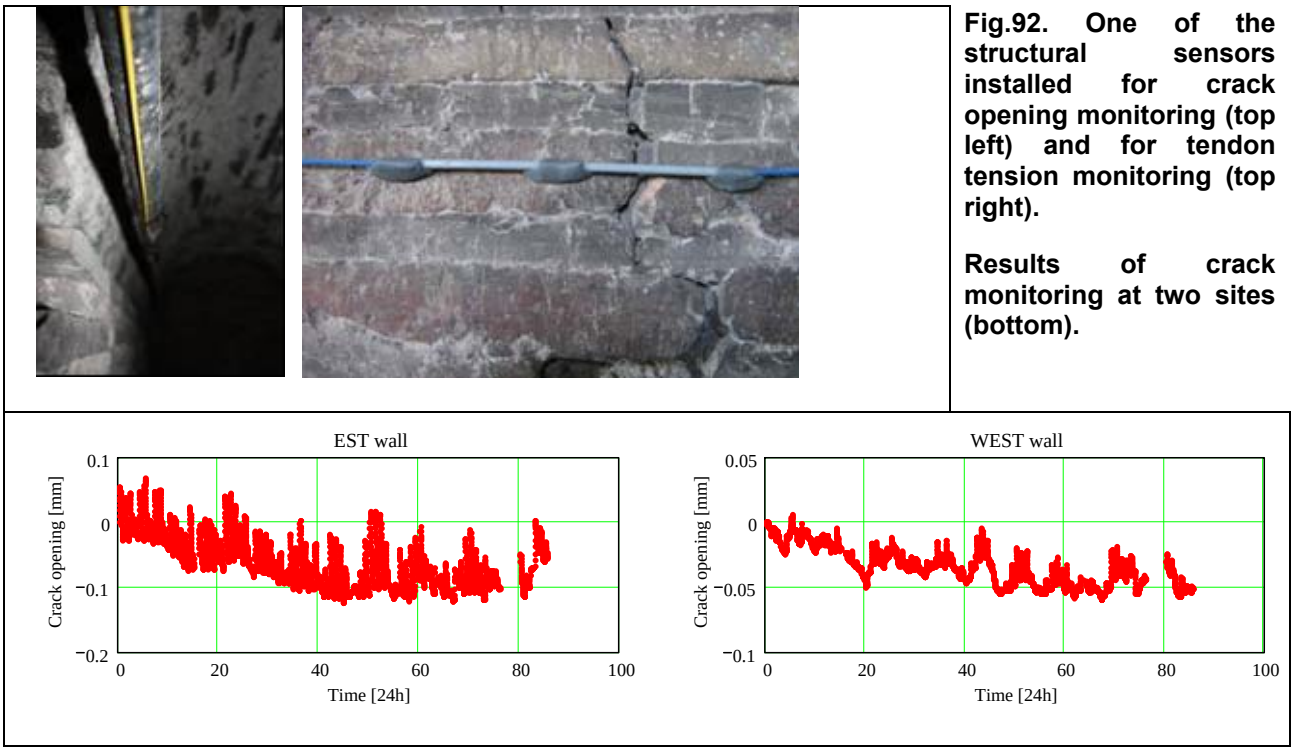

Fig.92. One of the structural sensors installed for crack opening monitoring (top left) and for tendon tension monitoring (top right).

Results of crack monitoring at two sites (bottom).

Figure 92 shows one of the structural sensors installed for crack monitoring and sample results of crack monitoring at two sites: crack opening shows strong correlation with thermal night/day cycling and average environment temperature.

3.6.3 Development of smart composite materials

FBG sensor have already found important applications in the development of 'smart' composite materials, i.e. composite materials with embedded sensors that performself-monitoring of the experienced thermal and structural stresses. Adopted technical solutions relay on the embedding of FBG sensors in the resin matrix of the composite, but such solution can be hardly used for structural patches for strengthening or repairing civil engineering structure to be produced in-situ. The availability of Glass/Carbon Fibre Textiles with woven FBG sensors would offer an effective solution for in-situ production of smart composites for civil engineering retrofitting works.
In the framework of the Research Project MAMAS (MIUR-FAR, led by CETMA), an innovative technique aimed to the development of a Glass Fiber Textile with woven FBG sensors has been tested. FBG sensors were woven in a commercial grade textile and its usage was tested simulating in-situ production of reinforcing patches on small scale concrete beams. Reinforced beams were subjected to Flexural Bending Test in order to verify the monitoring capability of the developed smart reinforcing patches in real working condition. Figure 93 shows two sample specimens subject to testing: sample shown in the picture on the left is a textile laminated patch prototype, sample shown in the centre is a

small size beam reinforced by the developed smart textile; the graph on the left compares results from the sensor embedded in the smart textile with the results from a reference traditional sensor. Results show that the embedded FGB sensors provide correct measurement of the Strain experienced by the beam, thus validating the developed technique; future work is planned for improvement of features and industrial engineering.

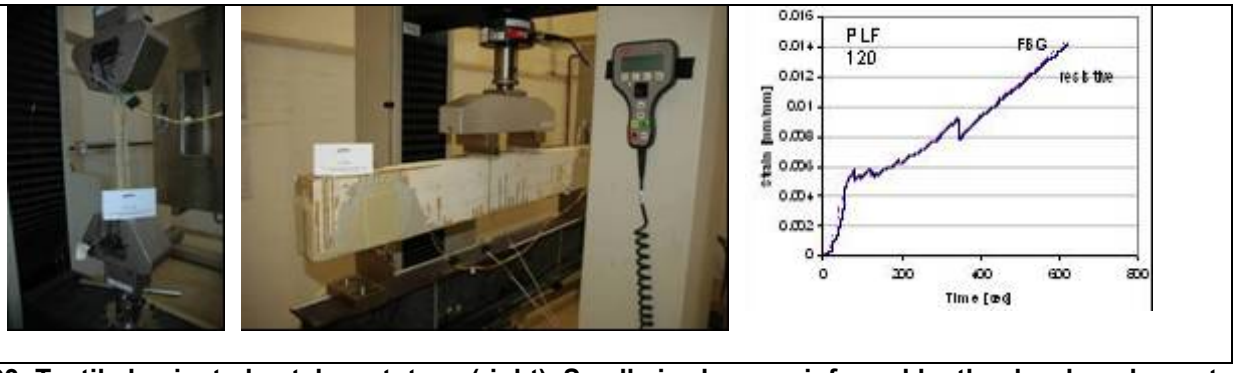

Fig.93. Textile laminated patch prototype (right). Small size beam reinforced by the developed smart textile (centre). Comparison of results from the sensor embedded in the smart textile with the results from a reference traditional sensor (left).

3.7 Seismological Activities

The activities in seismological field, performed in cooperation with the UTPRA-PREV laboratory, concerns the evaluation of seismic hazard at regional and local scale by the acquisition, interpretation and analysis of geological, geotechnical, geophysical and historical data.

3.7.1 New seismic zonation of Latium Region

Latium Regional Administration and ENEA signed an Agreement of Research aimed at the definition of a new approach for the regional seismic zonation in 2007. The resulting study, completed in 2010 (Fig. 94), was based on two methodologies: an historical and seismological analysis of the regional seismicity and a statistical and spatial analysis of the uniform hazard response spectra related to sites included into the Latium boundary. The historical analysis produced an evaluation of the maximum historical intensity in every Municipality, together with the information on magnitude and epicentral distance of the related events; these data were subsequently used in querying international accelerometric databases in order to select a set of real ground-motion recordings. The statistical analysis outlined, by a cluster technique, six groups of spectra which characterise the regional seismic hazard and can be used to associate each Municipality to the proper Seismic Zone.

The results were used to guide the new seismic zonation passed as Regional Rule in 2009; the selected accelerograms, scaled to the hazard level of each Municipality, represent the official reference input time-histories to be used in Regional seismic microzonation analyses.

Subsequently, by the activities of a Working Group composed of experts from Civil Protection National Department, ENEA, University of Rome “Sapienza” - Department of Earth Science, ISPRA and the Latium Board of the Geologists Association, the Guide-

Lines for the Seismic Microzonation analysis in the Latium region have been edited and passed as Regional Rule in December 2010.

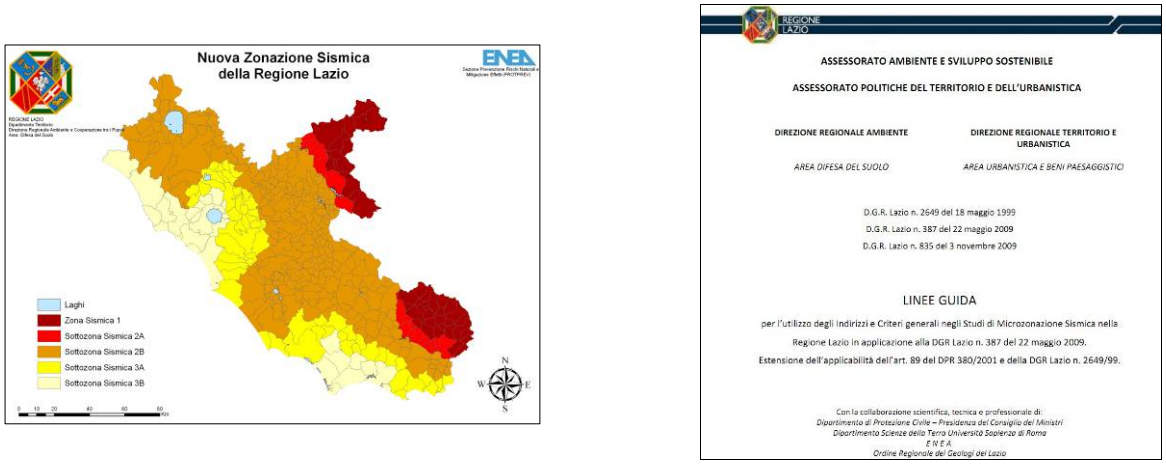

Figure 94 - The new seismic zonation of Latium region: map resulting from an historical and seismological analysis of the regional seismicity and astatistical and spatial analysis of the uniform hazard response spectra (left); cover of the Guide-Lines released (right).

3.7.2 Seismic microzonation of the Roio area

After the 2009 L'Aquila seismic sequence, Italian National Civil Protection Department promoted the seismic microzonation analysis of the damaged localities. A working group made up of experts from ENEA, Latium Region administration and University of Rome "Sapienza", attended to the study of some hamlets of L'Aquila municipality, located in the Roio area. After geological, geomorphological and geotechnical surveys, it was possible to draw a Level 1 microzonation map, aimed at the identification of zones potentially prone to local seismic amplifications. In the meantime, a temporary velocimetric and accelerometric array was deployed in order to record aftershocks and analyse the local seismic response by spectral ratio techniques. Moreover, a seismic noise survey was performed in order to characterise the seismic response of the Level 1 areas by the horizontal to vertical spectral ratio analysis. All these information were used as input data for some 1D and 2D numerical models, obtaining the final Level 3 microzonation map, to be used for local planning (fig. 95). The activity in conducted in the framework of an on going 5 year ENEA-CERI agreement signed in 2006.

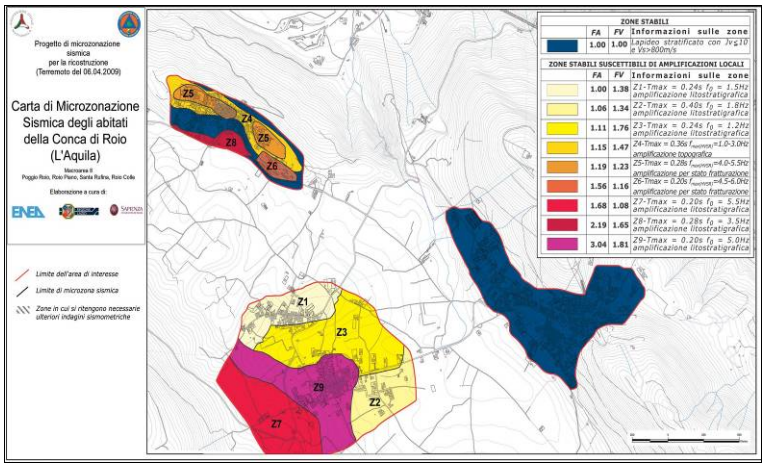

Figure 95 – Level 3 microzonation map of the Roio area (AQ) drawn up after the 2006 L'Aquila seismic sequence.

3.7.3 Development of an accelerometric Data Bank

In the last years, ENEA collected a great amount of three components waveform recorded by an accelerometric network.

Focusing on the 1997 Umbria-Marche seismic series, 177 recordings acquired in 9 ENEA accelerometric stations and related to 99 seismic events with maximum values of magnitude Mw=6.0 has been analised and stored in a relational database structure (Fig. 96). These information can improve both seismological and engineering knowledge of local seismic response.

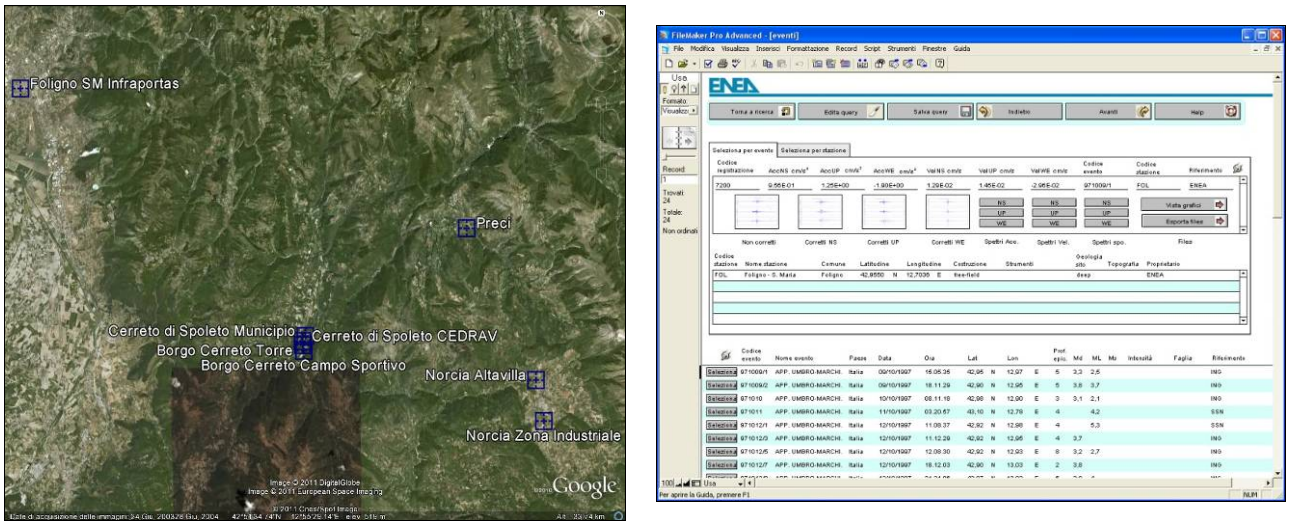

Figure 96 - Distribution of the 9 ENEA accelerometric stations located in the Umbria region since 1997 (left); Example of a query output, obtained by the ENEA accelerometric Data Bank mainly related to the 1997 Umbria-Marche seismic series (right).

4. Radiation Sources Laboratory

4.1 Mission and infrastructures

The Radiation Sources Laboratory performs R&D work in the fields of generation of coherent radiation and in the acceleration of charged particles. Research activities include emerging technologies in photonics and microlithography, development of laser systems and accelerators for scientific, industrial and medical applications.

Current activities are focussed on:

- Design and constructions of high energy-per-pulse excimer lasers, plasma driven X-ray sources and their applications;
- Design and constructions of Free Electron Laser (FEL) sources for the generation of electromagnetic radiation in the Far InfraRed and in the Terahertz region;
- Development of low-energy electron accelerators for material processing, medical applications and as a driver for FELs;
- Development of medium-energy proton accelerators for cancer therapy

These activities are undergoing a rapid development worldwide with an increasing number of applications such as microlithography in the extreme ultraviolet, X-ray microscopy of biological systems, effects of electromagnetic radiation, imaging systems applied to material characterization, biology, biomedicine and, more recently, art conservation studies.

The facilities formerly developed by UTAPRAD-SOR and utilized for current activities include:

- Excimer laser laboratory
- Soft X-ray plasma sources laboratory
- Compact FEL (90 – 150 GHz)
- FEL-CATS (400 – 700 GHz)
- TOP-LINAC
- 5 MeV Electron LINAC

4.1.1 Funding and projects

2010 has been a particularly important year as it saw the signature of the agreement with the Regional Government of Lazio for the implementation of the proton therapy system IMPLART in collaboration with the National Institute of Health and IFO (Institute Physiotherapy Hospital, Rome). Another important initiative in early 2010 was the presentation to the 'Regione Lazio' of a proposal for the modernization of research laboratories that included three separate projects: CETRA (Center of Excellence for Terahertz Radiation and Applications), the EGERIA Facility, the Solid State Laser Laboratory and Spectroscopy (now UTAPRAD-MFN). CETRA and EGERIA are also part of the initiatives of new research infrastructures (RI) recently evaluated among the "emerging projects" in the Italian roadmap defined by the Ministry of Education, University and Scientific Research.

Moreover the Radiation Source Laboratory has been actively involved in the realization of the SPARX FEL, a joint project between ENEA, CNR, INFN and the University of Rome

"Tor Vergata", aimed at the development of a Free Electron Laser in the VUV and X-ray regions. The major results obtained in 2010 are shortly described in the following.

4.2 Short-wavelength Sources and Applications

In the extreme ultraviolet (EUV) spectral region (20 eV - 280 eV) laser-plasma and discharge-plasma sources can produce energies per pulse and repetition rates sufficient to be considered a valuable alternative to synchrotrons and short-wavelength free-electron lasers (X-FELs) in many irradiation experiments, namely when the peak power and the brightness are more important than the average power and when it is not required a narrow spectral band. In fact, synchrotron beam-lines are often over-subscribed by factors of three or more; despite the widely-acknowledged advantages of synchrotron radiation, there is not enough to go round. Due to the cost of such sources (more than 100M€ to build, about 1M€ per beam-line per year to run) this is likely to remain the case. The same considerations apply for short-wavelength FELs that are being developed in different countries, as their size and costs are similar to synchrotrons. In this strategic frame, laser-plasma and discharge-plasma sources available in the market, such as those here, are alternative, table-top, cheaper, and more accessible sources which can offer at least some of the synchrotrons performance.

4.2.1 The multipurpose Laser-Plasma-source and Micro-Exposure-Tool EGERIA

The activity is mainly focused on the development and application of a Micro-Exposure-Tool (MET) for micro- and nano-lithography. The MET is a complex apparatus comprising a laser-driven plasma source called EGERIA, a debris mitigation system, an optical collector and an accurate optical projection system able to print a pattern with a spatial resolution better than 100 nm. It is worth mentioning two other experimental activities, respectively concerning the surface coloration of linen textiles for reproducing archaeological images, and the proof of a novel anti-counterfeiting system based on an invisible writing method which uses lithographic techniques on luminescent materials. The experimental results have shown that this technology is suitable to fabricate robust anti-counterfeiting tags, which are almost impossible to counterfeit and can be applied to almost every kind of objects, independent of their shape and size. This technology is patent-pending.

The Laser-Produced-Plasma facility called EGERIA (**E**xtreme ultraviolet light **G**eneration for **E**xperimental **R**esearch and **I**ndustrial **A**pplications) is based on the use of a XeCl excimer laser whose beam is focused on a metal tape placed in a vacuum chamber, thus creating a plasma which recombines and emits pulsed radiation. The features of the emitted radiation (i.e. spectral range, peak intensity, pulse duration in the nanosecond range) can be managed by adjusting the laser beam intensity on target and by selecting the target material. The spectral range spanned by EGERIA is between 20 eV and 1800 eV. A debris mitigation system (two ENEA patents) reduces by three orders of magnitude the debris emitted by the tape target, thus allowing almost clean irradiations in the EUV.

Presently, the plasma source EGERIA is an international-level facility that has been used by biologists (*in vivo* X-ray microscopy of bacteria, DNA repair, micro-radiography), hysicists (heavy ions generation, X-ray atomic spectroscopy, micro-devices for photonics,

contact-lithography, imaging of sub-micrometric structures on optically active materials) and industry (writing arbitrary pattern on anti-counterfeiting tags).

The Micro-Exposure-Tool (MET) EGERIA is a complex apparatus comprising the EGERIA source, an optical collector and an accurate optical projection system able to print pattern with a spatial resolution better than 100 nm. In 2010 the MET-EGERIA has been evaluated by the Italian Ministry of Education, University and Research (MIUR) as "Emerging Project" in the National Roadmap of Research Infrastructure.

The MET-EGERIA is used for projection-lithography to generate pattern with a sub-micrometer spatial resolution. Figure 97 shows a top view of the EGERIA source chamber and of the MET chamber. Both vacuum chambers are placed in a clean room, as shown in Figure 98.

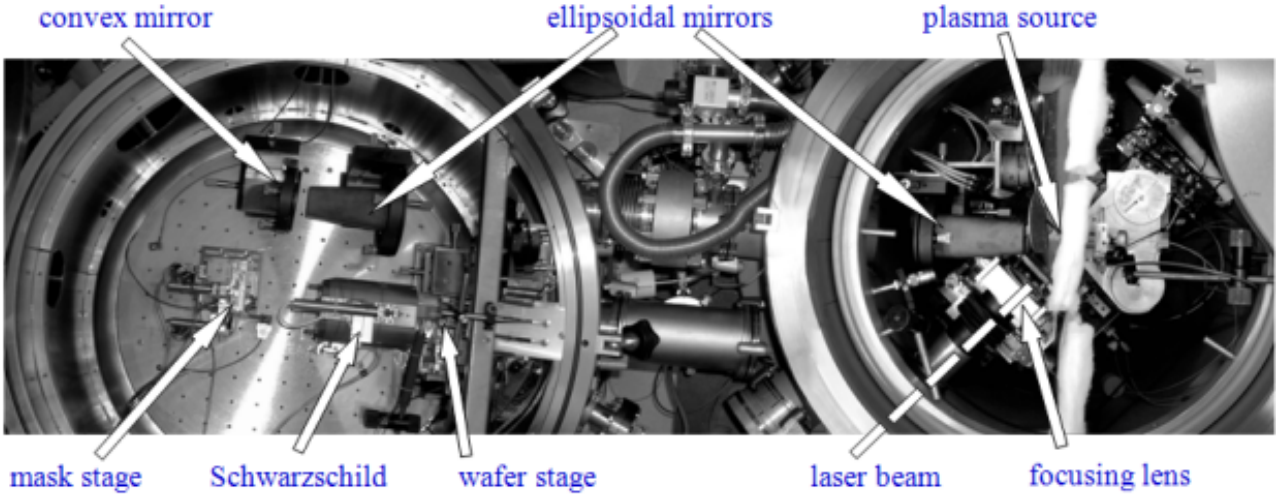

Figure 97 - ***Top picture of the EGERIA vacuum chamber (right) where the laser-plasma is generated and of the Micro Exposure Tool high-vacuum chamber (left) where high resolution pattern are written either on a photoresist or on a fluorescent material.***

Figure 98 - ***The EGERIA source and the Micro Exposure Tool inside the clean room.***

During 2010, the laser plasma source EGERIA was used to irradiate several samples in the extreme ultraviolet spectral region (20 eV < hv < 280 eV)

in cooperation with European Institutes and with other ENEA Laboratories. EGERIA has been recently implemented with new absolute photodiodes, in order to obtain absolute EUV dose measurements with an uncertainty of few percent.

A particularly interesting experiment has been carried out in the frame of a collaboration with the Birmingham University (UK). Different samples of a new kind of negative photoresists for extreme ultraviolet lithography (EUVL), synthesized at the Birmingham University, have been irradiated at different EUV dose levels in order to obtain the photoresist response curve. The results (see Figure 99) are still under analysis.

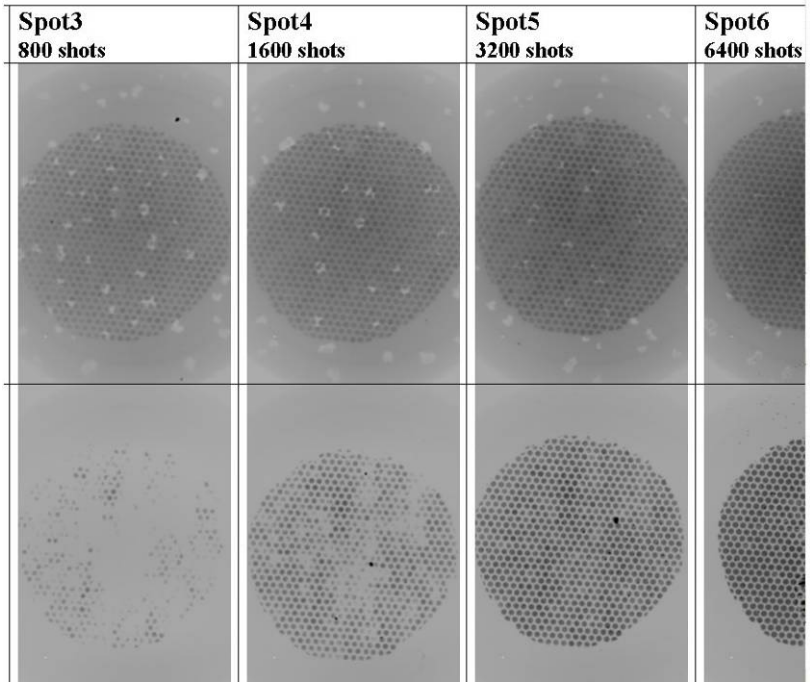

Figure 99 - ***Negative photoresists of type "A" (upper row) and of type "B" (lower row), from Birmingham University, exposed to different EUV dose values through a mask having hexagonal holes placed at a distance of 1 mm from the resist. The photoresists are observed under an optical microscope in reflection mode (after development of the resists). The darker regions correspond to higher photoresist thickness.***

From Figure 99, the different sensitivity and contrast of the two types of photoresist are evident. Further experiments in cooperation with the Birmingham University are planned after completing the analysis of these first results.

It is worth noticing that the research on innovative photoresists for EUVL has a great relevance in the semiconductor roadmap (http://www.itrs.net/), where the issue of high-sensitivity and high-spatial resolution resists is of paramount importance.

4.2.2 Discharge-plasma source of EUV radiation

A xenon Discharge Produced Plasma (DPP) EUV incoherent radiation source was jointly designed by ENEA Frascati and the Physics Department of L'Aquila University in the frame of the FIRB-EUVL project (2003-2008) and was assembled and tested in L'Aquila University. In April 2010 the apparatus has been transferred to our laboratory, where it is operating since November 2010 after several improvements and optimizations, in order to obtain a stable and reliable operation, see Figure 100 (picture and scheme). In particular, the Xe injection system has been rebuilt, and the discharge modulator and circuit

diagnostics have been improved. In addition, the vacuum chamber devoted to irradiation experiments and target positioning has been modified and connected to the source to obtain a larger radiation cone available for irradiations. The DPP is based on the generation of a xenon plasma column (10 mm in length and 0.5 mm in diameter) in an alumina capillary tube.

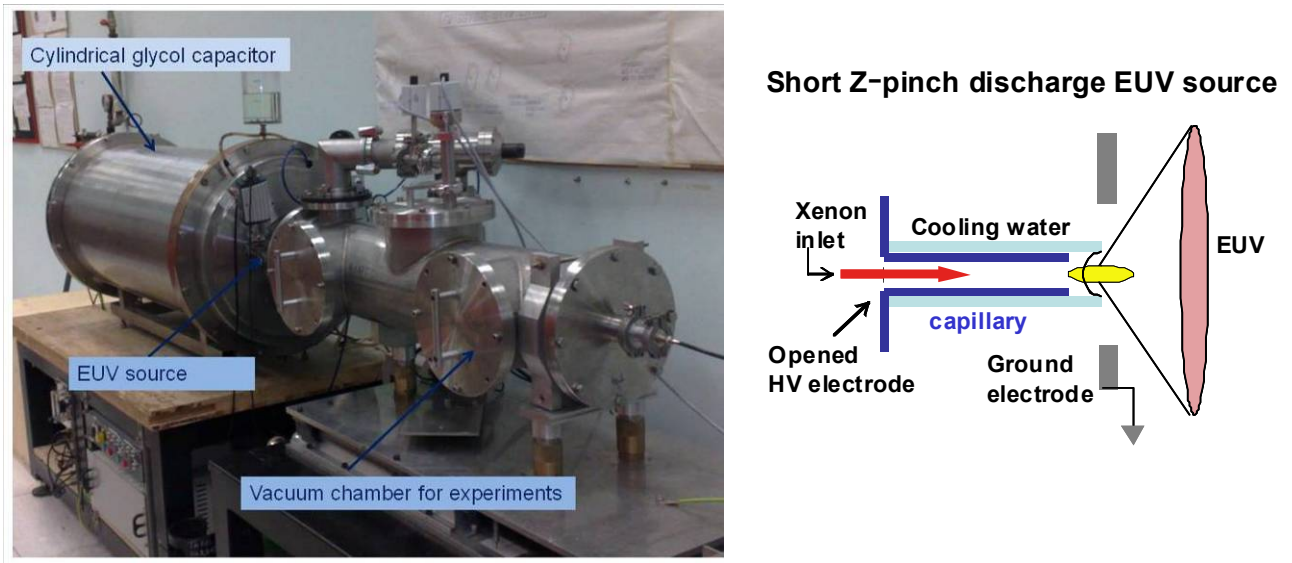

Figure 100 - ***DPP source operating at the ENEA Frascati Research Centre (UTAPRAD): picture with indication of main components (left); operating scheme (right)***

After evacuating the capillary down to a residual pressure of about 10^{-6} mbar, a small Xe flow (~ 5 standard cubic centimeter per minute) is injected, maintaining an equilibrium pressure of about $5 \cdot 10^{-3}$ mbar in the vacuum chamber connected to the source. The Xe plasma is generated by a short and intense current pulse (10 kA, 250 ns) flowing in the capillary filled by pre-ionized low pressure Xe. The current pulse is obtained by properly discharging in the capillary a 50-nF glycol low-inductance cylindrical capacitor, charged up to (20 - 25) kV. The plasma, pinched towards the capillary axis by the magnetic field produced by the high-current, is heated up to a temperature of (30 - 40) eV and after recombination it emits radiation in the (10 – 20) nm wavelength region, as shown in Figure 101.

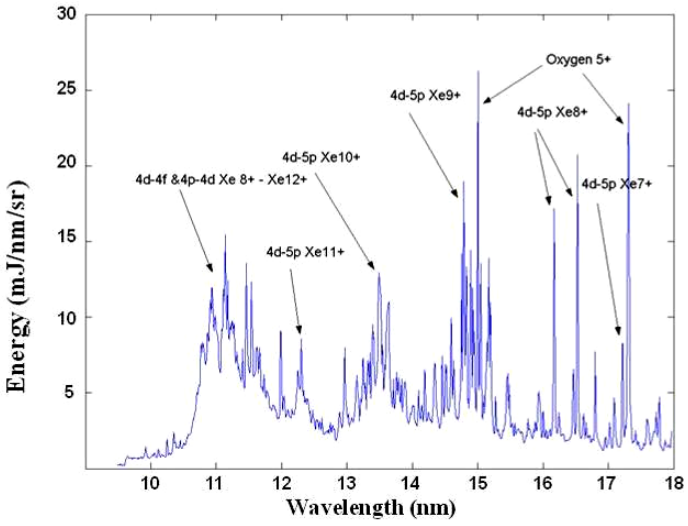

Figure 101 - Typical spectrum of the radiation emitted by the DPP.

At a repetition rate of 10 Hz, the source stability is better than 5% r.m.s. The conversion efficiency of the energy stored in the capacitor into EUV radiation is 0.3% on 2π sr at λ = 13.5 nm (which is the wavelength of interest for the next generation EUV lithography) on a 2% bandwidth. The EUV radiation pulses have a 60 ns FWHM (see Figure 102) and an energy of ~ 4 mJ/sr/shot at λ = 13.5 nm within the 2% bandwidth, whilst the energy emitted on the whole band (10 – 20) nm is about one order of magnitude larger.

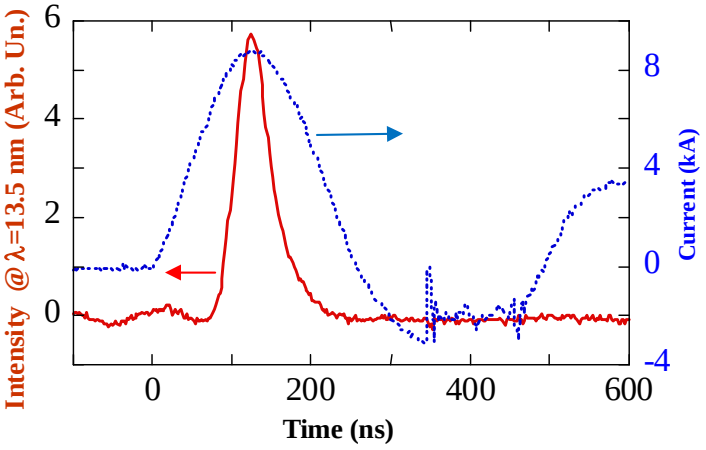

Figure 102 - *Time evolution of the discharge current and of the radiation emission.*

The emitted radiation can be collected in a 60° aperture-cone in the vacuum chamber dedicated to the experiments. The wavelength and the shape of the emission peaks depend on both the nature and flow of the used gas and on discharge parameters, so that the source can be optimized for different specific applications like imaging, microscopy, spectroscopy, microlithography, photo resist testing as well as color centre generation, material ablation, EUV optics diagnostics, X-ray fluorescence, and so on. As a consequence, the DPP frames within the laboratory research line on the EUV radiation generation and relevant applications. It may greatly improve the range of future collaborations and R&D activities.

In addition to its further characterization and optimization, it is planned to use the DPP in the framework of the anti-counterfeiting technique developed and patented by ENEA.

4.2.3 Invisible writing method as a novel anti-counterfeiting technique

A recent update of the Organisation for Economic Co-operation and Development (OECD) has estimated in $250 billion (in 2007) the worldwide value of international trade in counterfeit and pirated goods. This means that the available anti-counterfeiting techniques (fluorescent and thermo-chromatic inks/dyes, de-metallization, radio-frequency, surface engraving, micro-texts and holograms) used so far do not offer a good protection from unauthorized copying or replication. As a consequence, up till now there is no absolute certitude that the documents, objects, currency, identity/credit/debit cards, commercial/artistic objects, forensic documents, dangerous wastes, pharmaceutical products, copyright protection systems protected by existing anti-counterfeiting techniques are genuine.

Using the short-wavelength radiation emitted by EGERIA, we have exploited the capability to write an invisible image on a fluorescent film that can be used as a tag for identification

and traceability. This is a novel anti-counterfeiting system that prevents cloning and allows a security degree tailored on the customer's demand, up to a marking that is impossible to counterfeit. The reading technique comprises a small device that catches the invisible image and, if required, provides a digital decoding of the same image. The reading device has the capability to communicate with local or remote computer systems, and, if required, it can be based on a simple mobile phone digital camera.

During 2010, we made a prototype of anti-counterfeiting tag applied to a plastic substrate, commonly used for credit or identity cards. The ENEA MNF Lab deposited a thin film of luminescent material on the plastic. After the deposition, we exposed the film to the EGERIA radiation trough a contact (transmission) mask, thus transferring an invisible image on it, and then the card was protected by a standard 25-μm-thick plastic coating. The final result is shown in Figure 103. The invisible pattern can be observed only using the specific ENEA patented reading technique.

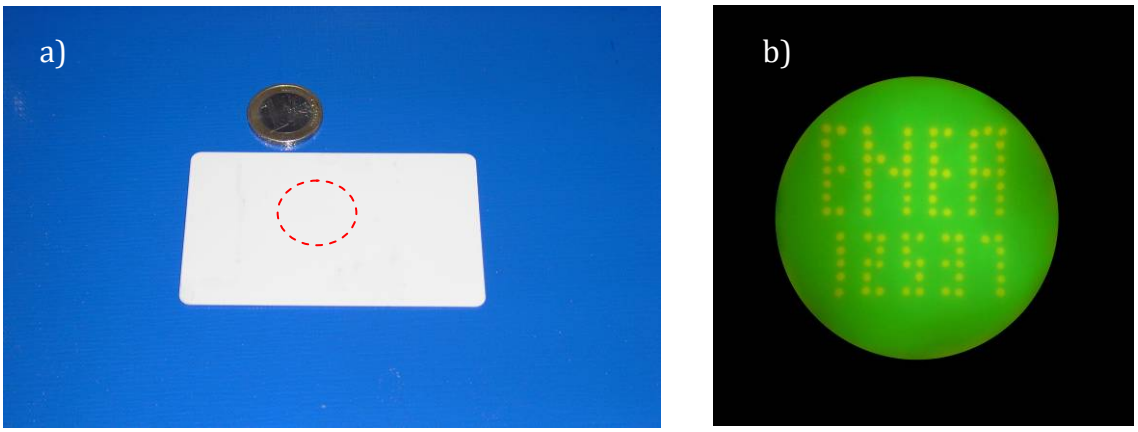

Figure 103 - ***a) Picture taken under natural light illumination of a standard plastic card (85 mm×54 mm) with an invisible mark within the dashed area written by the radiation emitted by EGERIA. b) picture of the same dashed area shown in a), but with the pattern made visible by means of the compact and portable ENEA reading system prototype.***

4.2.4 Linen textile coloration by nanosecond Laser pulses

The main interest in obtaining a permanent yellowish coloration of linen textiles is the search of a mechanism possibly leading to the formation of the Turin Shroud image: in fact, to date no one, not even with state-of-the-art technology has ever duplicated the Shroud image in all its chemical and physical characteristics, and the very thin (about 200 nm) coloration depth is one of the most difficult to replicate features of the Shroud image.

During 2010, in collaboration with ENEA MNF Laboratory, we obtained experimental results showing that a short and intense burst of 193-nm excimer laser radiation provides a linen coloration having many peculiar features of the body image embedded into the Turin Shroud, including the hue of color, the color penetration depth and the lack of fluorescence, see Figure 104.

Most importantly, thanks to the accurate characterization of both laser irradiation parameters and coloration results at the fiber level, we have recognized distinct physical and photo-chemical processes that account for both the experimentally achieved coloration and latent coloration. These processes may have played an important role in the generation of the body image on the Shroud of Turin.

During 2010 these results have been published in international journals, and their relevance echoed by several media (newspapers, websites, telecasts) pushed a group of Shroud's scholars (members of the international Shroud Science Group) to assign to ENEA the organization of the International Workshop on the Scientific approach to the Acheiropoietos Images (IWSAI 2010) that was held at the ENEA Frascati Center 4 through 6 May, 2010.

Figure 104 - ***Microscope view of a single fiber of linen colored after excimer laser irradiation at λ = 193 nm. The mechanical damage in the middle shows a colorless medulla, suggesting the color penetrates only the primary cell wall of the fiber, which is about 0.2 μm thick. The fiber has an average diameter of 20 μm.***

4.3 Terahertz Sources and Applications

Terahertz radiation covers the frequency range between 100 GHz and 10 THz (i.e. a wavelength between 3 mm and 30 μm), which spans the spectral interval between the microwave and the infrared regions of the electromagnetic spectrum. THz radiation has been raising a growing interest in recent years due to a variety of applications in the field of biology, biomedicine, environmental sciences and homeland security, in particular regarding the development of imaging techniques that allow the identification and investigation of structural and functional properties of a variety of materials. The development of coherent, tunable and powerful sources of THz radiation is therefore an important issue addressed by a number of research groups in the world.

4.4.1 Terahertz Free Electron Lasers

Two Free Electron based sources of the THz radiation are currently available at the ENEA laboratories in Frascati, covering altogether the spectral range from 90 GHz to 0.7 THz. These two sources are the first two FELs realized in Italy and, as far as the Compact FEL is concerned, it has been the second realized in Europe.

The ENEA Compact FEL (Fig. 105), is based on a 5 MeV Microtron providing an electron beam with 4 A peak current in 13 ps bunches. The electron beam is injected into a 8-period permanent magnet undulator (λ_u=2.5 cm) and the emitted radiation is stored in a hybrid resonator, which utilizes a WR42 waveguide for transverse confinement of the mode and wire-grids electron transparent mirrors (ETM) for the longitudinal confinement.

Figure 105 - View of the ENEA Compact FEL facility.

Peak power in excess of 3kW is obtained in the micropulse at 130 GHz. Micropulses occur with 330 ps spacing in a 4 μs long macropulse, which is repeated at 10 Hz. When the beam is focused to a spot size of about 0.5x1 cm^2 a peak electric field greater than 2 kV/cm is obtained in the micropulse. The vacuum chamber of the ENEA Compact FEL can also host different interacting structures like metal gratings and dielectric loaded wave-guides.

The second source, named FEL-CATS (Fig. 106), is based on a 2.5 MeV Linac powered by a 15 MW Klystron. The electrons accelerated by the Linac enter into a RF device that correlates their distribution in energy and phase. This correlation creates an intrinsic order within the electron bunch in such a way that coherent emission occurs with a single passage inside the undulator and without the use of any optical cavity. Power levels up to several kilowatt have been measured over a pulse length of about 5 μs. The absence of resonators, and the use of a short length undulator, result in a broad band emission from 400 μm up to 800 μm.

Figure 106 - View of the ENEA FEL-CATS facility

The peculiar temporal structure of the radiation emitted by these sources allows the investigation of the effects of high peak power, while maintaining a low average power incident on the sample, typically few mW, thus avoiding heating effects. A variety of biological systems have been studied with the ENEA Compact FEL in the frame of the European project THz-BRIDGE. More recently a reflective THz imaging setup has been developed and devoted to the study of hydration conditions in living plants and soils.

During 2010 a proposal has been submitted to the Regional Government of Lazio to establish an interdisciplinary Research Infrastructure, CETRA, specifically devoted to the development of THz sources and their application in biomedicine, cultural heritage conservation, material studies, security and telecommunications.

4.4.2 THz imaging

THz imaging has seen a tremendous development in recent years with a range of applications extending from the analysis of epithelial systems to the early detection of cancer, from mail inspection of illicit content to airport security systems.

A versatile reflective THz imaging system has been developed at ENEA-Frascati and is illuminated by the THz Compact FEL. The FEL radiation is coupled first into a focusing cone followed by a circular to rectangular waveguide transition, which matches the cone output to a series of two WR6 10 dB directional couplers. A probe end is attached to the second directional coupler directing the 130 GHz radiation to the surface of the sample under investigation. The side outputs of the two directional couplers provide a reference signal of the FEL radiation incident on the sample and the signal reflected by the sample respectively. Both signals are detected by Schottky diodes at room temperature. A variable attenuator allows the relative adjustment of the reference signal to the reflected signal within the response range of the Schottky diode during calibration (see Figure 107).

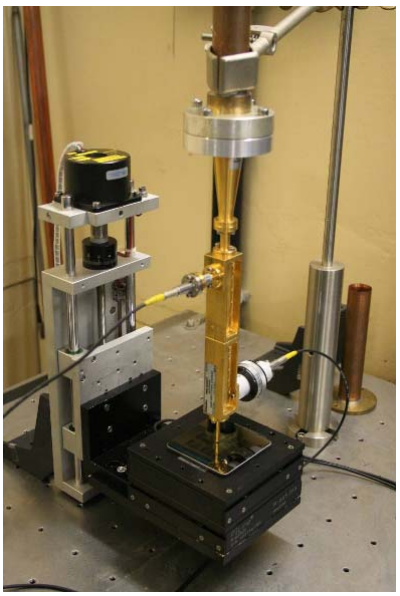

Figure 107 - ENEA THz Imaging system

The sample under investigation is placed on top of a XY translational stage driven by piezo-motors with 50 mm travel range on both axes. The distance between the sample and the imaging probe along the z axis can be adjusted by means of a stepper-motor driven stage. To obtain an image the sample is scanned at a maximum rate of 5 pixel/s, the reflected signal is normalized to the reference signal to compensate for any power fluctuation of the source during the scan. Collected data are stored in matrix form to be subsequently analyzed by an image processing software.

4.4.3 Measurements on artworks

Using the ENEA THz facility, extensive measurements have been carried out in collaboration with international partners in order to verify the possibility of setting up a common project regarding the exploitation of THz imaging techniques on paintings and artworks. Within the framework of a bilateral agreement signed between the Italian and Japanese foreign offices we started a collaboration with Dr. Kaori Fukunaga, from NICT Tokio in Japan, that initiated us to this fascinating discipline, being she the first scientist that had the idea to apply THz radiation for the study of art work in order to provide a tool for the conservation of cultural heritage In particular as far as the investigation of hidden paintings is concerned. The project is called THz-Arte.

The first experiment was performed on a painting made with natural pigments and gold, an partly covered by a 1.5 mm layer of whitening that has been analysed in the visible, at THz in transmission using the broad band source at NICT, and finally in reflection at Frascati with our FEL source. The whitening layer resulted to be perfectly transparent in the THz range and, due to the phase contrast control, in ENEA we obtained clearer image right over the plaster cover; the whitening acted as an antireflection coating.

After the first experimental successes the work proceeded with other images realised by Dr. Fukunaga; the one reported in Fig. 108 it's a tempera representing a lady Mary's dress. Part of the detail of the dress has been covered with "Gesso di Volterra", a kind of plaster. The detail covered is now made by two different pigments: indigo and cinnabar over gold. The THz image shows how the ENEA imaging device is capable to reveal not

only the painting covered as being completely uncovered, but also to distinguish the two different pigments showing to us that they have two different refractive indices at the FEL frequencies.

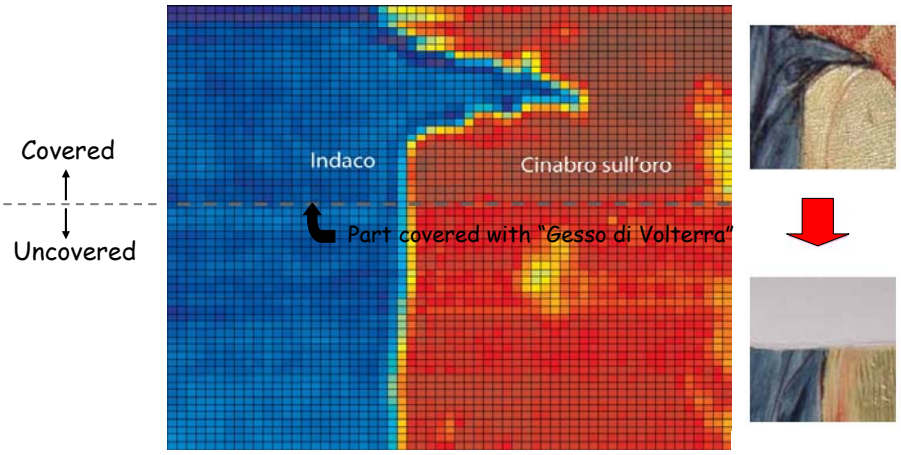

Figure 108 - ***Tempera sample – detail of Lady Mary dress***

"Gesso" is not the only material transparent to the THz radiation generated by the ENEA FEL. Several tempera art crafts, again realised by NICT has been analysed partly covered with lampblack and white plaster; the results demonstrate that the radiation can pass also through these different materials.

Many interesting experimental studies have been performed in order to exploit the phase contrast technique. Looking at the THz images of Figure 109, the figures show the visible image of two details of a tempera model specimen before and after covering with gesso. The THz reflection images have been taken optimizing the phase contrast acting on the probe-sample distance. Since gold is extremely reflective, the gold part is clearly observed under gesso, even tiny pieces can be recognized. Not only metals but also reflective pigments such as cinnabar can be detected under gesso.

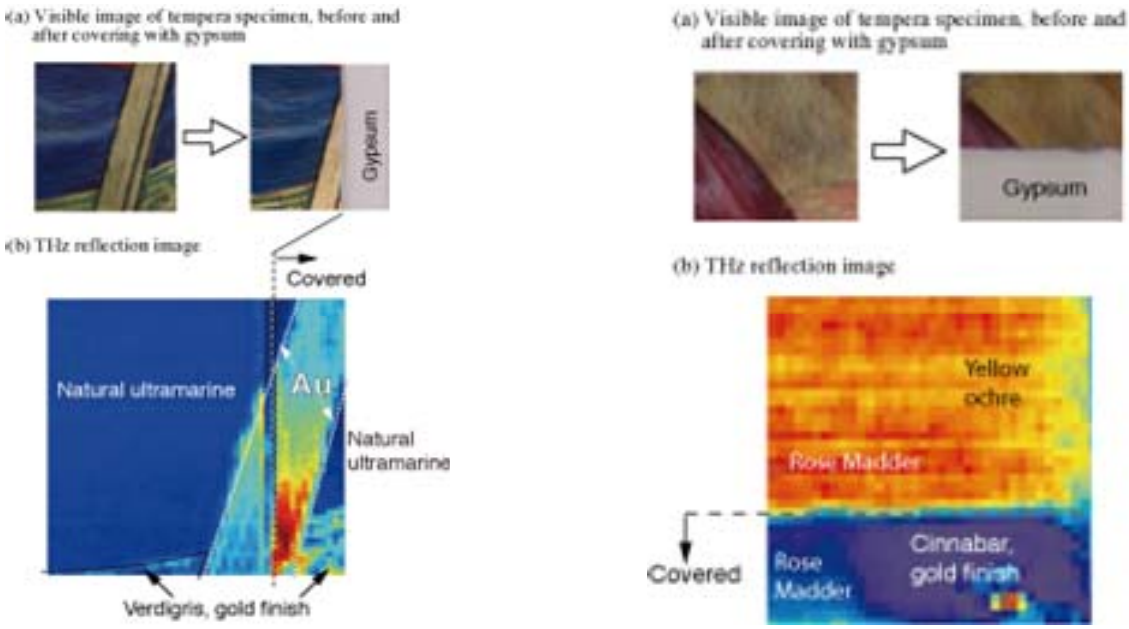

Figure 109 - ***Enhanced phase contrast THz images; in a) the verdigris is much more evident in the covered area respect to the uncovered. The same happens in b) where, we hardly distinguish the rose madder from yellow ochre***

The previous preliminary test demonstrated the potentials of phase-contrast technique as a tool with which it is possible to optimise the contrast among pigments response in reflection. Phase profiles of several pigments have been analyzed for a mosaic composed

by 4 different colors . The distance of the waveguide probe from the sample can be set at a position where the difference between phase profiles is maximized (see Figure 110).

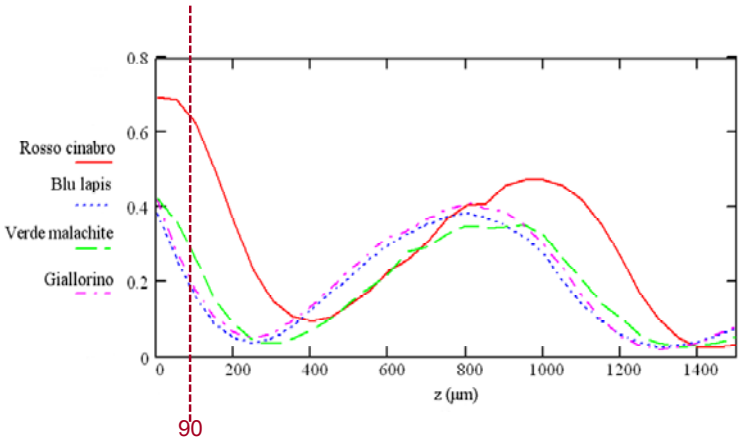

Figure 110- ***A phase profile scan, is performed changing the distance between the tip of the probe and the sample. This action can be repeated for any pigment generating four scanning profiles. There is a value that maximise the phase differences among the pigment responses.***

The THz image of the four colour mosaic is reported in Figure 111. A great contrast among three out of four pigments is evident while for two of them we hardly have a distinguishable fingerprint.

The possibility of obtaining spectral information about the sample was then investigated. By using the described scanning system it is possible to perform such a task, measuring the reflectivity while changing the distance between the sample and the probe (z-scan).

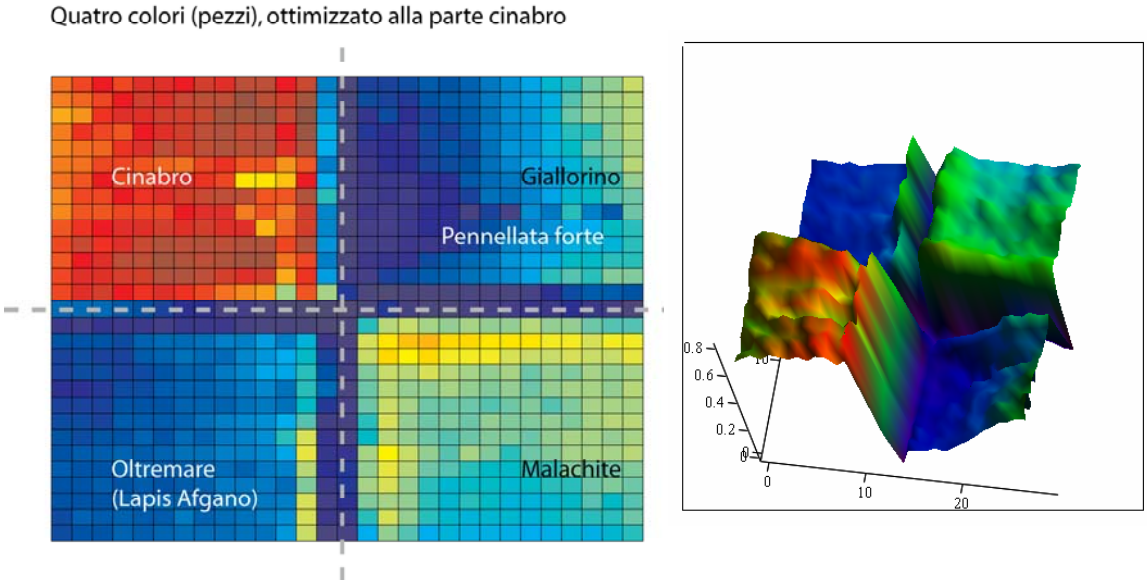

Figure 111 - ***A 2D THz scan of a mosaic composed by 4 different colors acquired at a distance where the phase contrast is maximum. Three pigments out of four are clearly distinguishable.***

The complex refraction index of the material is calculated by fitting the measured power z-profile with a model which takes into account the diffraction from the rectangular aperture of the output probe and the interference with the wave reflected from the sample. Resulting refraction index data are reported in Table VIII.

Table VIII - ***Real and imaginary part of the refraction index and absorption coefficient of different materials obtained using the phase sensitivity feature of the scanning system.***

Material	Re(n)	Im(n)	$\alpha(cm^{-1})$
COP	1.04	0.81	25.01
Blue Cobalt Oil on COP Plate	1.46	0.06	1.81
Blue Cobalt Acrylic on COP	1.30	0.26	8.06
Oil	1.15	0.36	11-36
Wax	1.32	0.28	8.35
Balsam	1.42	0.11	3.10

Further measurements are foreseen to verify the possibility of resolving pigments in a complex artwork, together with the ability of performing the measurements utilizing the second ENEA FEL source operating at shorter wavelength: FEL-CATS.

4.4.4 THz imaging detectors

The ENEA THz imaging facility at present makes use of shottky diodes as reliable and efficient THz detectors, and utilizes a x-y scanning platform in order to perform a bidimensional scan of the sample under investigation. Such a configuration requires some minutes to obtain a complete image of the sample, especially if high resolution is required. Moreover the scanning area is limited by the excursion limits of the scanning platform. It was then decided to verify the possibility of developing a new type of THz detector, based on High Electron Mobility Transistors (HEMT) in view of its possible integration in an imaging matrix, able to perform “one shot” THz measurements. HEMT used as THz detectors have been recently investigated where the detection mechanism is related to plasma wave excitations. A collaboration has been established between ENEA, CNR-IFN and SELEX SI in order to study the THz detection performance of such device. In order to study the THz detection process in a HEMT device, an active two dimensional near field imaging has been performed utilizing the reflective imaging system at the ENEA center of Frascati. The device under study is a double gate depletion GaN HEMT which is a standard high frequency device with a unity gain frequency at 30 GHz.

4.4.5 The IRMMW-THz 2010 International Conference

The IRMMW-THz Conference series is the oldest and largest forum devoted to the wide spectral range extending from the infrared to the millimeter wave region. The conference topics include infrared, terahertz and millimeter wave sources and components as well as far-infrared detectors and instrumentation. It also deals with applications as diverse as space science, biology, bio-medicine, cultural heritage conservation, environmental and material sciences, telecommunications and security. The conference typically alternates between Europe, Asia and USA on a three year cycle. The 2008 conference was held at CalTech Pasadena, CA (USA) and the 2009 conference was held in Busan, Korea.

The 35th International Conference on Infrared, Millimeter, and Terahertz Waves, IRMMW-THz 2010 was hosted by ENEA and held in Rome from September 5 to 10, 2010. The venue of the event was the "Angelicum" - Pontificia Università San Tommaso d'Aquino, located in the heart of the oldest area of the city of Rome. The success of the event is witnessed by the unprecedented record of 640 delegates registered at the conference coming from 36 countries from all over the world. Detailed info on the Conference is available at the website www.irmmw-thz2010.org.

Fig. 112 illustrates the geographical distribution of the participants indicating a strong contribution from Europe, as it usually happens for the continent hosting the conference. The chart also shows a strong Asian participation, mainly from Japan and Korea, which has become significant during the recent years of the conference. The numbers related to the North-American participation indicate a stable presence of scientists from this area.

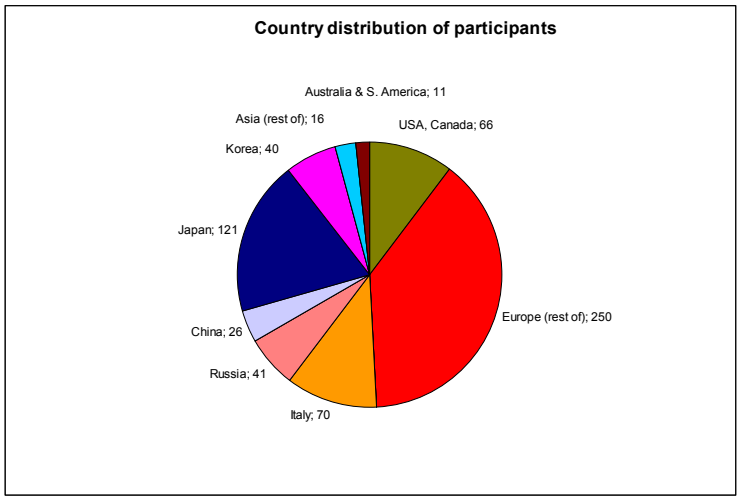

Fig. 112 – Distribution of participant to IRMMW-THz Conference per country

In Table IX we also report the distribution of participants per country in the years 2005 – 2010 clearly showing the positive trend and the record attendance achieved in Rome.

Due to the large number of participants and papers, the conference program has been articulated on joint Plenary Sessions, of two invited talks each, opening each day, followed by six parallel technical sessions every day. The Plenary Speakers have been selected on the basis of suggestions given by the Program Committee, the International Organizing Committee and the International Advisory Committee. Plenary lectures are intended to provide the state of the art of the most advanced research in the Infrared, Millimeter wave and Terahertz region, together with the overview of historical developments and new input and ideas from nearby fields.

The conference has offered the attendee a chance to participate in a wide range of topic areas that span all aspects of Infrared, Terahertz and Millimeter-Wave (IR, THz, and MMW) technology and applications from quantum physics, plasma physics, radio astronomy, biology and environmental science, to art conservation, material science, and security. The recent technological development in the Terahertz region has also stimulated the presence of industrial companies at the conference with the set-up of a Technical Exhibit, which has proven to be an important occasion to exchange information and contacts between the academic world and the industry. Fifteen companies have shown their products at the Technical Exhibit.

Overall 635 papers have been presented during IRMMW-THz-2010. Besides the 12 Plenary Talks, the conference counted 68 keynote talks and 235 oral talks, together with 320 posters presented in four afternoon sessions in the wonderful frame of the cloister of the Angelicum.

The Conference Proceedings have been published in electronic form only by the IEEE Microwave Theory and Techniques Society and are available on the IEEE Xplore Digital Library website. The publication references are: IEEE Catalog Number: CFP10IMM-ART, ISBN: 978-1-4244-6657-3.

Table IX - Number of participant to IRMMW-THz Conference per country in the last 6 years

	USA 2005	**China 2006**	**UK 2007**	**USA 2008**	**Korea 2009**	**Italy 2010**
	Williamsburg (VA)	**Shanghai**	**Cardiff**	**Pasadena**	**Busan**	**Rome**
USA, Canada	101	60	55	124	73	**66**
Europe (rest of)	99	123	134 (Excl. UK)	157	139	**250** (Excl. IT)
Italy						**70**
Russia	58	48	52	46	51	**41**
UK			85			
China		224				**26**
Japan						**121**
Korea					100	**40**
Asia (rest of)	116	117 (Excl. China)	178	130	204 (Excl. Korea)	**16**
Australia & S. America	8	9	19	19	9	**11**
TOTAL	382	581	523	476	576	**641**

4.4 Accelerators Development

The scientific experience acquired in many years of activity in the field of particle accelerators structures, devices and equipments, today constitutes an important national presidium for service and further development. It can satisfy the increasing demand of the scientific community, the industry, the medical community with its need of new therapy and diagnostics, and moreover it stimulates the training of new human resources. The field of particle accelerators is cross-sectional to many activities: in particular the accelerator activities deal physical technologies employing ionising particles and X rays for special applications (treatment of the materials) and for medicine. In the applications of non-ionising radiation, in particular with free electrons laser (FEL), electron accelerators are used as a powerful driver. In the following we briefly describe the main accelerators operating or under development at the ENEA Frascati Centre (UTAPRAD).

4.4.1 Electron accelerators

We list here the main developments:

1) Pulsed (4 μs) S band (3 GHz) standing wave linear accelerator with electron energy in the range 3 to 5 MeV and 0.2 A macropulse current, used for irradiation test and studies on the effects of the interaction of electrons with matter for scientific, medical and industrial applications (Figures 113, 114).

Figure 113 – *5-MeV Linac*

Figure 114 – *Output window of the 5-MeV Linac*

In the frame of various collaborations with private and public institutions irradiation experiments were carried out on cross linking of polymers, degradation of pesticides, degradation of phenols in olives' waste water, degradation of polychlorobiphenyls (PCB) present in oils of transformers, sterilization of water infected by pathogenic agents, control of the effects of the on the functionality of the blood cells, generation of x-rays radiation by Bremsstrahlung.

2) Pulsed (4 μs) S-band (3 GHz) standing wave linear accelerator with a maximum energy of 3 MeV (see Figure 115), equipped with a particular device for the manipulation of the e-beam, used as pilot for the generation of electromagnetic radiation in the sub-millimeter (0.4 – 0.8 THz) by means of magnetic undulators. During 2010 this device has been moved to a new bunker in the frame of a reorganization of the accelerator activities.

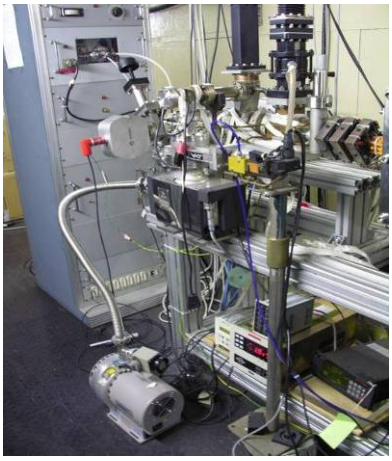

Figure 115 - *Pulsed S-band*

3) Circular accelerator (microtron) in S-band (3 GHz) with a maximum energy of 5 MeV, 0.3 A, 4 μs used as pilot of a compact FEL for the generation of electromagnetic radiation in the millimetre-wave region (90 - 150 GHz) (Figures 116, 117)

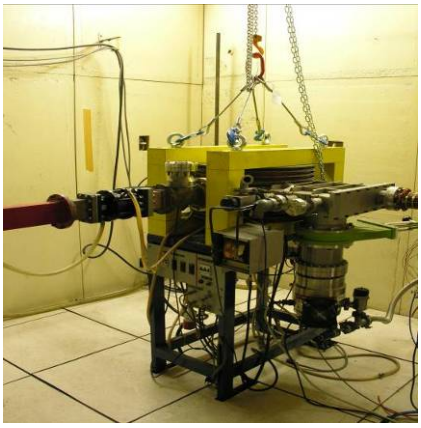

Figure 116 – *The microtron*

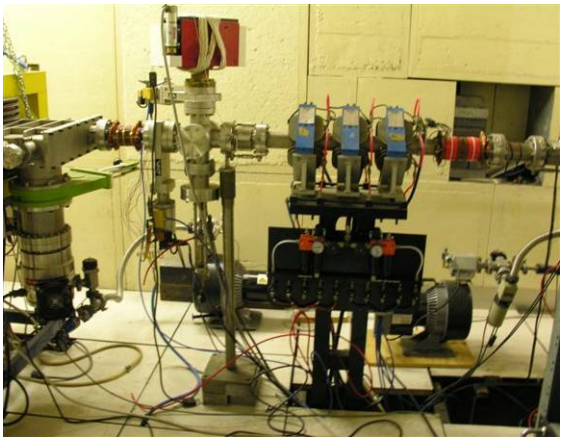

Figure 117 – *Beam transport channel with a triplet of quadrupoles*

4) Pulsed (4 μs) S-band (3 GHz) standing wave linear accelerator with variable energy from 3 MeV to 12 MeV, and average current of approximately 1 mA, developed in collaboration with the national industry, and employed in the hospitals for intra-operative radiating therapy (IORT).

4.4.2 Proton accelerator facility (ISPAN and IMPLART Projects)

This facility is based on a Linear proton accelerator in UHF band (425 MHz) with an energy of 7 MeV (Convention ISS-ENEA), which is used both for the production of radioisotopes for medical diagnostics and as a booster for further accelerating structures in band S for a 230 MeV of final energy for the oncologic therapy with protons (TOP-IMPLART) (Figure 118).

During 2010 many activities have been performed on the proton accelerator facility. In particular we can identify two macro-lines of activity:
1- bunker layout setting;
2- machine development.

The project, named IMPLART, is financed by Regione Lazio and provides a collaboration between ENEA, ISS (Italian Institute for Health) and IFO (Institute for the study and the cure of the human cancer pathology) for the construction of the 230 MeV facility at the San Raffaele (IFO) Hospital in a hall realized and devoted exclusively to this type of adron-radiotherapy for the treatment of a wide category of cancers.

Regarding the bunker layout in ENEA-Frascati Sinchrotron building, the FEL-CATS facility has been moved to another bunker to gain the necessary space for the new placement of the Accsys PL7 (7 MeV proton accelerator).and subsequent development to reach higher energy values. Such operation has caused a modification of both the security and control system. The cooling system also has been modified and new wire and optical connection for the PL 7 have been prepared.

At the same time a new control room has been set up closer to the machine, making a refurbishment of the PL7 control system. A new floor was prepared in the bunker to obtain the physical space necessary to allocate the vertical magnet (Fig. 119), the beam transport channel, and the accelerating SCDTL sections (up to 24 MeV of proton energy).

Figure 118 - Pictures of the interior of the proton accelerator bunker: RF power supplies (left), wave guide of the RFQ and the RFQ module up to 3 MeV of proton beam energy (right).

A special magnet stand was designed and constructed, which offers the possibility of adjusting the magnet position with micrometrical corrections. To this purpose new magnet polar expansions, a new vacuum chamber, and the holder of Petri dishes have been designed and constructed to deliver a vertical proton beam to biological samples. Calculations and numerical simulations about the proton beam trajectory in a magnetic field were performed.

Another activity has been devoted to the modeling of the beam transport channel, taking into account the best beam phase space conditions for injection in the subsequent sections of the machine, to achieve a proper matching between the 7 MeV accelerator (operating with 425 MHz RF field) and the accelerator section raising the energy up to 24 MeV with 3 GHz RF field.

Figure 119 - The vertical bending magnet with its stand and some of the personnel of the proton accelerator laboratory team (from left Dr. Carpanese Dr. Picardi and Mr. Ampollini)

4.4.3 Contribution to the SPARC and SPARX Projects

During 2010 the accelerator group has also participated to the SPARC project in collaboration with INFN-Frascati and MAT Laboratory. Advanced beam dynamics experiments have been carried out for the optimisation of the “velocity bunching” scheme. Preliminary tests have been performed on the generation of train of electron bunches in the picoseconds regime (COMB Experiment) to drive plasma wave (PWFA mechanism). The contribution has been devoted to the experiment planning, results analysis with e-beam dynamic calculations and participation to data records.

Further studies have dealt with beam dynamics in the SPARC Energy upgrade from 180 to 250 MeV employing compact RF structures in the C-band, and on the revised Technical Design Report of the SPARX FEL for a final energy of the accelerator up to 750 MeV.

4.4.4 New developments

In 2010 a collaboration started with ADAM – Geneve, a society for accelerators development, in order to develop two compact electron linear accelerators in the C-band (5712 MHz) at electron energies of 5 MeV (Figure 120) for X-rays production and 12 MeV (Figure 121) for medical application (IORT) respectively. ENEA designed the two structures, calculated the beam dynamics and modelled the RF systems. Furthermore the tuning of the structures was performed at the mechanical workshop of TSC-Fiumicino (Rome). The structures will be powered by a 2 MW C-Band magnetron provided by ADAM Company.

Useful indications from compact-FEL experiments at 150 GHz indicated solutions for an improvement of the performances of the 5-MeV driver microtron, mainly on lanthanum exaboride emitters and new solid state compact RF modulators complexes.

Figure 120 – ***5-MeV C-Band linac under test***

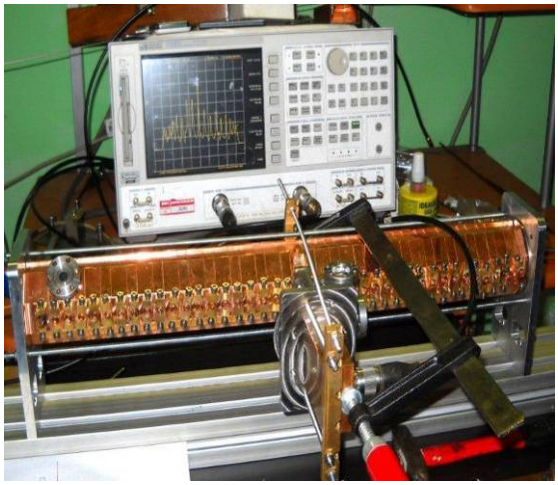

Figure 121 – ***12-MeV C-Band linac under test***

4.5 "Olocontrollo Emulativo" Technology

The cybernetic model of Synthetic Intelligence, named *GIASONE,* has conceived and implemented that emulates synthetically the process intrinsic in the intelligent biological system. Since the early '80s, an innovative research has begun starting from analysis of the knowledge of how the human process by "perceptions" leads to the "actions". The research is based on a new technological philosophy, using different cultural approaches, and the project target is to emulate the own behaviour of a biological intelligence.

Starting from *GIASONE* a new technology, named "Olocontrollo emulativo", was implemented and intelligent machines, or intelligence phases to conventional machines, were made emulating part of human intelligence process. During 2010 *GIASONE* has been integrated with emotional processes, necessary for intentionality and movement activities.

Using the cybernetic model conceived, several intelligent technological applications were designed and realized, in collaboration with several Large, Small and Medium Enterprises covering different application fields. The activities carried out in 2010 and the main results achieved are described in the following:

4.5.1 Activities and project results

SMART FLEX, is a prototype of a video inspection system to upgrade an already existing workstation. The system - implemented in collaboration with CRF (FIAT Research Center) and COMAU/Robotics - detects, in a default space, the position of some body parts "not related". The system reconstructs inside the volumetric environment and provides the location of various objects in the environment, to the control movements system of a robot gripping. The system solves the problem of fixed and predetermined position of the parties

in the industrial processes. The prototype realized at ENEA has a high level of versatility that makes it directly usable in different application fields.

ADAPTIVE PROSTHESIS, in people who use prosthesis, a considerable discomfort is generated by some physics events as: pressure peaks; friction between the stump and the interior of the reservoir; temperature increasing; sweating increasing etc. The aim of the project, is to create, in collaboration with the Santa Lucia Foundation and the ITOP company, a transfemoral prosthesis that dynamically adapts its volumetric shape to stump state. At moment the research and laboratory tests are being carried out on pressure sensors for use in this adaptive prosthesis. In the framework of this project, a thesis work has been carried out with the University Cattolica Del Sacro Cuore Medicina E Chirurgia "A. Gemelli", Terapia Occupazionale: "*Comportamento Occupazionale e Modello Cibernetico".* The thesis main focus is about the use of the cybernetic model GIASONE, in the domain of Occupational Science, allows additional access in the investigation of methodological issues and in designing solutions related to the dynamics of behaviour sciences.

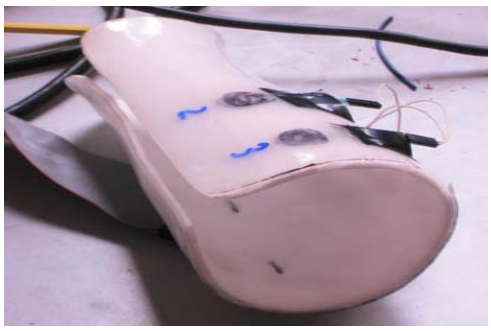

Fig. 122 - ***Pressure sensors test prototype***

ROBOTIC ARM, in collaboration with UTTRI a joint proposal has been made for the mechanization of fruit and vegetable harvest through a robotic arm. The proposal also provides product traceability by laser marking. The aim is to implement a project with the participation of industrial partners, that are already in the market for the construction of machines for the food industry.

BIC (Business Innovation Center) collaboration, during the year 2010, several contacts were undertaken with BIC-Colleferro and some companies, belonging to the same BIC, to analyze possible joint projects. This activity has led to organization of a workshop held at ENEA in May 2010, and the birth of some project ideas to be developed in 2011 as Domotics, industrialization of VISIO System, and remote domestic care.

VISIO is our perception system that was created for industrial robotics. When Visio is applied to humans becomes a device capable of converting an image captured by a camera into a tactile image. VISIO, is a complex system that allows a blind person to rebuild the environment through a skin stimulation. Several meetings with blind people were made and devoted to the description of cybernetic model and about to use of VISIO finalized to the industrialization of VISIO System.

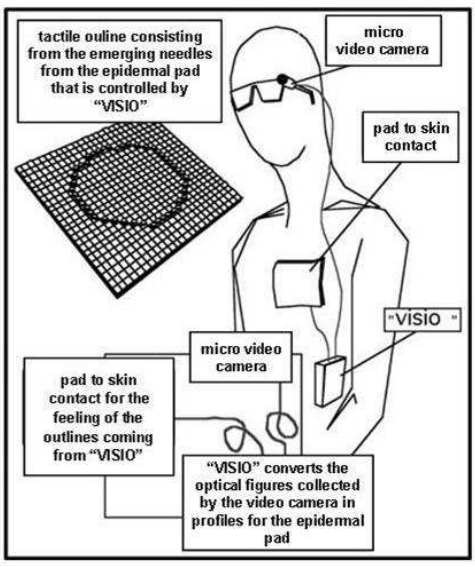

Fig. 123- ***Functional schema of VISIO***

5. Coordination of accelerator development for medical applications

The coordination activities in the field of accelerator development for medical applications followed three main lines in 2010: ISPAN, C-Band, TOP IMPLART

ISPAN project (2009 - 2011) aims to producing in a linac-based proton low energy facility for cellular and small animal radiobiology studies at Frascati Laboratories of ENEA. The program, partially funded by Regione Lazio, is conducted by NRT company, with ENEA the major technical consultant. Two SDCTL accelerating structures were designed and modeled and the drawing were passed to the companies NRT and CECOM in charge of their construction, other beam transport elements were collected.

Two **C-Band** linear accelerators were designed and constructed in the frame of a collaboration with ADAM S.A., a new Geneva company which aim to constructing medical accelerators, The two structures are described in the UTAPRAD-SOR Section.

The **TOP-IMPLART** program (Terapia Oncologica con Protoni, Intensity Modulated Proton Linear Accelerator for RadioTherapy) that aims at constructing an innovative Proton Linear Accelerator for Protontherapy in collaboration with ISS and IFO, was definitely approved for 11 M€ funding and an agreement was signed between Regione Lazio and ENEA for delivering the funds in four fiscal years starting 2011. The Program was also presented to the media by Regione Lazio. As to the design, it was revised in depth and many contacts were taken with several companies, mostly located in Lazio, which have the necessary expertise for the construction.

6. Technology transfer coordination

The Technology transfer coordination activities carried out in 2010 were focused on the following main aspects:

1) Co-organization of the workshop “ENEA incontra le imprese” (ENEA meets enterprises), held in Frascati Research Centre on May, 25th 2010
2) Preparation and participation to the meetings of the “Network of Technology Transfer Contact Points”. This is a recently established coordination panel, formed by ENEA personnel - not necessarily depending from the Technology Transfer Unit (UTT) - involved in technology and knowledge transfer activities in their respective units. The Network is intended to provide a link between ENEA personnel allocated to technical and scientific units and UTT, with the aim to collect requirements, provide support and disseminate information on technology transfer policies.
3) Participation on behalf of UTAPRAD to the ENEA initiative aimed at setting up a permanent scientific collaboration with the “Villa Reale and Parco di Monza” Consortium. The latter is in charge of restoring and re-launching the former royal residence and the annexed park located in Monza, one of the biggest and most important historical villas in Europe.
4) Support to the ENEA UTAPRAD personnel related to technology transfer demands (patent filing, establishment of spin-off companies etc.).

Personnel in 2010

UTAPRAD – Technical Unit for the Development of Applications of Radiations - Director dr. Roberta Fantoni (Roberta.fantoni@enea.it)

Direction staff members

Emilia Batisti, Elisabetta Borsella, Giorgio Fornetti, Anna Pagliardini, Luigi Picardi, Ilaria Sergi, Giulio Tuccinardi

Guests

Susanna Carroccia

UTAPRAD-STG – Administration and Management service – Director dr. Tiziana Giuli (tiziana.giuli@enea.it)

STG staff members

Paola Chiappini, Tiziana Vari

UTAPRAD-DIM – Diagnostics and Metrology Laboratory – Director dr. Antonio Palucci (antonio.palucci@enea.it)

DIM staff members

Lorella Addari, Paolo Aristipini, Florinda Artuso, Luisa Caneve, Roberto Carletti, Dario Cataldi, Roberto Chirico, Francesco Colao, Luigi De Dominicis, Antonella De Ninno, Giovanni Dipoppa, Mario Ferri De Collibus, Luca Fiorani, Gianfranco Giubileo, Massimiliano Guarneri, Maurizio Guarracino, Antonia Lai, Violeta Lazic, Giovanni Leggeri, Giacomo Lorenzoni, Salvatore Marullo, Ivano Menicucci, Marcello Nuvoli, Roberto Ricci

Research fellows

Massimo Francucci, Maria Sighicelli, Valeria Spizzichino

Guests

Adriana Puiu, Dave Poreh, Pilar Ortiz, Sonja Jovicevic

UTAPRAD-MAT – Mathematical Modelling Laboratory – director dr. Giuseppe Dattoli (giuseppe.dattoli@enea.it)

MAT staff members

Franco Ciocci, Luca Giannessi, Marcello Quattromini, Elio Sabia, Ivan P. Spassovsky, Amalia Torre

Research fellows

Mario Del Franco

UTAPRAD-MNF Photonics Micro and Nano-structures Laboratory – director dr. Rosa Maria Montereali (rosa.monterali@enea.it)

MNF staff members

Francesca Bonfigli, Sabina Botti, Doriano Brogioli, Luciano Cantarini, Michele A. Caponero, Rosaria D'Amato, Roberto D'Imperio, Stefano Libera, Guido Martini, Salvatore Paolini, Alessandro Peloso, Andrea Polimadei, Antonino Santoni, Gaetano Terranova, Maria Aurora Vincenti, Alessandro Zini

Research fellows

Rocio Martinez Morillas, Rajesh Menon M. R., Ernst Popovici, Lavinia Gavrila-Florescu

Guests

Hypolito José Kalinowski

UTAPRAD-SOR - Radiation Sources Laboratory – director dr. Gian Piero Gallerano (gianpiero.gallerano@enea.it)

SOR staff members

Alessandro Ampollini, Rosanna Balvetti, Maria Laura Bargellini, Marco Battaglia, Sarah Bollanti, Ezio Campana, Mariano Carpanese, Gemma Casadei, Domenico De Meis, Paolo Di Lazzaro, Andrea Doria, Antonio Fastelli, Alessandra Filippini, Francesco Flora, Emilio Franconi, Emilio Giovenale, Giovanni Messina, Luca Mezi, Daniele Murra, Loredana Puccia, Concetta Ronsivalle, Davide Vicca, Consuelo Zampetti

Research fellows

Alberto Petralia, Vincenzo Surrenti

Research Products

Peer reviewed papers

1. Fantoni R., Fiorani L., Loreti S., Palucci A., Lazzara L., Nardello I. “Remote and in-situ seawater bio-optical description during the XVIII oceanographic expedition” *Optoelectronics and Advanced Materials – Rapid Communications* **4**, 754-758 (2010)
2. Fantoni R., Fiorani L., Okladnikov I. G., Palucci A. ”Local observations of primary production in the Ross Sea: results of a lidar-calibrated satellite algorithm” *Optoelectronics and Advanced Materials – Rapid Communications* **4**, 759-763 (2010)
3. Fantoni R., Fiorani L., Okladnikov I. G., Palucci A.”Comparison of SeaWiFS, MODIS-Terra, MODIS-Aqua and MERIS satellites in the Southern Ocean” *Optoelectronics and Advanced Materials – Rapid Communications* **4**, 764-768 (2010).
4. Poreh D., Fiorani L. “Software for analyzing and visualizing laser remote sensing (LIDAR) data” *Journal of Optoelectronics and Advanced Materials* **12**, 1231-1236 (2010)
5. Cisek M., Colao F., Demetrio E., Di Cicco A., Drozdowska V., Fiorani L., Goszczko I., Lazic V., Okladnikov I. G., Palucci A., Piechura J., Poggi C., Sighicelli M., Walczowski W., Wieczorek P. “Remote and local monitoring of dissolved and suspended fluorescent organic matter off the Svalbard” *Journal of Optoelectronics and Advanced Materials* **12**, 1604-1618 (2010)
6. Fiorani L., Caneve L., Colao F., Fantoni R., Ortiz P., Gómez M. A., Vázquez M. A. “Real-time diagnosis of historical artworks by laser-induced fluorescence” *Advanced Materials Research* **133-134**, 253-258 (2010)
7. S. Marullo, R. Santoleri, V. Banzon,3 R. H. Evans, and M. Guarracino: A diurnal-cycle resolving sea surface temperature product for the tropical Atlantic, Journal of Geophysical Reserach, VOL. 115, C05011, doi 10.1029/2009JC005466, 2010
8. Artuso F., Chamard P., Chiavarini S., di Sarra A., Meloni D., Piacentino S., Sferlazzo D.M., Tropospheric halocarbons and nitrous oxide monitored at a remote site in the Mediterranean, Atmospheric Environment. **44** (2010) 4944-4953.
9. L. Caneve, A. Diamanti, F. Grimaldi, G. Palleschi, V. Spizzichino, F. Valentini, Analysis of fresco by laser induced breakdown spectroscopy, Spectrochim. Acta **B 65** (2010) 702-706.
10. L. De Dominicis, M. Ferri de Collibus, G. Fornetti, M. Guarneri, M. Nuvoli, R. Ricci, M. Francucci “Improving underwater imaging in an amplitude modulated laser system with radio frequency control technique” Journal of the European Optical Society - Rapid Publications **5**, 10004 (2010), 10004-1 – 10004-5, ISSN 1990-2573.
11. R. Ricci, M. Francucci, L. De Dominicis, M. Ferri de Collibus, G. Fornetti, M. Guarneri, M. Nuvoli, E. Paglia, and L. Bartolini, "Techniques for Effective Optical Noise Rejection in Amplitude-Modulated Laser Optical Radars for Underwater Three-Dimensional Imaging", EURASIP Journal on Advances in Signal Processing, Hindawi Publishing Corporation, Vol. **2010**, 2010.
12. G. Giubileo, A. Puiu, “Photoacoustic Spectroscopy of Standard Explosives in the MIR Region”, Nucl. Instr. and Meth. **A 623** (2010), 771-777.
13. G. Giubileo, A. Lai, D. Piccinelli, A. Puiu, “Laser diagnostic technology for early detection of pathogen infestation in orange fruits”, Nucl. Instr. and Meth. **A 623** (2010), 778-781.
14. Marullo et al., “A diurnal cycle resolving sea surface temperature product for the tropical Atlantic”, Journal of Geophysical Reserach, **115**, C05011, doi 10.1029/2009JC005466, 2010.
15. A. De Ninno, A. Congiu Castellano “Deprotonation of Glutamic Acid Induced By Weak Magnetic Field: An FTIR-ATR Study” Bioelectromagnetics, DOI 10.1002/bem.20631 (2010)
16. A. De Ninno “La Scoperta di una nuova fonte energetica: dalla prova di principio alla realizzazione di un prodotto”, DAXXIX , Anno XI-n.3- Novembre 2010
17. A.M.Popov, F.Colao, R.Fantoni “Spatial confinement of laser-induced plasma to enhance LIBS sensitivity for trace elements determination in soils” J. Anal. At. Spectrom., (2010), **25**, pp.837-848.
18. F.Colao, R.Fantoni, P.Ortiz, M.A.Vazquez, J.M.Martin, R.Ortiz, N.Idris, Quarry identification of historical building materials by means of laser induced breakdown spectroscopy, X-ray fluorescence and chemometric analysis, Spectrochim. Acta **B 65** (2010),.688-694.
19. M. Ferrario, D. Alesini, A. Bacci, M. Bellaveglia,R. Boni M. Boscolo, M. Castellano, E. Chiadroni, A. Cianchi, L. Cultrera,G. Di Pirro,L. Ficcadenti,D. Filippetto,V. Fusco, A. Gallo,G. Gatti,L. Giannessi, M. Labat, B. Marchetti, C. Marrelli,M. Migliorati,A. Mostacci, E. Pace, L. Palumbo, M. Quattromini,C. Ronsivalle, A. R. Rossi, J. Rosenzweig,L. Serafini,M. Serluca, B. Spataro,C. Vaccarezza,and C. Vicario ““Experimental Demonstration of Emittance Compensation with Velocity Bunching”, PHYSICAL REVIEW LETTERS, **104**, 054801 (2010)

20. G. Dattoli and K. Zhukovsky “Appèl polynomials series expansions” Int. Math. Forum 5, **14**, 649-662 (2010)
21. G. Dattoli, B. Germano, M. R. Martinelli and P. E. Ricci “Negative derivative and special functions” Appl. Math. Comput. **217**, 3924-3928 (2010)
22. M. Agostino,C. Pellegrini, L. Giannessi and S. Reiche “Comparative study of non-ideal beam effects in high gain harmonic generation and self-seeded free electron lasers” Phys. Rev. Special Topics, **13**, 070701 (2010).
23. M.A.Vincenti, T.Marolo and R.M.Montereali, *Advanced Optical Spectroscopy of Luminescent Color Centers in Lithium Fluoride Thin Films,* Radiation Measurements **45** (2010) 359-361
24. F.Bonfigli, S.Almaviva, I.Franzini, R.M.Montereali, A.Cedola, S.Lagomarsino, D.Pelliccia, *Visible Emitting Color Centers in Lithium Fluoride for X-ray Imaging Applications,* Radiation Measurements **45** (2010 599-601 http://dx.doi.org/10.1016/j.radmeas.2009.09.011
25. R.M.Montereali, S.Almaviva, F.Bonfigli, A.Cricenti, A.Faenov, F.Flora, P.Gaudio, A.Lai, S.Martellucci, E.Nichelatti, T.Pikuz, L.Reale, M.Richetta, M.A.Vincenti, *Lithium Fluoride Thin Films Detectors for Soft X-Ray Imaging at High Spatial Resolution,* Nuclear Instruments and Methods **A 623** (2010)758-762 http://dx.doi.org/10.1016/j.nima.2010.02.089
26. R.M.Montereali, T.Marolo, M.Montecchi, E.Nichelatti, *Spectral Investigation of Colour Centres in Gamma Irradiated Lithium Fluoride Thin Films,* Nuclear Instruments and Methods **B 268** (2010) 2866-2869 http://dx.doi.org/10.1016/j.nimb.2010.03.020
27. E.Nichelatti, S.Almaviva, F.Bonfigli, I.Franzini, R.M.Montereali, M.A.Vincenti, *Photoluminescence from Colour Centres Generated in Lithium Fluoride Thin Films and Crystals by Extreme-Ultraviolet Irradiation,* Nuclear Instruments and Methods **B 268** (2010) 3035-3039.
28. F.Somma, R.M.Montereali, M.A.Vincenti, S.Polosan, M.Secu, *Radiation Induced Defects in Pb^{2+}-Doped LiF Crystals,* Optical Materials **37** (2010) 1309-1312.
29. F.Bonfigli, S.Almaviva, F.Flora, R.M.Montereali, A.Reale, A.Ritucci, P.Zuppella, *Color-Center Photoluminescent Nano-Patterns Induced in Lithium Fluoride by Soft X-Ray Laser Beam,* J. Non-Crystalline Solids **356** (2010) 1968-1971
30. M.Barbagallo, L.Cosentino, G.Greco, R.M.Montereali, A.Pappalardo, C.Scirè, S.Scirè, M.A.Vincenti, and P.Finocchiaro, *Development of a Thermal Neutron Detector based on Scintillating Fibers and Silicon Photomultipliers* Review of Scientific Instruments **81**(2010) 093503
31. S.Botti, L.Cantarini, A. Palucci, *Surface-enhanced Raman spectroscopy for trace-level detection of explosives*, J. Raman. Spectrosc. 2010, 41, 866-869
32. R.D’Amato, M.Falconieri, F.Fabbri, V.Bello, E.Borsella, *Preparation of luminescent Si nanoparticles by tailoring the size, crystallinity and surface composition,* J. Nanopart. Res., **12**, 1845-1858 (2010) DOI 10.1007/s11051-009-9746-3..
33. M.A.Caponero, P.Corvaglia, A.Largo, G.Maddaluno, *Development and Some Investigative Testing of Smart Structural FRP Devices with Embedded Fiber Optic Sensor for Health Monitoring of Civil Structures,* Advances in Structural Engineering **13** (2010) 905-925.
34. M.A.Caponero, A.Coricciati, P.Corvaglia, G.Fardin, A.Largo, *Production and Characterisation of Multifunctional Textile for Masonry Retrofitting and Health Monitoring,* Sensors & Transducers Journal, **9** (2010) 28-38.
35. M. Venturini,M. Migliorati,C. Ronsivalle,M. Ferrario and C. Vaccarezza “Dynamics of longitudinal phase-space modulations in an rf compressor for electron beams”, PHYSICAL REVIEW SPECIAL TOPICS - ACCELERATORS AND BEAMS **13**, 080703 (2010)
36. P. Di Lazzaro: “Laser produced plasmas for bio-photonics” in Biophotonics: Spoectroscopy, Imaging Sensing and Manipulation, B. Di Bartolo and J. Collins Eds. NATO SPS Series, (Springer, 2010) pp. 305 - 319. ISBN 978-94-007-0028-4 ISSN 1874-6500.
37. P. Di Lazzaro, D. Murra, A. Santoni, G. Fanti, E. Nichelatti, G. Baldacchini: “Deep Ultraviolet radiation simulates the Turin Shroud image” Journal of Imaging Science and Technology **54**, 040302-(6) (2010)
38. G. Fanti, J.A. Botella, P. Di Lazzaro, T. Heimburger, R. Schneider, N. Svensson: “Microscopic and macroscopic characteristics of the Shroud of Turin image superficiality” Journal of Imaging Science and Technology **54**, 040201-(8) (2010)
39. L. Reale, J. Kaiser, L. Pace, A. Lai, F. Flora, A. Angelosante, A. Tucci, P. Zuppella, L. Mancini, et al.: “Detection of lead in zea mays by dual-energy X-ray microtomography at the SYRMEP beamline of the ELETTRA synchrotron and by atomic absorption spectroscopy”, Microscopy Research And Technique **73**, pp. 638–649, (2010).
40. J. Colgan, J. Abdallah Jr, A. Ya. Faenov, T. A. Pikuz, I. Yu Skobelev, F. Flora, M. Francucci and S. Martellucci: “Model calculations and measurements of the emission of a barium plasma in the spectral range of high-n Rydberg levels in a near Ni-like state”, J. of Physics B: Atomic, Molecular and Optical Physics, **43**, p. 175701-(9), (2010).

Books and Book Chapters

1. Fiorani L., Mitev V. (eds.) "Recent Advances in Atmospheric Lidars" *INOE Publishing House*, Bucharest, Romania (2010)
2. Fiorani L. "Questo pazzo pazzo inverno" (in Italian) *Città Nuova ONLINE* (26-01-2010) e *Città Nuova* **2**, 55 (2010)
3. Fiorani L., Pasini A. "Il pianeta che scotta: capire il dibattito sui cambiamenti climatici" (in Italian) *Città Nuova*, Roma, Italy (2010)
4. Fiorani L., Aiuppa A., Buongiorno F., Colao F., Del Bugaro D., Fantoni R., Giudice G., Giuffrida G., Guerrieri L., Guida R., Kataev M. Y., Kataev S. G., Liuzzo M., Lonchin A. V., Palucci A., Spinetti C., Sykhanov A. Y. "Chemicomorphological characterization of Etna's plume by atmospheric lidar, satellite radiometers and in-situ measurements" Manakos I., Kalaitzidis C. (eds.), Imagin[e,g] Europe, *IOS Press*, Amsterdam, The Netherlands (2010) pp. 122-130
5. Colao F., Fantoni R., Fiorani L., Menicucci I., Nuvoli M., Palucci A., Terranova G. "Lidar identification of oil spills during the PRIMI cruise" Barale V., Gower J. F. R., Alberotanza L. (eds.), Proceedings "Oceans from Space" Venice 2010, *Joint Research Centre of the European Commission*, Ispra, Italy (2010) pp. 65-66
6. Colao F., Fantoni R., Fiorani L., Palucci A., Sighicelli M. "Laser-induced fluorescence measurement of sea water bio-optical parameters during the SESAME campaign" Barale V., Gower J. F. R., Alberotanza L. (eds.), Proceedings "Oceans from Space" Venice 2010, *Joint Research Centre of the European Commission*, Ispra, Italy (2010) pp. 67-68
7. Fantoni R., Ferri De Collibus M., Fornetti G., Francucci M., Guarneri M., Ricci R., Caneve L., Colao F., Fiorani L., Palucci A., Dell'Erba R., Blasi L., Di Falco V., Moriconi C. "Laser scanning technologies for 2D and 3D imaging and characterization of decorated monumental surfaces" Ferrari A. (ed.), Proceedings 4th International Congress on "Science and Technology for the Safeguard of Cultural Heritage on the Mediterranean Basin", *AIC & Fondazione Roma-Mediterraneo*, Rome, Italy (2010) pp. 419-428
8. Fiorani L. "Lidar application to lithosphere, hydrosphere and atmosphere" Koslovskiy V. V. (ed.), Progress in Laser and Electro-Optics Research, *Nova Science Publishers*, Hauppauge, USA (2010) pp. 21-75
9. Artale V., V. Rupolo, F. Raicich, S. Marullo, S. Calmanti, G. Sannino, G. Fusco: "Variabilità, trend e cambiamenti climatici delle masse d'acqua del Mar Mediterraneo nel XX secolo". In "I cambiamenti climatici in Italia: evidenze, vulnerabilità e impatti" a cura di Sergio Castellari e Vincenzo Artale (Centro Euro-Mediterraneo per i Cambiamenti Climatici). Libro pp. 590.

Patents

1. Caneve L., Colao F., Fiorani L., Palucci A. "*Radar laser portatile per la diagnostica remota di superfici"* Brevetto *RM2010A000606 (2010)*

Conference Proceedings

1. S. Botti, M. Carpanese, L. Cantarini, G. Giubileo, V. Lazic, S. Jovicevic, A. Palucci, A. Puiu, "Trace detection of explosive compounds by different laser-based techniques at the ENEA Laboratories", Proc. of SPIE Vol. **7665** (2010), 76650O-1.
2. Salusti E., R. V. Rupolo and S. Marullo: "East Mediterranean Transient and Dense Water Dynamics in the Aegean Sea, 2010" - Rapp. Comm. Int. Mer Medit. Vol. 39 - page 175.
3. Napolitano E., R. Iacono , S. Marullo and V, Artale: "Aspects of the Surface Tyrrhenian Sea Summer Circulation 2010" - Rapp. Comm. Int. Mer Medit. Vol. 39 - page 147
4. Marullo S., V. Artale and R. Santoleri: "The SST Multi-Decadal Variability In The Atlantic-Mediterranean Region 2010" - Rapp. Comm. Int. Mer Medit. Vol. 39 - page 140
5. V. Lazic, A. Palucci, S. Jovicevic, M. Carpanese, C. Poggi, E. Buono, Detection of explosives at trace levels by Laser Induced Breakdown Spectroscopy (LIBS), SPIE Vol. 7665, p. 76650V, 1-9.).
6. L.Caneve, F. Colao, V, Spizzichino, "Analysis of biofilms from Roman catacombs by laser induced fluorescence and multivariate analysis", Proc. of CMA4CH, Application of Multivariate Analysis and Chemometry to Cultural Heritage and Environment 3rd ed., Taormina, 26-29 September 2010, pp. 29-31.

7. C. Vaccarezza, E. Chiadroni, M. Ferrario, G.Dattoli, L. Giannessi, M. Quattromini, C. Ronsivalle, M.Venturini, M. Migliorati, "Microbunching Instability Effect Studies and Laser Heater Optimization for The SPARX FEL Accelerator" , Proc. IPAC10 Conference, Kyoto (Japan) p.1779
8. M. Ferrario, D. Alesini, F. Anelli, M. Bellaveglia, M. Boscolo, L. Cacciotti, M. Castellano, E. Chiadroni, L. Cultrera, G.Di Pirro, L. Ficcadenti, D. Filippetto, S. Fioravanti, A. Gallo, G. Gatti, E. Pace, R. Sorchetti, A. Mostacci, C.Vaccarezza, L. Giannessi, A. Petralia, C. Ronsivalle,A. Bacci, V. Petrillo, A.R. Rossi, L. Serafini,O. Limaj, M. Moreno, M. Serluca,A. Cianchi, B. Marchetti,C. Vicario, PSI,J. Rosenzweig, H. Tomizawa, "Advanced Beam Dynamics Experiments with The SPARC High Brightness Photoinjector" , Proc. IPAC10 Conference, Kyoto (Japan) p.2311
9. L. Giannessi, A. Petralia, G. Dattoli, F. Ciocci, M. Del Franco, M. Quattromini, C. Ronsivalle, E. Sabia, I. Spassovsky, V. Surrenti, IT. D. Filippetto, G. Di Pirro, G. Gatti, M. Bellaveglia, D. Alesini, M. Castellano, E. Chiadroni, L. Cultrera, M. Ferrario, L. Ficcadenti, A. Gallo, A, Ghigo, E. Pace, B. Spataro, C. Vaccarezza, A. Bacci, V. Petrillo, A.R. Rossi, L. Serafini ,M. Serluca, M. Moreno, L. Poletto, F. Frassetto,J.V. Rau, V. Rossi Albertini, IT. A. Cianchi, A.Mostacci, M Migliorati, L. Palumbo, G. Marcus, P. Musumeci, J.Rosenzweig, M. Labat, F. Briquez, M. E. Couprie, B. Carré, M.Bougeard, D. Garzella ,G. Lambert, C.Vicario "FEL Experiments At SPARC: Seeding with Harmonics Generated in Gas",Proc. 32nd International FEL Conference MAX Lab. Sweden, (August 2010)
10. L. Giannessi, A. Petralia, G. Dattoli, F. Ciocci, M. Del Franco, M. Quattromini, C. Ronsivalle, E.Sabia, I. Spassovsky, V. Surrenti D. Filippetto, G. Di Pirro, G. Gatti, M.Bellaveglia, D. Alesini, M. Castellano, E. Chiadroni, L. Cultrera, M. Ferrario, L. Ficcadenti, A.Gallo, A, Ghigo, E. Pace, B. Spataro, C. Vaccarezza, A. Bacci, V. Petrillo, A.R.Rossi, L. Serafini,M. Serluca, M. Moreno, L. Poletto, F. Frassetto,J.V. Rau, V. Rossi Albertini, A. Cianchi, A.Mostacci, M Migliorati, L. Palumbo, G. Marcus, P. Musumeci, J.Rosenzweig, S. Spampinati, M. Labat, F. Briquez, M. E. Couprie, B. Carré, M. Bougeard, D. Garzella, G. Lambert.C.Vicario "FEL Experiments at SPARC: Operation in Seeded and Chirped Mode" , Proc. 32nd International FEL Conference MAX Lab. Sweden, (August 2010)
11. F.Bonfigli, S.Almaviva and R.M.Montereali, *Confocal Microscopy on Light-emitting Nanostructures and X-ray Imaging Detectors Based on Color Centers in Lithium Fluoride*, AIP Conference Proceedings **1275** (2010)170-173.
12. H.J.Kalinowski, R.M.Montereali, M.A.Vincenti, R.N.Nogueira, *Visible photoluminescence in coloured lithium fluoride under ultra-violet continuous wave excitation*, IOP Publishing, Journal of Physics: Conference Series **249** (2010) 012002.
13. R.M.Montereali, S.Almaviva, F.Bonfigli, I.Franzini, D.Pelliccia, A.Cedola, S.Lagomarsino, *F and F-aggregates colour centres in lithium fluoride for high spatial resolution x-ray imaging*, IOP Publishing, Journal of Physics: Conference Series **249** (2010) 012003.
14. F.Bonfigli, M.Montecchi, R.M.Montereali, E.Nichelatti, M.Piccinini, F.Somma, *Colour-centre concentrations in broad-band light-emitting strip waveguides in Lithium Fluoride*, IOP Publishing, Journal of Physics: Conference Series **249** (2010) 012004.
15. O.Goncharova, R.M.Montereali and G.Baldacchini, *Thin film structures with nanocrystals: an origin of enhanced photo response*, IOP Publishing, Journal of Physics: Conference Series **24**9 (2010)012063.
16. F.Bonfigli, P.Gaudio, I.Lupelli, E.Nichelatti, M.Richetta, M.A.Vincenti and R.M.Montereali, *Characterization of LiF-based Soft X-Ray Imaging Detectors by Confocal Fluorescence Microscopy*, IOP Conference Series: Materials Science and Engineering **15** (2010) 012025.
17. F.Somma, P.Aloe, F.D'Acapito, R.M.Montereali, S.Polosan, M.Secu, M.A.Vincenti, *Optical and X-ray Absorption Spectroscopy in Lead Doped Lithium Fluoride Crystals*, IOP Conference Series: Materials Science and Engineering **15** (2010) 012035.
18. M.A.Vincenti, G.Baldacchini, V.S.Kalinov, R.M.Montereali, A.P.Voitovich, *Spectroscopic Investigation of F, F_2 and F_3^+ Color Centers in Gamma Irradiated Lithium Fluoride Crystals*, IOP Conference Series: Materials Science and Engineering **15** (2010) 012053.
19. S.Polosan, M.Secu, C.Logofatu, F.Somma, R.M.Montereali, M.A.Vincenti, *Radiation Induced Defects in Tl^+-Doped LiF Crystals*, IOP Conference Series: Materials Science and Engineering 15(2010)012081.
20. R.M.Montereali, F.Bonfigli, V.Mussi, E.Nichelatti, A.Santoni, S.Scaglione, *Optical investigation of metallic lithium colloids and F centres in ion-assisted LiF thin films*, IOP Conference Series: Materials Science and Engineering **15** (2010) 012017
21. M.Falconieri, E.Borsella, R.D'Amato, F.Fabbri, E.Trave, V.Bello, G.Mattei, Y.Nie, D.Wang, *On the Red Photoluminescence Emission from Surface-Oxidised Silicon Nanocrystals*, AIP Conference Proceeding BONSAI Project Symposium: Breakthroughs in Nanoparticles for Bio-Imaging, Vol**. 1275**, 50-57 (2010) doi:10.1063/1.3505082.
22. R.D'Amato, M.Falconieri, E.Borsella, *Synthesis and Photoluminescence of Ytterbium-doped Silicon Nanocrystals*, AIP Conference Proceeding BONSAI Project Symposium: Breakthroughs in Nanoparticles for Bio-Imaging, Vol. **1275**, 75-79 (2010) doi:10.1063/1.3505086.

23. I.Rivolta, B.Lettiero, A.Panariti, R.D'Amato, V.Maurice, M.Falconieri, N.Herlein, E.Borsella, G.Miserocchi, *Si-based Nanoparticles: a biocompatibility study*, AIP Conference Proceeding BONSAI Project Symposium: Breakthroughs in Nanoparticles for Bio-Imaging, Vol. **1275**, 94-97 (2010) doi:10.1063/1.3505090.
24. D. Filippetto, M. Bellaveglia, E. Chiadroni, A. Gallo, A. Mostacci, A. Cianchi, B. Marchetti, C. Ronsivalle,"High Brightness Beam Measurement Techniques and Analysis at SPARC", Proc. IPAC10 Conference, Kyoto (Japan) p.939
25. M. Venturini, M. Migliorati, C. Ronsivalle,M. Ferrario, C. Vaccarezza "Microbunching and RF Compression" , Proc. IPAC10 Conference, Kyoto (Japan) p.1776
26. D. Alesini, A. Bacci, M. Bellaveglia, R. Boni, G. Di Pirro, M. Ferrario, L. Ficcadenti, A. Gallo,F. Marcellni, A. Mostacci, E. Pace, B. Spataro, C. Vaccarezza, C. Ronsivalle, L. Palumbo, V. Spizzo, "Beam Energy Upgrade Of The Frascati FEL Linac with a C-band RF system", Proc. IPAC10 Conference, Kyoto (Japan) p.3682
27. C. Ronsivalle, L. Picardi,P. Antici, A. Mostacci, M. Migliorati, L.Palumbo,D. Alesini "Hybrid Schemes for the Post-Acceleration ff Laser Generated Protons" , Proc. IPAC10 Conference, Kyoto (Japan) p.4363.
28. R. Balvetti, M.L. Bargellini, M. Battaglia, A. Botticelli, G. Casadei, A. Filippini, A. Guidoni, E. Pancotti, L. Puccia, L. Rubini, C. Zampetti, F. Bernardo,A. Grandinetti, B. Mussi, G. Bozanceff, C. Iencenelli,"From Natural Intelligence To Synthetic Intelligence Through Cybernetic Model" Proceedings Congresso DRANS2010 p. 216-220.
29. P. Di Lazzaro: "Ipotesi scientifiche sulla formazione dell'immagine sulla Sindone" 30GIORNI, Aprile 2010, pp. 72 – 75.
30. P. Di Lazzaro, D. Murra, A. Santoni, G.- Baldacchini: "Sub-micrometer coloration depth of linens by vacuum ultraviolet radiation", Proc. International Workshop on the Scientific approach to the Acheiropoietos Images, edited by P. Di Lazzaro (2010) pp. 3 – 10.
31. D. Murra, P. Di Lazzaro: "Sight and brain, an introduction to the visually misleading images", Proc. International Workshop on the Scientific approach to the Acheiropoietos Images, edited by P. Di Lazzaro (2010) pp. 31 – 34.

Papers presented at Conferences

1. Colao F., Caneve L., Fantoni R., Fiorani L. "Laser scanning techniques for remote 2D hyperspectral imaging of decorated monumental surfaces" 30th EARSeL Symposium, *EARSeL*, Paris, France (2010)
2. Poreh D., Fiorani L., Colao F., Palucci A. "IDL script for visualizing Laser remote sensing (Lidar) data" International Conference on Environmental Observations, Modeling and Information Systems ENVIROMIS 2010, *SCERT,* Tomsk, Russia (2010)
3. Fiorani L., Colao F., Palucci A., Poreh D. "First simultaneous measurement of water vapor concentration, extinction coefficient and transport of a volcanic plume by differential absorption lidar"25th International Laser Radar Conference, *ICLAS*, St. Petersburg, Russia (2010)
4. Fiorani L., Colao F., Palucci A., Poreh D. "Lidar characterization of volcanic plumes" 4th International Workshop on Optoelectronic Techniques for Environmental Monitoring, *INOE*, Cluj, Romania (2010)
5. S. Marullo, R. Santoleri , V. Banzon , R.H. Evans , M. Guarracino, K. Nittis: "Challenges to generating satellite-based diurnal SST fieldsfor the Mediterranean Sea". Oceans From Space Venice 2010.
6. P. Bergamaschi, M. Corazza, A.T. Vermeulen, A.J. Manning, M. Athanassiadou, P. Bousquet, R. Thompson, M. Heimann, K. Trusilova, U. Karstens, J. van Aardenne, S. Monni, E. Popa, L Haszpra, J. Moncrieff, R. Neubert, E. Nisbet, T. Aalto, F. Meinhardt, L. Ries, M. Steinbacher, S. O'Doherty, F. Artuso, S. Piacentino, and E. Dlugokencky. "*Inverse modeling of European CH_4 and N_2O emissions"*, NitroEurope General Assembly and Open Science Conference, Solothurn-Switzerland, 1-4 February 2010.
7. F. Artuso, S. Piacentino, M. D. Sferlazzo, A. di Sarra, D. Meloni, F. Monteleone, P. Chamard, M. Frezzotti. "Atmospheric emissions of N_2O deduced from long-term observations at the Mediterranean Island of Lampedusa". EGU General Assembly 2010, Vienna.
8. F.Artuso, P. Spezzano, D. Cataldi, S. Becagli, R. Udisti, M. Mansueto, C. Bommarito, D. M. Sferlazzo, "Characterization of PAHs in atmospheric particulate at a remote site in the Mediterranean", 36th International Symposium on Environmental Analytical Chemistry, Rome, Italy, 5th-9th October 2010.
9. A. Palucci, M. Caponero. "Tecnologie opto-elettroniche per Security e Safety XVII Giornata di Studio sull'Ingegneria delle Microonde Elettronica abilitante per l'ambiente sicuro", 9 Giugno 2010 Università di Roma "Tor Vergata" Villa Mondragone, Monte Porzio Catone (Roma).

10. A. Palucci. “Laser Spectrometer for water quality analysis” – ACTCLEAN Food industry 2010 - Resource Efficiency and Environmental Legal Compliance in Food Industry - Slovakia - 24.11.2010, Bratislava (**invited lecture**).
11. A. Palucci. “Lessons learned from ENEA FISLAS project on explosive trace detection”. CRESCENDO (Coordination action on Risk, Evolution of threatS and Context assessment by an Enlarged Network for an R&D rOadmap) MEETING "CBRNE" March 24th 2010, Brussels (**invited lecture**).
12. S. Botti, M. Carpanese, L. Cantarini, G. Giubileo, S. Jovicevic, V. Lazic, A. Palucci, A. Puiu: “Trace detection of explosive compounds by different laser-based techniques at the ENEA Laboratories”, SPIE Vol. 7665, p. 76650V, 1-12.
13. V. Lazic, “LIBS on water: analysis of aerosols and of solid samples covered by water” **(invited lecture**), conference LIBS, September 2010, Memphis (USA).
14. L. Caneve, S. Almaviva, F.Colao, “LIBS project: Set up of a chamber for testing LIBS, Meeting on Task TA TGS-01-04, Material deposition and composition of walls”, Frascati, 8-9 March 2010.
15. R.Fantoni , S. Almaviva, L.Caneve, F.Colao, G. Maddaluno, “LIBS characterization of inner tile superficial layers inside fusion reactors”, Proc. of SASP 2010, Innsbruck, Austria.
16. L. De Dominicis, M. Ferri de Collibus, G. Fornetti, M. Guarneri, M. Nuvoli, R. Ricci, M. Francucci "SLIM, Subsea Laser Imaging and Metrology for the inspection of subsea infrastructures" II Technical Meeting on Optoelectronic technologies for the Oil and Gas Industry, Aberdeen (UK), November 4, 2010
17. C. Neri, M. Ferri De Collibus, M. Florean, G. Mugnaini, M. Pillon, F. Pollastrone, P. Rossi 26th Symposium on fusion technology – SOFT 2010 - Porto – Portugal “Iter in vessel viewing system design and assessment activities”.
18. G. Giubileo, “Biopsia ottica nella diagnostica dei tumori”, Workshop Oncogenesi tra Scienza e Clinica Medica – OSCM; Frascati, 10-11 Giugno, 2010.
19. Botti S., Cantarini L., Falconieri M., Giubileo G., Puiu A., Stacchini P., “Olive oil adulteration sensing with laser spectroscopy”, 36° International Symposium on Environmental Analytical Chemistry - ISEAC; Rome, October 5-9, 2010.
20. G. Dattoli, M. Quattromini, E. Sabia and V. Surrenti FEL2010 "Free-Electron-Laser-and-Positronium – stimulated annihilation” (Malmo Svezia August 2010)
21. G. Dattoli “Free Electron Lasers” 35-th International Conference on Infrared Millimeter and Terahertz waves **(invited lecture)**
22. L. Giannessi *SPARC Operation in Seeded and Chirped Mode*, presented at the 32 FEL conference 2010, Malmo, Sweden
23. L. Giannessi, *Seeding the SPARC Free electron laser amplifier*presented at the “Seeded FEL Sources and Time Resolverd Experiments Workshop” Adriatic Guesthouse Trieste, Italy 14-15 December 2010
24. F.Bonfigli, S.Almaviva and R.M.Montereali, *Confocal Microscopy Characterization of Light-Emitting Nanostructures and X-ray Imaging Detectors based on Color Centers in Lithium Fluoride*, BONSAI Symposium, Breakthroughs in Nanoparticles for Bio-Imaging, Frascati-Rome, Italy, April 8-9, 2010, P3-23.
25. M.A.Vincenti, G.Baldacchini, F.Bonfigli, P.Chiacchiaretta, R.M.Montereali, R.B.Pode, *Annealing e Degradazione di Film Sottili di Alq_3*, Convegno Fotonica 2010, 12° Convegno Nazionale delle Tecnologie Fotoniche, Pisa, 25-27 maggio 2010.
26. F.Bonfigli, S.Almaviva, F.Flora, A.Lai, R.M.Montereali P.Gaudio, M.Richetta, L.Reale, A.Faenov, T.Pikuz, *LiF-based X-ray Imaging Detectors for Micro-Radiographies of Biological Samples*, Convegno Fotonica 2010, 12° Convegno Nazionale delle Tecnologie Fotoniche, Pisa, 25-27 maggio 2010.
27. R.M.Montereali, S.Almaviva, F.Bonfigli, M.A.Vincenti, R.Nogueira, H.J.Kalinowski**,** *Reticoli Luminescenti Prodotti tramite Laser a Bassa Potenza in Cristalli e Film di Fluoruro di Litio Colorati con Raggi Gamma,* Convegno Fotonica 2010, 12° Convegno Nazionale delle Tecnologie Fotoniche, Pisa, 25-27 maggio 2010.
28. P.Finocchiaro, M.Barbagallo, L.Casentino, G.Greco, G.Guardo, R.M.Montereali, A.Pappalardo, C.Scirè, S.Scirè, M.A.Vincenti, *A thermal neutron mini-detector with SiPM and scintillating fibres*, 2010 Symposium on Radiation Measurements and Applications, SORMA XII and Workshop DNDO, May 24-28 2010, Michigan, USA.
29. F.Bonfigli, D.Hampai, R.M.Montereali, M.A.Vincenti and S.B.Dabagov, *Combination of LiF Detectors with Polycapillary Optics for X-ray High Resolution Imaging*, EXRS 2010 European Conference on X-Ray Spectrometry, Figueira da Foz, Coimbra, Portugal, 20-25 June 2010.
30. R.M.Montereali, F.Bonfigli, E.Nichelatti, A.Santoni, S.Scaglione, V.Mussi, *Optical Investigation of Metallic Lithium Colloids and F-Centers in Ion-Assisted LiF Thin Films*, Abstracts EURODIM 2010, 11th Europhysical Conference on Defects in Insulating Materials, Pécs, Hungary 12-16 July 2010, 10.4.
31. F.Bonfigli, P.Gaudio, I.Lupelli, E.Nichelatti, M.Richetta, M.A.Vincenti and R.M.Montereali, *Characterization of LiF-based Soft X-Ray Imaging Detectors by Confocal Fluorescence Microscopy*,

Abstracts EURODIM 2010, 11th Europhysical Conference on Defects in Insulating Materials, Pécs, Hungary 12-16 July 2010, 13.1.

32. F.Somma, P.Aloe, F.D'Acapito, R.M.Montereali, S.Polosan, M.Secu, M.A.Vincenti, *Optical and X-ray Absorption Spectroscopy in Lead Doped Lithium Fluoride Crystals*, Abstracts EURODIM 2010, 11th Europhysical Conference on Defects in Insulating Materials, Pécs, Hungary 12-16 July 2010, A14.
33. Olga Goncharova and Rosa Maria Montereali, *Toward the Control of Defects in Lithium Fluoride by using Multilayer Structures,* Abstracts EURODIM 2010, 11th Europhysical Conference on Defects in Insulating Materials, Pécs, Hungary 12-16 July 2010, A52.
34. M.A.Vincenti, G.Baldacchini, V.S.Kalinov, R.M.Montereali, A.P.Voitovich, *Spectroscopic Investigation of F, F_2 and F_3^+ Color Centers in Gamma Irradiated Lithium Fluoride Crystals*, Abstracts EURODIM 2010, 11th Europhysical Conference on Defects in Insulating Materials, Pécs, Hungary 12-16 July 2010, A73.
35. S.Polosan, M.Secu, C.Logofatu, F.Somma, R.M.Montereali, M.A.Vincenti, *Radiation Induced Defects in Tl^+-Doped LiF Crystals*, Abstracts EURODIM 2010, 11th Europhysical Conference on Defects in Insulating Materials, Pécs, Hungary 12-16 July 2010, B65.
36. M.A.Vincenti, E.Di Bartolomeo, S.Licoccia, A.Rufoloni and R.M.Montereali**,** *Morphological Investigation of Ultra-Thin Lithium Fluoride Films*, X International Conference on Nanostructured Materials, Nano2010, September 13-17, 2010, Roma – Italy, p. 80.
37. F.Bonfigli, I.Chiamenti, L.N.Costa, A.S.L.Gomes, L.Dominici, H.J.Kalinowski, F.Michelotti, R.M.Montereali, M.A.Vincenti, *Guide d'Onda basate su Centri di Colore nel Fluoruro di Litio Prodotte mediante Impulsi Laser al Femtosecondo*, XCVI Congresso Nazionale Societa' Italiana di Fisica, Bologna, 20-24 Settembre 2010, p.109.
38. R.M.Montereali, S.Almaviva, F.Bonfigli, M.A.Vincenti, *Spettroscopia e Microscopia Ottica per lo Studio della Fotodegradazione di Film Organici di Alq_3*, XCVI Congresso Nazionale Societa' Italiana di Fisica, Bologna, 20-24 Settembre 2010, p.109.
39. E.Nichelatti, F. Bonfigli, M.A.Vincenti, and R.M.Montereali, *Optical Modelling of an Alq_3-based Organic Light-Emitting Diode*, 15th International Workshop on Inorganic and Organic Electroluminescence & 2010 International Conference on the Science and Technology of Emissive Displays and Lighting & XVIII Advanced Display Technologies International Symposium, St-Petersburg, Russia, Sept. 27 – Oct. 1, 2010, p.90-91.
40. G.Baldacchini, P.Chiacchiaretta, R.M.Montereali, R.B.Pode, M.A.Vincenti, *Degradation of Alq_3 Thin Films and Stretched Behavior*, 15th International Workshop on Inorganic and Organic Electroluminescence & 2010 International Conference on the Science and Technology of Emissive Displays and Lighting & XVIII Advanced Display Technologies International Symposium, St-Petersburg, Russia, Sept. 27 – Oct. 1, 2010, p.108-109.
41. F.Bonfigli, D.Brogioli, M.A.Vincenti, and R.M.Montereali, *Optical investigation of photo-bleaching effects in organic Alq_3 thin films*, 15th International Workshop on Inorganic and Organic Electroluminescence & 2010 International Conference on the Science and Technology of Emissive Displays and Lighting & XVIII Advanced Display Technologies International Symposium, St-Petersburg, Russia, Sept. 27 – Oct. 1, 2010, p.110-111.
42. F.Somma, P.Aloe, F.Bonfigli, M.A.Vincenti, F.D'Acapito, S.Polosan and R.M.Montereali, *Metal impurities in LiF: opportunity for X-ray imaging detectors development*, International Workshop on Extreme Ultraviolet Sources, University College Dublino, 13-15 Nov. 2010, p. 40.
43. I.Chiamenti, L.N.Costa, F.Bonfigli, M.A.Vincenti, R.M.Montereali, A.S.L.Gomes, L.Dominici, F.Michelotti, H.J.Kalinowski, *Characterization of Optical Waveguides Produced by Femtosecond Laser in Lithium Fluoride Crystals*, 2nd Mediterranean Photonics Conference, Eilat Israele, 29 Nov. – 2 Dec. 2010.
44. D.Brogioli, R.Zhao and P.M.Biesheuvel, *Capacitive double-layer expansion: a novel technique for generating energy from the mixing of sea and river water*, "Wetsus Congress 2010", Leeuwarden, NL, 18-19 Oct. 2010.
45. S.Botti, L.Cantarini, M.Falconieri, G.Giubileo, A. Puiu, *Olive oil adulteration sensing with laser spectroscopy,* 36 Symposium on Environmental Analytical Chemistry, Roma 5-9 Ottobre, 2010.
46. E.Borsella, R.D'Amato, F.Fabbri, M.Falconieri, E.Popovici, *Laser synthesis of nanoparticles: from research to applications*, NanotechItaly2010, International Conference, Promoting responsible innovation, Venezia, 20-22 ottobre 2010.
47. E.Borsella, R.D'Amato, F.Fabbri, M.Falconieri, E.Trave, V.Bello, G.Mattei, Y.Nie, D.Wang, *On the role of NBOHC (Non-Bridging Oxygen Hole Centres) in the red photo-luminescence emission from Si nanocrystals*, E-MRS 2010 Spring Meeting, Symposium Silicon-based nanophotonics, Strasbourg (France), 7-11 giugno 2010.
48. A.Seyhan, U.Guler, M.Falconieri, R.D'Amato, E.Borsella, R.Turan, *Photo-Luminescence Bleaching In Free Standing Si Nanocrystals Prepared By Laser Assisted Silane Prolysis*, , E-MRS 2010 Spring Meeting, Symposium Silicon-based nanophotonics, Strasbourg (France), 7-11 giugno 2010.

49. R.D'Amato, M.Falconieri, E.Borsella, *Synthesis and photoluminescence of Ytterbium-doped Silicon nanocrystals*, BONSAI project Symposium, Breakthroughs in nanoparticles for bio-imaging, Frascati, Roma, 8-9 aprile 2010.
50. M.Falconieri, E.Borsella, R.D'Amato, F.Fabbri, E.Trave, V.Bello, G.Mattei, Y.Nie, D.Wang*, On the red photoluminescence emission from silicon-based nanoparticles*, BONSAI project Symposium, Breakthroughs in nanoparticles for bio-imaging, Frascati, Roma, 8-9 aprile 2010.
51. E.Borsella, R.D'Amato, M.Falconieri, N.Herlin, V.Maurice, O.Sublemontier, F.Huisken, T.Schmidt, G.Mattei, E.Trave, *Luminescent Silicon based Nanoparticles by laser pyrolysis*, BONSAI project Symposium, Breakthroughs in nanoparticles for bio-imaging, Frascati, Roma, 8-9 aprile 2010.
52. I.Rivolta, B.Lettiero, A.Panariti, R.D'Amato, V.Maurice, M.Falconieri, N.Herlin, E.Borsella and G.Miserocchi, Si-based *Nanoparticles: a biocompatibility study*, BONSAI project Symposium, Breakthroughs in nanoparticles for bio-imaging, Frascati, Roma, 8-9 aprile 2010.
53. A.Seyhan, U.Guler, M.Falconieri, R.D'Amato, E.Borsella, R.Turan, *Study of The Photo-Luminescence Bleaching in Si Nanocrystals Prepared by Laser Assisted Silane Pyrolysis*, BONSAI project Symposium, Breakthroughs in nanoparticles for bio-imaging, Frascati, Roma, 8-9 aprile 2010.
54. M.A.Caponero, A.Coricciati, P.Corvaglia, G.Fardin, A.Largo, *Multifunctional textile for masonry retrofitting, ICST2010 - Fourth International Conference on Sensing Technology*, Lecce (Italy) 3-5 June 2010
55. R.Capobianco, M.Caponero, A.Caratelli, U.Ianniruberto, *Un Monitoraggio delle Temperature del Calcestruzzo in un Getto di Grande Spessore*, Le Nuove Frontiere del Calcestruzzo Strutturale, Salerno (Italy), 22-23 Aprile 2010.
56. G.Miceli, L.M.Vinci, E.Guarneri, A.Doria, G.P.Gallerano, E.Giovenale, G.Messina, A.Petralia, I.Spassovsky, V.Surrenti, "Villa Romana del Casal di Piazza Armerina, mappatura del degrado biologico sotto il pavimento musivo mediante radiazione Terahertz", XVI Colloquio AISCOM, Palermo, marzo 2010.
57. C. Ronsivalle, "RF compression and microbunching", Relazione orale presso la XVIII Conferenza RiNEm (Riunione Nazionale di Elettromagnetismo), Universita' del Sannio, Benevento 6-10 settembre 2010
58. C. Ronsivalle, "Acceleratori per terapia oncologica", Relazione orale "Workshop "Oncogenesi: tra scienza e clinica medica", ENEA-Frascati, 10-11 giugno 2010
59. S. Sandri, M. Benassi, G. Ottaviano, L. Picardi, L. Strigari, "Neutron field analysis for a proton therapy installation", Third European IRPA Congress, Helsinki, Finlandia, 14 - 18 Giugno 2010
60. G.P. Gallerano, "Le NIR nella ricerca e nell'industria: il caso della radiazione Terahertz", (**Invited lecture)** Giornate Siciliane di Radoprotezione, Sicarusa 3 -5, Giugno 2010
61. G.P. Gallerano, "THz-BRIDGE seven years later: is a unifying view of the interaction of e.m. radiation with biological systems possible?" (**Invited lecture)**, International Workshop of the Project "Genotoxic Effects of Terahertz Radiation in vitro?", PTB Braunschweig, Germany, December 6-7, 2010
62. A.Doria, G.P.Gallerano, E.Giovenale, E.Guarneri, G.Messina, G.Miceli, A.Petralia, I.Spassovsky, V.Surrenti, L.M.Vinci, "Studying biodegradation of mosaics using THz and mm-wave radiation", Poster session, 35th International Conference on Infrared, Millimeter and Terahertz Waves, IRMMW-THz2010, Roma 5 - 10 Settembre 2010
63. B. Bisceglia, A.Doria, G.P.Gallerano, E.Giovenale, G.Messina, A.Petralia, I.Spassovsky, "An innovative non invasive technique for treatment of works of art: MM and THz waves for diagnostics and conservation", Poster Session, 35th International Conference on Infrared, Millimeter and Terahertz Waves, IRMMW-THz2010, Roma 5 - 10 Settembre 2010
64. F. Soldovieri, I. Catapano, L. Crocco, M. R. Scarfì , A. Doria, E. Giovenale, G. P. Gallerano, A. Petralia, "A simple electromagnetic model for buried interface detection via THz holographic data", 35th International Conference on Infrared, Millimeter and Terahertz Waves, IRMMW-THz2010, Roma 5 - 10 Settembre 2010
65. M.Ortolani, E.Giovine, A.Di Gaspare, S.Cibella, R. Leoni, G.Torrioli, F.Evangelisti, V.Foglietti, M.S.Vitiello, G.Scamarcio, A.Cetronio, C.Lanzieri, M.Peroni, A. Doria, E. Giovenale, A. Petralia, G.P.Gallerano, "Perspectives in the Design of Monolithic Focal Plane Arrays for Terahertz Active Spectroscopic Imaging" 35th International Conference on Infrared, Millimeter and Terahertz Waves, IRMMW-THz2010, Roma 5 - 10 Settembre 2010
66. E. Giovine, A. Di Gaspare, M. Ortolani, F. Evangelisti, V. Foglietti, A. Cetronio, D. Dominijanni, C. Lanzieri, M. Peroni, A. Doria, E. Giovenale, I. Spassovsky, and G. P. Gallerano, "AlGaN/GaN Heterostructure Transistors for the Generation and Detection of THz Radiation" 35th International Conference on Infrared, Millimeter and Terahertz Waves, IRMMW-THz2010, Roma 5 - 10 Settembre 2010

67. S. Bollanti, P. Di Lazzaro, F. Flora, L. Mezi, D. Murra, A. Torre, F. Bonfigli, R.M. Montereali, M.A. Vincenti, “Sistema innovativo di marcatura invisibile per applicazioni in anticontraffazione/tracciabilità”, Nanoforum, Torino, 15-17 Giugno 2010.
68. S. Bollanti, P. Di Lazzaro, F. Flora, L. Mezi, D. Murra, A. Torre, F. Bonfigli, R.M. Montereali, M.A. Vincenti, “Invisible marking system and relevant reading method for applications in anti-counterfeiting and traceability”, Nanoforum, Torino, 15-17 Giugno 2010.
69. P. Di Lazzaro, “La sacra Sindone, indagine su un mistero”, (**Invited lecture)**, Seminario nell’ambito della Settimana della cultura Italiana nel mondo, Ambasciata Italiana a Riga (Lettonia), 21 Ottobre 2010.
70. P. Di Lazzaro: “Sub-micrometer coloration depth of linens by vacuum ultraviolet radiation”, (**Invited lecture) -** IWSAI Frascati 4 Maggio 2010.
71. R. Balvetti, M.L. Bargellini, M. Battaglia, A. Botticelli, G. Casadei, A. Filippini, A. Guidoni, E. Pancotti, L. Puccia, L. Rubini, C. Zampetti, F. Bernardo,A. Grandinetti, B. Mussi, G. Bozanceff, C. Iencenelli, “GIASONE : un modello cibernetico per l’autonomatica”, Congresso Annuale Società Italiana di Fisica, XCVI Congresso Nazionale (Bologna, 20 - 24 Settembre, 2010).
72. R. Balvetti, M.L. Bargellini, M. Battaglia, A. Botticelli, G. Casadei, A. Filippini, A. Guidoni, E. Pancotti, L. Puccia, L. Rubini, C. Zampetti, F. Bernardo,A. Grandinetti, B. Mussi, G. Bozanceff, C. Iencenelli *From Natural Intelligence To Synthetic Intelligence Through Cybernetic Model,* The International Symposium on Design and Research in the Artificial and the Natural Sciences: DRANS 2010 Orlando/Florida Jun. 29, 2010 - Jun 29, 2010.

Technical reports

1. F. Artuso. Rapporto ESF (European Science Foundation) dal titolo “Optimization of CH4 and N2O continuous measurements at Lampedusa ENEA station”.
2. F. Artuso, A. Genovese, D. Cataldi. Rapporto per il Progetto MUSS Industria 2015 riguardante lo stato dell’arte sulle emissioni da biocombustibili.
3. L. De Dominicis, M. Ferri de Collibus, G. Fornetti, M. Guarneri, M. Nuvoli, R. Ricci, L. Bartolini, M. Francucci “Theoretical determination of power backscattered by the medium for an amplitude-modulated laser-radar in an underwater environment” RT/2010/36/ENEA, ISSN/0393-3016.
4. E.Nichelatti, R.M.Montereali, M.A.Vincenti, F.Di Pompeo, E.Segreto, N.Canci, F.Cavanna, Optical Characterization of Organic Light-Emitting Thin Films in the Ultraviolet and Visible Spectral Ranges, RT/2010/31/ENEA.
5. E.Nichelatti, F.Bonfigli, R.M.Montereali, M.A.Vincenti “Attività modellistica ottica per il progetto tecvim e sua applicazione a diodi organici emettitori di luce basati su tris (8-idrossichinolina) alluminio”, RT/2010/52/ENEA.
6. F.Fabbri, G.Terranova, R.D’Amato, B.Pignon, N.Herlin, B.Miao, P.Simon, E.Popovici, “Produzione e caratterizzazione di nanoparticelle di biossido di titanio mediante pirolisi indotta da laser di precursori liquidi,” RT/2010/53/ENEA.
7. Lai A. Sighicelli M. Valente F. 2010 “Studio dell’interazione pianta-patogeno, Brassica olearacea-Phoma lingam, attraverso l’analisi d’immagine dei parametri fotochimici correlati all’emissione di fluorescenza della clorofilla a”. RT/2010/49/ENEA
8. Lai A. Sighicelli M. Valente F. 2010 “Analisi d’immagine dei parametri fotochimici dell’emissione di fluorescenza della clorofilla a per la valutazione di una patologia su pianta elicitata e sviluppata lontano dal punto d’infezione “ RT/2010/50/ENEA
9. Lai A. Sighicelli M. 2010 “Valutazione dell’emissione di fluorescenza della clorofilla a e della risposta fotochimica correlata di Populus x euramericana (pioppo) clone I-214 cresciuto in presenza di alte concentrazioni di zinco.” RT/2010/51/ENEA.

Invited seminars

1. F. Artuso, A. di Sarra. “Misure di gas serra nel Mediterraneo: la stazione di Osservazioni Climatiche dell’ENEA a Lampedusa” tenutosi il 7 Aprile presso l’ISAC CNR di Roma Tor Vergata.
2. R.M. Montereali, seminario su invito presso l’Università degli Studi di Roma Tor Vergata Dipartimento di Fisica, Scienza dei Materiali, Roma, 28 aprile 2010, *Materiali a larga banda di emissione per dispositivi emettitori di luce.*
3. F. Bonfigli, seminario su invito presso l’Università degli Studi di Roma Tor Vergata Dipartimento di Fisica, Scienza dei Materiali, Roma, 20 maggio 2010, *Nuovi rivelatori di immagine a lettura ottica per raggi X.*
4. D. Brogioli, presentazione su invito a "Wetsus Congress 2010", 18-19 ottobre 2010, Leeuwarden, NL; autori: D. Brogioli (UTAPRAD-MNF), R. Zhao e P. M. Biesheuvel (Wetsus, NL), Capacitive double-layer expansion: a novel technique for generating energy from the mixing of sea and river water.

5. R.M. Montereali, relazione su invito, Conferenza Photonica 2010 su "I progressi della fotonica nelle scienze mediche biologiche" in Salone delle Tecnologie Innovative, Hi. Tech EXPO 2010, Fiera di Milano, 17-18 Novembre 2010, Nuove Tecnologie per Imaging Microscopico nella Biomedicina.
6. G.P. Gallerano, "Interaction of THz radiation with biological systems: unifying view or interdisciplinary approach?" Invited, Cerimonia inaugurale del "Center for THz-Bio Applications Systems" Seoul University, Korea, 9 -10 Marzo 2010.
7. L. Giannessi, *The SPARC FEL* International Center for Relativistic Astrophysics Network (Pescara) October 4, 2010
8. L. Giannessi, *First seeding experimets at SPARC*, HHG2 Workshop, Lund, Sweden, 5-7 May 2010

Events organization

- "BONSAI Symposium: Breakthroughs in Nanoparticles for Bio-Imaging" 8-9/04/2010, ENEA Frascati.
- "International Workshop on the Scientific Approach to the Acheiropoietos Images", IWSAI, ENEA-Frascati, May 4-6, 2010;
- "I laboratori incontrano le piccole e medie imprese" a cura di ENEA e BIC-Lazio, ENEA-Frascati, May 25, 2010;
- "Workshop Oncologia tra clinica medica e scienza", ENEA-Frascati, June 10-11, 2010;
- "International Conference on Infrared and Millimeter, and Terahertz Waves", IRMMW-THz 2010, Roma, September 5-10, 2010.